A Holocene Trace Chemistry Record from Law Dome Ice Cores

Christopher Thomas Plummer
BSc, BAntSci (Hons)

Submitted in fulfilment of the requirements for the degree of
Doctor of Philosophy

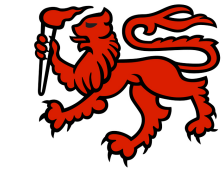

UNIVERSITY*of*
TASMANIA

February 2018

Declaration

This thesis contains no material which has been accepted for a degree or diploma by the University or any other institution, except by way of background information and duly acknowledged in the thesis, and to the best of my knowledge and belief no material previously published or written by another person except where due acknowledgement is made in the text of the thesis, nor does the thesis contain any material that infringes copyright.

Signed:_____

Christopher Thomas Plummer

Date: 21 February 2018

Authority of Access

This thesis may be made available for loan and limited copying and communication in accordance with the Copyright Act 1968.

Abstract

The short instrumental period from the Southern Hemisphere presents challenges to assessing long term variability in the climate system. Proxy records developed from ice core data provide an opportunity to address this issue. Following new analysis of ice cores from the high snowfall Dome Summit South (DSS), Law Dome, East Antarctica, the full Holocene chemistry records of sea salts, sulphate and methanesulphonic acid (MSA) from this site are presented for the first time. The records have been annually layer counted to 333 BCE +13/-7 years; comparable or better than the presently available, sub-annual resolution Antarctic ice core records covering 2,000 years. The annually dated record has been used to construct proxy records of El Nino-Southern Oscillation, Australian drought, and improve the accumulation record for the site. The detailed volcanic history from DSS has been used to refine the timing of the Kuwae (Vanuatu) eruption to between 1456 and 1458 CE. This eruption is one of the largest of the past 2,000 years and constraining its timing and separating it from a 1453 CE Northern Hemisphere event improves volcanic forcing estimates. Beyond the layer counting ages were based on an ice flow model with dating ties to other Antarctic ice core records.

This study indicates aerosols at DSS were primarily dry deposited at the Last Glacial Maximum (LGM) through to 12,000 years before 2000 CE (b2k). From 12,000 b2k wet deposition of aerosols increased in dominance, with the current wet deposited regime reached by approximately 7,500 b2k. Sea salt concentrations at DSS were lowest at 12,000 b2k. From 12-8,000 b2k sea salt concentrations increased markedly, corresponding with the timing of ice sheet retreat, bringing the DSS site relatively closer to the coast. This increase is also observed at inland Antarctic sites, although is more extreme at DSS. Sulphate concentrations at DSS remained largely unchanged through this period suggesting more of the larger sea salt particles were being deposited at DSS as the ice sheet retreated. However sea salt concentrations continued to gradually increase after the ice sheet retreat had occurred, only stabilising by 5,000 b2k.

The increase in sea salt concentrations following the ice sheet retreat are consistent with an increase in wind speed across the Southern Ocean and a southward shift of the westerly wind belt bringing greater aerosol loads. This is supported by other proxy data and modelling studies which suggest increases in cyclonic activity in the circumpolar trough, a contraction of the Antarctic High and possible strengthening or shift in position of the zonal westerly wind belt around Antarctica. However the evidence from the Law Dome sea salt record cannot rule out a northward shift of the mean wind belt over open waters. The more gradual change in sea salt concentrations from 8-5,000 b2k is not clearly observed in other inland Antarctic ice cores. It is possible that small changes in the westerly winds around Antarctica would be more strongly observed in the coastal DSS core than inland Antarctic sites. Agreement between solar insolation and sea salt concentrations suggest insolation is an important driver of changes to processes affecting sea salt deposition at DSS in the Holocene.

An inverse relationship between the sea salt record and sea surface temperature (SST) reconstructed from marine sediment cores is observed, potentially driven by increased wind speed or cyclogenesis over the Southern Ocean releasing greater latent heat from the sea surface, increasing atmospheric moisture and sea salt aerosol loads. A positive correlation between sea salt concentrations and sea ice presence reconstructions off the Dronning Maud Land coast suggest either regional coherence in sea ice formation or another control such as SST or wind advection of ice floes is affecting sea ice formation. No consistent relationship between SST, sea ice and MSA over millennial timescales is evident in this study, possibly reflecting the complex relationship between MSA production and deposition.

Acknowledgements

This research would not have been possible without my supervisors: Mark Curran, Andrew Moy, Tessa Vance, Tas van Ommen and Kelvin Michael. They have shown great patience and support and always made themselves available when needed and I am grateful for that. I'd like to thank Meredith Nation and Sam Poynter for their support with the core processing, sample analysis and ability to perform jigsaw puzzles at -18°C. I acknowledge Sune Rasmussen for his Matlab expertise which helped considerably with the core dating. I thank Cheryl not only for her vial washing, but for ideas and useful discussions. I also extend my gratitude to the staff of the ACE CRC and AAD for their help and support during my PhD.

I would also like to thank the original DSS drill teams of the late 80s and early 90s. When DSS was drilled to bedrock it was quite an achievement, and I hope those that were involved are happy to know that their efforts over a quarter of a century ago are still bearing fruit today.

My appreciation also goes to the members of the Aurora Basin North (ABN) field team. The opportunity to head to Antarctica and be involved in drilling a new ice core was a fantastic opportunity and greatly appreciated. The whole team were great to work with, but I'd like to especially thank the other members of the processing team Mana, Holly and Olivia, as well as my Casey cabin mate Olivier.

I also thank IMAS and UTAS for providing travel funds to present my work at the IPICS conference. I also gratefully acknowledge the Australian Postgraduate Award scholarship I received. And finally, I'd like to acknowledge my friends and family. Their encouragement has been invaluable and does not go unappreciated.

List of abbreviations

AICC2012 – Antarctic Ice Core Chronology 2012

ALC – Annual Layer Counted

AABW – Antarctic Bottom Water

B2K – Before 2000 CE

BCE – Before Common Era

CCSM3 – Community Climate System Model 3

CE – Common Era

CFA – Continuous Flow Analysis

CLIMAP – Climate Long-range Investigation, Mapping, and Prediction

$\delta^{18}O$ – Oxygen Isotope Ratio

δD – Deuterium to Hydrogen ratio

DI – Deionised Water

DML – Dronning Maud Land

DMS – Dimethyl Sulphide

DMSP – Dimethylsulfoniopropionate

DSS – Dome Summit South

EA – Elemental Analyser

EAIS – East Antarctic Ice Sheet

EDC – EPICA Dome C

EDML – EPICA Dronning Maud Land

ENSO - El Niño–Southern Oscillation

EPICA – European Project for Ice Coring in Antarctica

GICC05 – Greenland Ice Core Chronology 2005

GISP – Greenland Ice Sheet Project

GRIP – Greenland Ice Core Project

IAEA – International Atomic Energy Agency

IRMS – Isotope Ratio Mass Spectrometer

ITCZ – Intertropical Convergence Zone

LGM – Last Glacial Maximum

LoQ – Limit of Quantitation

MSA – Methanesulphonic Acid

MSLP – Mean Sea Level Pressure

μEq/L – Micro equivalents per litre

NADW – North Atlantic Deep Water

NGRIP – North Greenland Ice Core Project

NH – Northern Hemisphere

PDO - Pacific Decadal Oscillation

PMIP2 – Paleoclimate Modelling Intercomparison Project 2

PSC – Polar Stratospheric Cloud

SAM – Southern Annular Mode

SH – Southern Hemisphere

SLAP – Standard Light Antarctic Precipitation

SWW – Southern Westerly Winds

VEI – Volcanic Explosivity Index

VSMOW – Vienna Standard Mean Ocean Water

WAIS – West Antarctic Ice Sheet

Peer-reviewed publications related to this work

Plummer, C. T., Curran, M. A. J., van Ommen, T. D., Rasmussen, S. O., Moy, A. D., Vance, T. R., Clausen, H. B., Vinther, B. M., and Mayewski, P. A.: An independently dated 2000-yr volcanic record from Law Dome, East Antarctica, including a new perspective on the dating of the 1450s CE eruption of Kuwae, Vanuatu, Clim. Past, 8, 1929-1940, 2012. doi:10.5194/cp-8-1929-2012

Tessa R. Vance, Tas D. van Ommen, Mark A. J. Curran, **Christopher T. Plummer,** Andrew D. Moy, A millennial record of ENSO and eastern Australian rainfall from the Law Dome ice core, East Antarctica, J. Clim, 26, (3) pp. 710–725, 2013, doi: 10.1175/JCLI-D-12-00003.1

- Contributed timescale and sample analysis.

Roberts, J., **Plummer, C.**, Vance, T., van Ommen, T., Moy, A., Poynter, S., Treverrow, A., Curran, M., and George, S.: A 2000-year annual record of snow accumulation rates for Law Dome, East Antarctica, Clim. Past, 11, 697-707, 2015. doi:10.5194/cp-11-697-2015, 2015.

- Contributed layer counted dating for accumulation rate calculation, sample analysis and text.

Vance, T. R., J. L. Roberts, **C. T. Plummer**, A. S. Kiem, and T. D. van Ommen, Interdecadal Pacific variability and eastern Australian mega-droughts over the last millennium, Geophys. Res. Lett., 42, 129–137, 2015. doi:10.1002/2014GL062447

- Contributed timescale, analysis and text.

Roberts, J., Curran, M., Poynter, S., Moy, A., van Ommen, T., Vance, T., Tozer, C., Graham, F., Young, D., **Plummer, C**., Pedro, J., Blankenship, D., Siebert, M.: Correlation confidence limits for unevenly sampled data, Computers & Geoscience, 2016, doi: 10.1016/j.cageo.2016.09.011

- Contributed timescale and sample analysis.

Statement of Authorship

The following people and institutions contributed to the publication of work undertaken as part of this thesis:

Candidate: Christopher Plummer – Institute for Marine and Antarctic Studies, Antarctic Climate and Ecosystems Cooperative Research Centre
Author 1: Mark Curran – Antarctic Climate and Ecosystems Cooperative Research Centre, Australian Antarctic Division
Author 2: Tas van Ommen – Antarctic Climate and Ecosystems Cooperative Research Centre, Australian Antarctic Division
Author 3: Sune O. Rasmussen – Centre for Ice & Climate, University of Copenhagen
Author 4: Andrew D. Moy – Antarctic Climate and Ecosystems Cooperative Research Centre, Australian Antarctic Division
Author 5: Tessa R. Vance – Antarctic Climate and Ecosystems Cooperative Research Centre
Author 6: Henrik B. Clausen - Centre for Ice & Climate, University of Copenhagen
Author 7: Bo M. Vinther - Centre for Ice & Climate, University of Copenhagen
Author 8: Paul A. Mayewski – Climate Change Institute, University of Maine

An independently dated 2000-yr volcanic record from Law Dome, East Antarctica, including a new perspective on the dating of the 1450s CE eruption of Kuwae, Vanuatu

Located in Chapter 5

The candidate was the primary author, responsible for Law Dome volcanic identification, led the annual layer counting dating effort, flux calculations, inter-core comparisons and performed part of the chemical analysis and record synthesis and writing the manuscript (75%). Author 1 contributed to dating, flux calculations and analysis (8%). Author 2 provided assistance with flux calculations and dating (4%). Author 3 assisted with dating and providing NGRIP data (4%). Authors 4-5 assisted with dating and record synthesis (2%). Authors 6-7 contributed NGRIP data and calculation of NGRIP volcanic fluxes. Author 8 assisted with ice core analysis (1%).

Signed _____

Name: MARK CURRAN
Supervisor

Date: 15/9/2017

Signed

Name: NATHAN BINDOFF
Head of School
IMAS

Date: 23/10/2017

List of tables

List of figures

Contents

Chapter 1 – Introduction and literature review

1 Overview

Changes in climate systems are driven by both natural cycles and human influences. The importance of the latter has become has come under scrutiny, but the increasing anthropogenic influence on the climate system is difficult to assess with short instrumental records (IPCC, 2014). The ability to extend the climate record is possible through the use of proxies recorded in various natural climate responders, such as tree rings, corals, sediment deposits and ice cores. Extending climate records offers the opportunity to assess present climate changes in the context of a longer time period.

Ice cores are considered excellent climate archives due to the ability of snow to preserve atmospheric conditions at the time of snow deposition through trapping of air bubbles, aerosols and particles. Individual snowfall events accumulate as layers through time. By sampling through these layers by drilling an ice core it is possible to investigate the atmospheric conditions at the time of snow deposition. Ice cores have been retrieved from locations across the planet including mid-latitude high mountain areas (e.g. The Himalayas and Andes) and the high latitude ice sheets of Greenland and Antarctica. Polar regions are particularly useful for studies of past atmospheric changes as they are substantially isolated from other continents, where local continental dust and anthropogenic activities would dominate over climate signals (Legrand and Mayewski, 1997).

By exploiting the link between snow deposition and atmospheric chemistry it is possible to reconstruct past atmospheric and climate variability on timescales from annual to 800,000 year timescales. Ice core data has been used to reconstruct temperature histories (e.g. PAGES Consortium, 2013; Johnsen et al., 1995; Masson-Delmotte et al., 2011; Masson et al., 2000; Mayewski et al., 2004b; Simonsen et al., 2011; Vinther et al., 2009, 2006a) and changes in atmospheric circulation patterns (e.g. Aizen et al., 2004; Goodwin et al., 2004; Mayewski et al., 2004a; Souney et al., 2002; Vance et al., 2013).

Volcanic eruptions affect the climate system and ice cores offer an opportunity to accurately date these events and provide information on their relative size and potential impact on climate (Gao et al., 2007; Hammer et al., 1997; Robock, 2000; Sigl et al., 2013).

Dating terminology used in this thesis.

Calendar dates used in this thesis are denoted by CE or BCE for Common Era/Before the Common Era. For longer time periods the term "years before 2000 CE" (b2k) is used.

Thesis Aims

The key aims of this study were to:

- Acquire new chemistry data from the existing Law Dome, Dome Summit South (DSS) core to form a complete Holocene trace ion record for sea salts sodium and chloride, sulphate and methanesulphonic acid (MSA).
- Produce an annually layer counted timescale for the DSS core past 2000 years.
- Determine the timing and magnitude of volcanic events recorded in the layer counted portion of the DSS core.
- Investigate changes in Holocene chemistry at DSS.

Thesis structure

Chapter 1 provides a review of literature, providing background information related to the thesis aims. This includes details on atmospheric circulation, ice core chemistry, volcanic eruptions and their impact on climate.

Chapter 2 documents the DSS (Law Dome) ice cores used in this thesis. The ice sample preparation and analytical methods are also presented.

Chapter 3 establishes the ice core dating methods and techniques used for the DSS ice core. This includes the annual layer counting using seasonal varying chemical species and the age model for DSS using age ties.

Chapter 4 presents the Holocene trace ion chemistry records for DSS, and explores the relationship between the ice core chemistry and site changes, sea surface temperatures, and sea ice extent.

Chapter 5 is a peer reviewed publication on the 2000-year volcanic history from the Law Dome ice core record.

Chapter 6 provides a summary of findings in this thesis.

Chapter 7 offers recommendations and suggestions for further research.

1.1 Law Dome

The ice cores used in this study are from the Dome Summit South (DSS) site on Law Dome, a small ice cap located on the coast of Wilkes Land, East Antarctica (66°44′S 112°50′E) [Figure 1.1] with an approximate present elevation of 1395 m above sea level. Law Dome projects into a predominantly easterly atmospheric circulation pattern. Cyclonic systems that form over the Southern Ocean move across Law Dome where adiabatic cooling from orographic lifting precipitates snowfall (Bromwich, 1988). The easterly airflow gives rise to a snow accumulation gradient across the dome, with a high of 1.20 metres annually (ma^{-1}) ice equivalent on the eastern flank, to 0.17 ma^{-1} ice equivalent west of the summit (Curran et al., 2002; Morgan et al., 1997).

DSS is 4.6 km south-southwest of the Law Dome summit. This location was chosen as radio echo-sounding indicated an area of relatively flat bedrock and a reduced likelihood of flow disturbance to the overlying ice (Morgan et al., 1997). Flow disturbances in ice can distort the layers making interpretations of the ice core record more difficult (Morgan et al., 1997). The annual accumulation rate of 0.68 ma^{-1} ice equivalent at DSS (Roberts et al., 2015; van Ommen et al., 2004) is a result of the high cyclonic frequency across Law Dome and snowfall events are sufficiently frequent to allow the extraction of glaciochemical records with sub-annual resolution (McMorrow et al., 2001). High accumulation rates

reduce post-depositional changes to snow pack chemistry (Waddington et al., 1996). The absence of high gusts and generally low mean wind speed (8.3 m s^{-1}) reduce the post depositional reworking and mixing of surface snow (Adams, 1996). DSS has a mean low summer temperature of -12.6°C (Allison et al., 1993) and no melt events have been observed which would alter the chemistry record.

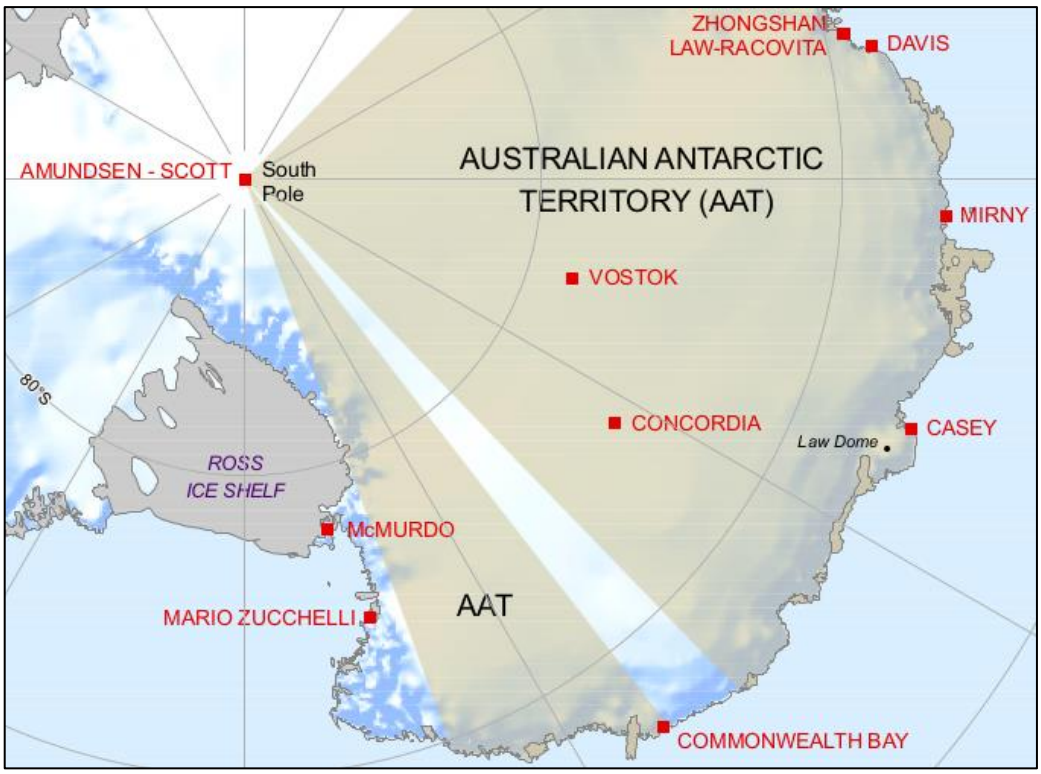

Figure 1.1- Location of Law Dome in East Antarctica. The DSS site is located 4.6 km from the Law Dome summit.

1.2 Atmospheric circulation

Global atmospheric circulation patterns are a key component driving the distribution of thermal gradients and wind patterns on the planet. These circulation patterns are a strong influence on the transport of aerosols to and around the Antarctic. Each hemisphere can be divided into 3 major circulation components; Hadley, Ferrel and polar cells [Figure 1.2]. Additionally, the formation and breakdown of the polar vortex has a significant impact on long range transport and deposition of aerosols to Antarctica.

Hadley cells are thermally-driven convection cells that dominate low-latitude circulation. Warm air rising at the equator reaches the tropopause and is forced poleward. The air cools as it flows from the equator, where the air

converges around the mid latitudes as it cools and sinks. This convergence of relatively warm, dry air results in a high pressure zone at the surface 30° either side of the equator, known as the subtropical high. Surface winds in the Hadley cell flow from the high towards the low pressure zone at the equator but are deflected towards the west by the Coriolis force. Where the winds meet about the equator is known as the intertropical convergence zone (ITCZ) in which the air rises again to complete the Hadley cell (Ahrens, 2012).

Not all surface air descending from the Hadley cell returns to the equator – some of this air moves towards the poles. As the air flows towards the poles it is deflected by the Coriolis force to give westerly surface winds. This air flows poleward where it converges with cold air flowing out from the poles around 60° latitude. This creates an area of low pressure at the surface called the polar front. Here, the warmer air rises, and some of this air then returned to the subtropical high to complete the Ferrel cell (Ahrens, 2012). The westerly winds are not constant, as areas of high and low pressure break up the surface flow pattern, introduced by baroclinic waves that develop spontaneously in response to instabilities in the large-scale flow pattern (e.g. differences in the thermal properties of land and water) (Wallace and Hobbs, 2006). Westerly flow in the Southern Hemisphere is more zonal than the Northern Hemisphere because there are fewer continental landmasses to introduce baroclinic instability in the Southern Hemisphere (Salby, 2012).

The polar cell in Antarctica is a zone of high pressure over the continent where a small amount of air migrates poleward from above the polar front in the upper troposphere cools and sinks over the interior. The weak polar cell is completed as the katabatic flow of cold air drains back out to the polar front. The Coriolis force results in easterly winds over the continent (Ahrens, 2012). The relative strength of the high pressure system over the continent affects the position of the westerly wind belt that encircles Antarctica and the ability for the cyclonic systems associated with the polar front to penetrate beyond the coastal margins (Kreutz et al., 2000; Mayewski et al., 2004a; Souney et al., 2002).

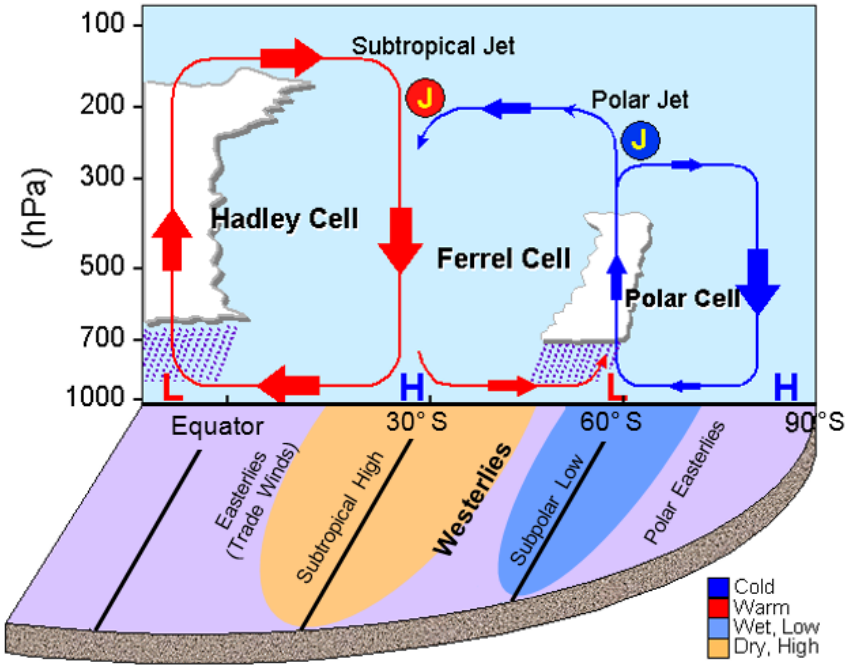

Figure 1.2 – General atmospheric circulation model. The three major meridional cells operating in each hemisphere, and their effect on winds and surface pressures. The size of the arrow indicates the relative strength of airflow. Modified from Li and Wang, (2003).

1.2.1 Polar Vortex

The Polar Vortex is a primary feature of Southern Hemisphere high-latitude stratospheric circulation. During the Antarctic winter cold stratospheric air over the continent is restricted from interacting with air from lower latitudes by a large-scale vortex circulation, bounded at its perimeter by strong eastward-flowing polar jetstream encircling the continent (Wallace and Hobbs, 2006). Rising temperatures in spring and weakening westerly winds around the vortex lead to its breakdown each summer. During the cold winter period high-level ice clouds called polar stratospheric clouds (PSCs) form in the vortex.

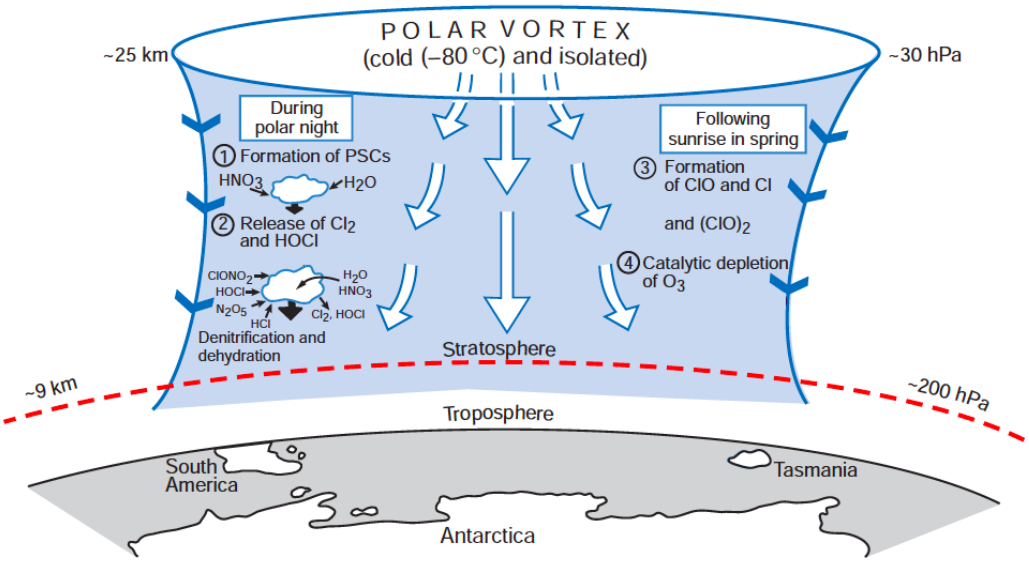

Figure 1.3 – Polar vortex over Antarctica. Large arrows show cold descending air. 1-4 show atmospheric chemistry taking place inside the vortex. Modified from Wallace and Hobbs, (2006).

Over Antarctica, two main types of PSCs have been observed:

Type I which condense near -78 °C and consist of a mixture of liquid and solid particles of nitric acid, water and sulfuric acid. Type I PSCs have been further sub-classified into 3 types:

> **Type Ia**: Contain nitric acid in trihydrate form.
>
> **Type Ib**: Supercooled ternary solutions formed by the uptake of H_2O and HNO_3 on the liquid stratospheric H_2SO_4/H_2O (background) aerosols (Khosrawi et al., 2011).
>
> **Type Ic**: Metastable HNO_3 and H_2O in solid phase (Tabazadeh and Toon, 1996).

Type II which form around -85 °C consist of a mixture of ice and water together with some dissolved nitric acid. Type II PSCs have larger crystals and are nucleated by smaller Type I or other atmospheric aerosols (Salby, 2012).

Gravitational settling or sedimentation of PSCs is thought to be an important process controlling deposition of nitrate to the Antarctic ice sheet (Legrand and Mayewski, 1997). The height of PSCs descends through winter closer to the tropospheric boundary where increased nitrate concentrations can be incorporated in tropospheric precipitation, leading to a small nitrate maximum observed in spring (Mayewski and Legrand, 1990; Mulvaney and Wolff, 1993).

1.3 Ice core chemistry

Ice core chemistry varies through time in response to changes in climatic conditions. The variations in chemistry can be exploited using proxy methods to produce paleoclimate interpretations. However, before such interpretations can be made it is essential to understand the source, transport and depositional regimes for each species. This study will primarily investigate the ions of sodium (Na^+), chloride (Cl^-), methanesulphonic acid (MSA^-) and sulphate (SO_4^{2-}) and the following literature review will discuss these in detail. In addition to these species, sections of ice were also analysed for nitrate (NO_3^-), hydrogen peroxide (peroxide) and stable isotopes of oxygen and hydrogen, which were used to produce the ice core timescale for this study. A review of depositional mechanisms and how they may affect interpretation of ice core records is also given.

1.3.1 Sea salt species

The term “sea salts” refers to measured trace ion species in an ice core derived from seawater sources. The major trace ion species with seawater sources investigated in this study are chloride (Cl^-), sodium (Na^+) and sulphate (SO_4^{2-}). Chloride and sodium in Antarctic ice cores originate mainly from sea salt (Röthlisberger et al., 2003; Wagenbach, 1996). Sulphate is a substantial component of seawater, however has significant biological sources and may be altered by fractionation processes, therefore cannot be as readily interpreted as a seawater species as Cl^- or Na^+.

The concentrations of sea salt species in Antarctic surface snow decrease exponentially with distance inland and elevation as the larger aerosols fall out during transport (Mulvaney and Wolff, 1994; Yang et al., 1996). This has important implications for interpretations of sea salt records as it suggests changes in concentrations of sea salt species are linked to the frequency and intensity of tropospheric aerosol transport to the ice core site (Kreutz et al., 1997).

1.3.2 Sea salt aerosol production

In Antarctic coastal regions sea salt is a major aerosol component with highest concentrations during winter (e.g. Jourdain et al., 2008; Wagenbach et al., 1998). For sea salt aerosols to be preserved in ice cores an effective atmospheric transport pathway is necessary. The methods for ejecting sea salt particles into the air over open water are mechanical tearing of water droplets from wave crests at high wind speeds (wave breaking) and the bursting of bubbles at the water surface (Gong et al., 1997; Norris et al., 2012). Once seawater droplets enter the air they evaporate thus concentrating or forming airborne crystals of sea salt that can be lofted into the atmosphere (Udisti et al., 2012). Sea salt spray in the atmosphere is a major source of cloud condensation nuclei where they affect cloud cover and albedo, scattering incoming radiation and reflecting a portion back to space (Quinn et al., 1996).

Non-sea salt sulphate ($nssSO_4^{2-}$) is the proportion of total sulphate in an ice core not from a seawater source. It is derived by multiplying the concentration of sodium by the ratio of sulphate to sodium in bulk seawater, and subtracting this from the total sulphate concentration (Rankin et al., 2000; Wagenbach et al., 1998). This method may result in negative values during winter periods around the Antarctic. Assuming the sodium concentration is seawater derived, negative values suggest a depletion in sulphate relative to the seawater ratio. One source for seawater ions depleted in sulphate is the highly saline surface brine pools formed on new sea ice (Rankin et al., 2000; Wagenbach et al., 1998; Wolff et al., 2003). The growth of sea ice expels sea salt particles from the ice matrix forming saline brine pools (Rankin et al., 2000; Wagenbach et al., 1998). As salinity increases and the temperature decreases below -8ºC, mirabilite ($Na_2SO_4 \cdot 10H_2O$)

is precipitated. This results in brine pools heavily depleted in sulphate and up to 13% of sodium relative to seawater (Rankin et al., 2002). Fractionation of other seawater species can occur at lower temperatures. Below -22ºC NaCl will precipitate, however sea ice temperatures this cold are normally associated with multi-year ice therefore we do not expect to see NaCl depletion (Rankin et al., 2002).

The transport pathway for fractionated aerosols from sea ice is still debated. Formation of frost flowers has been proposed as a mechanism (e.g. Kaleschke et al., 2004; Rankin et al., 2004, 2000; Wagenbach et al., 1998). Frost flowers are small centimetre-scale ice crystal growths that form on new sea ice. Analysis of frost flowers shows them depleted in sulphate relative to sodium (Rankin et al., 2000). Frost flower formation and entrainment of the sea salt aerosol requires specific meteorological conditions. The creation of new ice is essential to their formation, and temperatures need to be sufficiently low for fractionation to occur. Low wind speeds will not generate aerosols from flowers, and high winds speeds will destroy them (Rankin et al., 2000). Alvarez-Aviles et al., (2008) found evidence for an alternative aerosol pathway where frost flowers act as wicks drawing up brine from the surface pools, potentially enabling more effective wind-driven transport at lower speeds through an increased surface area. Studies of frost flowers in laboratories have shown they do wick up brine effectively, however have had difficulty in getting any aerosols from them, even when wind strengths were increased to cause them to break (Roscoe et al., 2011). This calls in to question the role frost flower formation has on sea salt aerosol formation, though the study notes that low humidity conditions were not assessed and that the dehydration of frost flowers may have a role.

Yang et al., (2008) suggested snow lying on sea ice as an important source of sea salt aerosol. They proposed several methods for sea salts to be incorporated with blowing snow; falling snow flooding of the sea ice surface, saltation across brine pools, and sea salt inputs from nearby leads and open waters. The snow can be dehydrated to provide a saline nucleus that is more easily lofted into the atmosphere. A chemistry transport model forced by blowing snow and frost flower emissions found blowing snow was the dominant winter sea salt source

(Huang and Jaeglé, 2016). The study found blowing snow emissions were greatest in regions with persistent strong winds over sea ice, while frost flower emissions were largest where open water and cold air temperatures are co-located.

The dominance of fractionated sea salts decreases moving inland and with increasing elevation, with greater than 80% fractionation at the sea ice surface and 5% or less at inland sites (Udisti et al., 2012; Wong, 2007). The estimated total sulphate depletion calculated for Law Dome is 33.4%, 15.1% of which is frost-flower derived (Wong, 2007) and this factor has been used to correct for the effects of fractionation when calculating $nssSO_4^{2-}$ on Law Dome ice cores (see section 1.4.1).

1.3.3 Sea salts and sea ice extent

Sea salts have been suggested as a possible proxy for sea ice extent (e.g. Wolff et al. 2003). In almost all Antarctic sites, sea salts exhibit a winter maximum, for example Law Dome, Halley Bay, Neumayer, DML, Concordia stations and WAIS divide (Curran et al., 1998; Sigl et al., 2013; Traufetter et al., 2004; Udisti et al., 2012; Wagenbach, 1996; Wagenbach et al., 1998) coincident with the annual increase in sea ice extent. If the dominant source of sea salts deposited to the ice sheet are from open ocean sources (i.e., bubble bursting and wave breaking processes described above) we might expect to observe higher sea salt concentrations during periods of less extensive sea ice (i.e. local summer) when the distance between the open ocean and those sites is shorter (Abram et al., 2013; Levine et al., 2014). This assumes the meteorology controlling production and transport of sea salts does not change throughout the year. Fractionation is evidence for at least some sea-ice derived sea salt source (see section 1.3.2). Attempts at calibrating annual sea salt data against annual sea ice extent have not been successful, likely due to local meteorological factors, changes in atmospheric transport and polynyas exerting greater influence on sea salt aerosols and overprinting the sea ice extent signal in the ice core record (Abram et al., 2013; Levine et al., 2014). However, the much larger changes in sea ice extent over glacial/interglacial cycles may allow sea salts to be used as a

proxy for sea ice extent during those periods (Levine et al., 2014; Wolff et al., 2003).

Sea salt records represented by sodium concentrations in Greenland and Antarctic ice cores show pronounced glacial/interglacial variations (Fischer et al., 2007b). In Antarctica, the sea salt flux is enhanced by a factor of 13 during the Last Glacial Maximum (LGM, 18-24,000 years ago) compared to the Holocene and varies by approximately a factor of 1-2 in parallel with Antarctic warm events (Fischer et al., 2007b). The continental source of sodium is much more important during glacial periods (Röthlisberger et al., 2002b). Global atmospheric dustiness is increased during glacial periods. During glacial times generally cold and dry conditions prevailed on land resulting in reduced forests, expansion of grass vegetation, and an increase of exposed lacustrine material due to lake level decrease. Stronger latitudinal thermal gradients led to generally more vigorous atmospheric circulation (Kohfeld and Harrison, 2001; Tegen, 2003; Yung et al., 1996).

1.3.4 Chloride depletion

Studies investigating changes in aerosols as a function of distance from oceanic source have observed chloride depletion relative to the expected seawater ratio of chloride/sodium in atmospheric aerosol particles (Virkkula et al., 2009; Wagenbach et al., 1998). However, chloride concentrations in snow show little or no significant post-depositional loss or enrichment (Virkkula et al., 2009) at coastal sites below 2000 m elevation (Bertler et al., 2005). At sites with higher elevation and further inland reactions of chloride with nitric and sulphuric acids in the atmosphere leads to the formation of hydrochloric acid (HCl) that eventually escapes the sea salt aerosol budget thus leaving the relative concentrations of sea salts depleted in chloride (Röthlisberger et al., 2003). This process is understood to be greater at low accumulation sites where readmission of HCl to the atmosphere takes place. Because of these uncertainties sodium is frequently used as a reliable marker of sea salt concentrations (Abram et al., 2013) however sodium may be depleted by up to 13% relative to seawater

concentrations due to frost flower formation (Rankin et al., 2002) and also has a low continental source through the Holocene (Röthlisberger et al., 2003).

At Law Dome, Curran et al., (1998) found the average seawater ratios of sodium and chloride closely matched those measured in ice cores from the site, which suggests post depositional loss or enrichment of chloride is minimal at Law Dome, likely due to the high accumulation rate and the site elevation (1370 m) being below the 2000 m elevation threshold (Bertler et al., 2005).

1.3.5 Previous sea salt studies from Law Dome

The annual sea salt cycle from Law Dome has a winter maximum and a period of low concentrations during summer as a result of the seasonal frequency, position and intensity of synoptic scale cyclonic events and regional variations in wind speeds (Curran et al. 1998). Lower-troposphere wind strength and atmospheric circulation modes control the formation and the transport of sea spray, thus sea salt concentrations measured in ice cores are useful for reconstructing changes in zonal wind intensity, cyclonic-system latitude and strength, polar vortex intensity and atmospheric circulation modes (e.g., Goodwin et al., 2004; Legrand and Mayewski, 1997; Petit et al., 1999; Udisti et al., 2012; Wolff et al., 2006). Links between large-scale atmospheric patterns such as the Southern Annular Mode (SAM), El Nino – Southern Oscillation (ENSO) and strength of the Antarctic High and the deposition of Law Dome sea salts have been found (Goodwin et al., 2004; Souney et al., 2002; Vance et al., 2013).

Mid-latitude winter mean sea level pressure (MSLP) in the south Indian and southwest Pacific oceans is strongly correlated with the May-June-July (MJJ) sea salt concentrations from Law Dome, and anti-correlated to the Southern Annular Mode (Goodwin et al., 2004). The Southern Annular Mode (SAM) is one of the dominant climate modes in the Southern Hemisphere. The atmospheric circulation of the SAM describes a predominantly zonally symmetric pattern characterized by a redistribution of atmospheric mass between the polar region (>60ºS) and a zonally symmetric ring around 45º-50ºS (Kwok and Comiso, 2002). The positive SAM phase is associated with an increase in the strength of the prevailing westerly winds in the Antarctic as well as a contraction of the

circumpolar trough poleward; while the negative phase has the opposite effect (Goodwin et al., 2004).

Work by Souney et al. (2002) found a significant positive correlation with June sea level pressure (SLP) measured from 12 stations across East Antarctica and the sea salt record from Law Dome. They argue that a significant correlation to SLP over such a broad area of East Antarctica suggests sea salt aerosol production and transport to Law Dome is related to the large scale atmospheric circulation system over the continent during winter - the Antarctic High. Their study found that maximum sea salt concentrations occurred during periods of high pressure anomalies over continental Antarctica, contemporaneous with the circumpolar trough being displaced northwards over open water.

A link between the summer concentration of sea salts and ENSO has been established (Vance et al., 2013). The Law Dome sea salt record for the months DJFM is correlated significantly with the Southern Oscillation Index (SOI) and ENSO sea surface temperature (SST) indices. The study also found that the Law Dome summer sea salt record correlated with annual rainfall in South Eastern Australia. Vance et al., (2015) further demonstrated that Law Dome sea salts are correlated with the Interdecadal Pacific Oscillation (IPO). The IPO is a low frequency SST anomaly in the Pacific Ocean operating on decadal to multi-decadal timescales that has a modulating effect on the ENSO signal (Power et al., 1999; Salinger et al., 2001). The negative IPO phase favours La Niña conditions over El Niño conditions (Risbey et al., 2009) and drought risk in Australia increases in positive phases of the IPO (Vance et al., 2015).

1.4 Sulphate in ice cores

The primary sources of sulphate to the Antarctic ice sheet are seawater and biogenic productivity with minor contributions from volcanic eruptions and anthropogenic emissions. Measured ice core concentrations are a total sulphate comprising all sources [Figure 1.4], which make interpreting records more difficult. Sea salts (including sea salt sulphate) were discussed in the previous section; therefore this section will focus on the other sulphate sources and the expression of and isolation of those signals from the total sulphate record.

1.4.1 Non-sea salt sulphate

Non-sea salt sulphate ($nssSO_4^{2-}$) is the component of total sulphate not derived from seawater. The $nssSO_4^{2-}$ is calculated using the ratio of sulphate and sodium concentrations using the seawater ratio of 0.1201 (r), and a fractionation correction (fc) according to equation 1 (Palmer et al., 2001).

$$nssSO_4^{2-} = [\text{total } SO_4^{2-}] - (r - fc) \times [Na^+] \qquad \textbf{Equation 1.}$$

The fractionation correction is necessary to account for the depletion of sulphate relative to sodium and at Law Dome is 0.033 (Palmer et al., 2002). Not correcting for fractionation can result in negative $nssSO_4^{2-}$ values during winter months, when salt concentrations are highest, and frost flower formation has the greatest effect on sea salt ion concentrations. Although fractionation predominantly affects winter sea salt concentrations, the correction is applied year-round because the boundaries between summer and winter snow are not distinct (Palmer et al., 2002). This has minimal effect on interpretation of the $nssSO_4^{2-}$ record because summer is the sea salt minima, and the sulphate signal is dominated by biogenic sources unaffected by fractionation.

The $nssSO_4^{2-}$ record has numerous components from marine and terrestrial biogenic, volcanic, anthropogenic and continental dust sources. It is dominated by marine biogenic aerosols from reduced sulphur gases, primarily dimethylsulphide (DMS) (Savoie et al., 2002). DMS is a product of atmospheric oxidation of dimethylsulphoniopropionate (DMSP) produced by certain phytoplankton (Charlson et al., 1987; Curran and Jones, 2000). The levels of $nssSO_4^{2-}$ recorded in ice cores can be considered indicative of summer biological activity in the Southern Ocean for coastal ice core sites (Curran and Jones, 2000; Wagenbach et al., 1998). The $nssSO_4^{2-}$ record has a strong seasonality with minimum values in August and rising sharply to peak during January with the summer increase in biological activity (Curran et al., 1998).

Volcanic contributions to the $nssSO_4^{2-}$ record are readily identified by a large increase from background levels (Curran et al., 1998; Dixon et al., 2004).

Volcanic eruptions emit sulphur gases that are oxidised to SO_4^{2-} in the atmosphere and appear as sharp peaks in the $nssSO_4^{2-}$ record lasting 2-3 years and abnormally elevated winter $nssSO_4^{2-}$ values.

The relative isolation of the Antarctic from continental dust and anthropogenic sulphate sources results in only minor contributions to the sulphate record from those sources and the signal is overprinted by much more dominant biogenic and volcanic sources (Curran et al., 1998; Graf et al., 2010; Minikin et al., 1998).

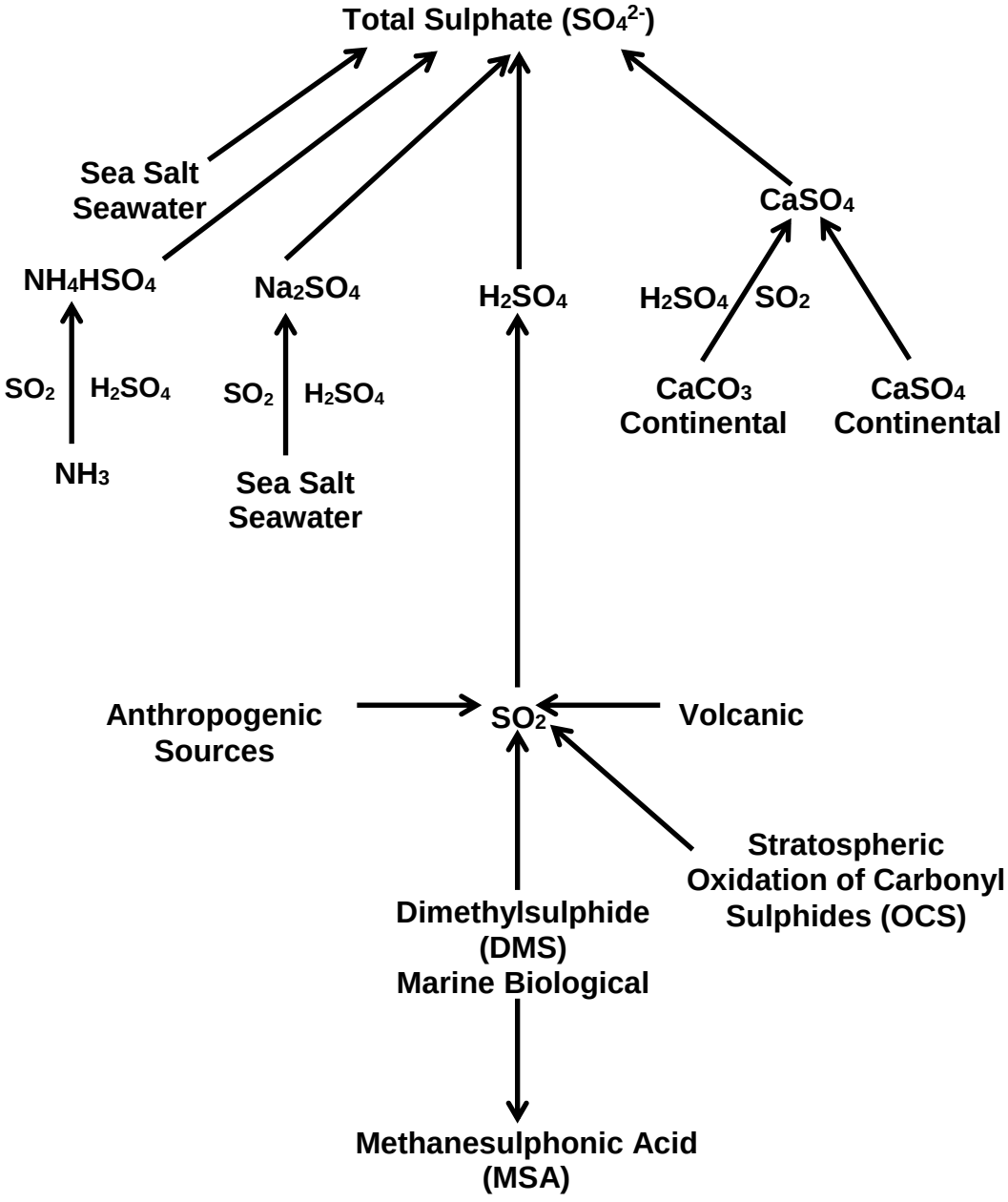

Figure 1.4 – Sources of sulphate in ice cores. Modified from Legrand and Mayewski, 1997

1.5 Methanesulphonic Acid

Methanesulphonic Acid (MSA) is one of the stable end-products of atmospheric oxidation of DMS, and has been used to estimate marine biogenic sulphur emissions (Savoie et al., 2002). The MSA seasonal cycle is similar to that of $nssSO_4^{2-}$; a clear summer maximum and values close to zero during winter. While $nssSO_4^{2-}$ has multiple sources, the only source for MSA is DMS (Curran et al., 1998). A major contributor to the MSA precursor species production are the coccolithophores and phytoplankton Phaeocystis sp., which is especially prevalent in the Southern Ocean (Gibson et al., 1990; Liss et al., 1994). Curran and Jones, (2000) found that the sea ice zone exhibited higher levels of DMS (and its precursor DMSP) during the spring-summer sea ice melt phase, where it is thought that the fresh water and nutrients released stimulate growth. As phytoplanktonic activity varies with sea ice melt, there is a corresponding variation in the amount of DMS produced. Growth rates of Phaeocystis respond positively to moderate temperature increases (Schoemann et al., 2005) in isolation, but other variables such as nutrient availability, grazing, and light availability are important to production. Other phytoplankton DMS contributors may behave differently.

Correlations between MSA concentrations and sea ice extent have been found at several ice core sites (e.g. Curran et al. 2003; Foster et al. 2006; Becagli et al. 2009). These studies have demonstrated that MSA can be used as a proxy for sea ice extent around Antarctica. Both positive and negative correlations with sea ice extent have been found, depending on the local aerosol transport pathways (Abram et al., 2013). A positive correlation between MSA and satellite-derived sea ice extent data has been found at Law Dome (Curran et al., 2003).

Post depositional changes to MSA in ice cores are known to occur and cause difficulty in sampling and interpretation of data (Curran et al., 2003; Mulvaney et al., 1992; Pasteur and Mulvaney, 2000; Wolff, 1996). MSA is known to diffuse through both firn and solid ice, where it migrates along grain boundaries from summer snow to the sea salt rich winter snow where it forms a stable cation salt (Pasteur and Mulvaney, 2000). The diffusion coefficient for

MSA in ice is $4.10 \pm 0.25 \times 10^{-13}$ m^2 s^{-1} (Roberts et al., 2009). This is greater than other common chemistry species measured in ice such as oxygen-18 or deuterium (2×10^{-15} m^2 s^{-1}) or nitric acid (10^{-14} m^2 s^{-1}) (Wolff et al., 1996). Ice cores and ice core samples have been shown to lose MSA to the atmosphere during storage, so analysis for MSA should ideally take place as soon as possible, or the samples be melted and refrozen to preserve MSA (Abram et al., 2008).

1.6 Nitrate

Nitrate in polar ice cores has a complex production and transport regime, and its interpretation is unclear. Sources of nitrate include tropical thunderstorms (Legrand, 1987), stratospheric oxidation of N_2O (from anthropogenic emissions), ionospheric dissociation of N_2, and polar stratospheric clouds via HNO_3 (Bertler et al., 2005). Nitrate has an austral summer maximum, which it has been suggested results from enhanced stratospheric transfer to the ice sheet during summer (Curran et al., 1998). The summer nitrate peak is often preceded by a smaller spring peak that has been attributed to gravity settling of particles (sedimentation) from polar stratospheric clouds (Bertler et al., 2005; Mayewski and Legrand, 1990). Post-depositional processes also complicate interpretation of the nitrate record. The nitrate record is affected by re-emission of particles to the atmosphere through wind pumping and air circulating through the porous firn layer and the potential for photolytic breakdown, especially at low accumulation sites (Legrand et al., 1996; Röthlisberger et al., 2002a).

1.7 Isotopes

The isotopic ratios of $H_2{}^{18}O$, $H_2{}^{16}O$ and ^2H_2O in the ice vary according to the degree of fractionation the water vapour underwent during transport from the moisture source region to the ice sheet [Fig 1.3]. Fractionation occurs due to the different saturation vapour pressure and molecular diffusivities of the heavier and lighter water molecules, respectively (Schlosser et al., 2008). The heavier water isotopes evaporate less readily and condense more easily. The ratios of oxygen and hydrogen (denoted by $\delta^{18}O$ and δD respectively) are reported as the deviation in parts per million from Vienna Standard Mean Ocean Water

(VSMOW) according to equation 2a and 2b. The values for $\delta^{18}O$ and δD in the Antarctic are negative due to the accumulated loss of heavier isotopes in poleward-moving air masses as they move to higher latitudes.

At high accumulation ice core sites large seasonal variations are preserved in the $\delta^{18}O$ and δD records. These variations are caused by the stronger temperature gradient between the moisture source regions and the ice sheet during the winter compared to the summer. Therefore isotopic values are lower (more negative) from winter snow than summer snow deposits. This seasonality can be used as a dating tool by counting of annual horizons. The ratios vary primarily as a function of atmospheric condensation temperature at time of the snowfall, but elevation, latitude and distance from open water source also have an influence. The isotopic ratios in an ice core can be used as a proxy for air temperature at the deposition site (Dansgaard, 1964). At Law Dome, the oxygen isotope ($\delta^{18}O$) maximum occurs around January 10 each year, which corresponds with the timing of the average summer temperature maximum at Casey station, 120 km north-northwest (van Ommen and Morgan, 1997).

$$\delta^{18}O = \left[\frac{\left(\frac{{H_2}^{18}O_{sample}}{{H_2}^{16}O_{sample}} \right)}{\left(\frac{{H_2}^{18}O_{VSMOW}}{{H_2}^{18}O_{VSMOW}} \right)} - 1 \right] \times 1000\ ‰ \qquad \textbf{Equation 2a}$$

$$\delta D = \left[\frac{\left(\frac{^{2}H_2O_{sample}}{H_2O_{sample}} \right)}{\left(\frac{^{2}H_2O_{VSMOW}}{H_2O_{VSMOW}} \right)} - 1 \right] \times 1000\ ‰ \qquad \textbf{Equation 2b}$$

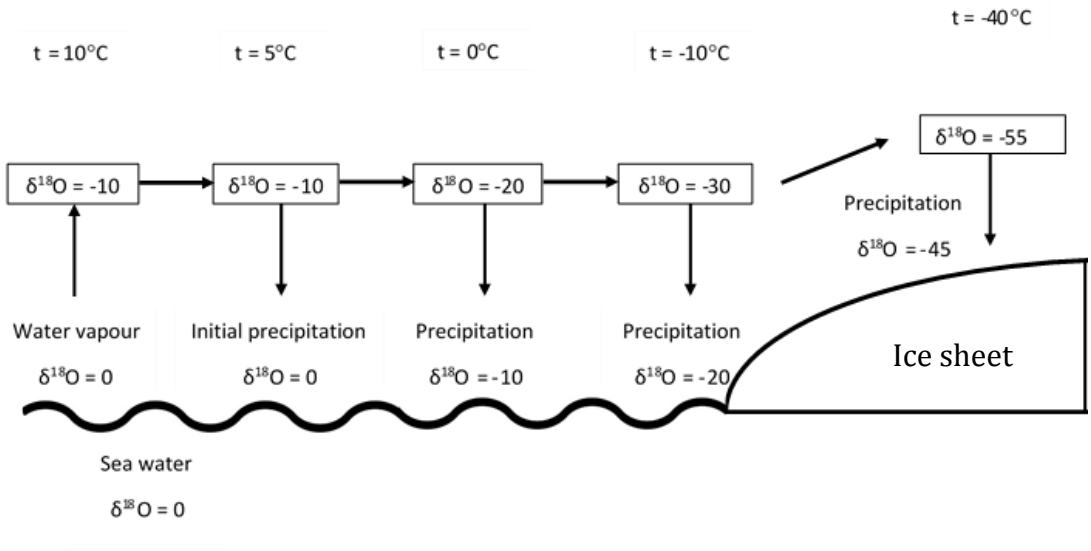

Figure 1.5 – Simple isotope fractionation model. The isotope record ($\delta^{18}O$) becomes progressively more fractionated polewards. Modified from Bradley, (1999).

1.8 Hydrogen Peroxide

Hydrogen peroxide (H_2O_2) is formed through photodissociation of ozone in the troposphere. As this only occurs in the presence of sunlight, a higher concentration of peroxide can be seen in summer precipitation in Antarctica (Thompson, 1992). Peroxide is found to be one of the clearest seasonal tracers in both Arctic and Antarctic high-accumulation ice cores (Sigg and Neftel, 1988). The H_2O_2 signal has a summer peak and has been used to assist the dating of Law Dome ice cores.

1.9 Climate impact of volcanic eruptions

Volcanic eruptions are an important natural forcing on Earth's climate system, therefore it is important to understand their impact. Volcanic events have been held responsible for cold periods throughout recorded history, with so called "volcanic winters" following major eruptions thought to have adversely affected human populations, cultures and vegetation (Stothers, 1999). One such example is the year following the 1815 eruption of Mount Tambora, Indonesia, named "the year without summer" after abnormally low temperatures were recorded

throughout Europe and North America (Stothers, 1984). The associated heavy rains, increased snow and frosts resulted in widespread crop failures which led to famine and disease (Stothers, 1984). In recent history, the June 15 1991 eruption of Mount Pinatubo, Philippines, was the largest stratospheric aerosol perturbation of the 20th century with the 30km high eruption plume injecting 30 Tg of aerosol to the atmosphere (McCormick et al., 1995). The eruption brought to an end several years of globally warm surface temperatures, with mean tropospheric temperatures showing a -0.7ºC anomaly in 1992, and a -0.2ºC anomaly in 1993 when compared to the 1958-1991 average, and accounting for ENSO patterns that should have caused tropospheric warming (McCormick et al., 1995).

Large volcanic eruptions inject sulphur gases (predominantly sulphur dioxide) into the stratosphere, which is oxidised to sulphuric acid (H_2SO_4) (Rampino and Self, 1984). Sulphur aerosols emitted during volcanic eruptions reflect incoming solar radiation, cooling the surface and troposphere while absorbing outgoing long wave radiation causing stratospheric warming (Robock, 2000). The decrease in temperature following an eruption is in the order of 0.4 – 1.2°C and primarily a result of the amount of sulphate aerosols injected to the stratosphere (McCormick et al., 1995; Rampino and Self, 1982; Robock, 2000). The fine ash particulates (tephra) ejected during eruptions may have a local climate impact, however most falls out of the atmosphere within days to weeks of the eruption and the small amount that remains in the stratosphere has a minimal impact on global climate (Rampino and Self, 1984, Rampino, 1982; Robock, 2000).

1.9.1 Volcanism recorded in ice cores

Volcanic eruptions are an important natural cause of climate change (Sigl et al., 2013). As archives of atmospheric chemistry, ice cores enable the relationship between volcanic sulphur emissions and climate forcing to be explored together with precise timing of events.

Evidence of volcanic eruptions being preserved in ice cores was first established in Greenland ice cores by Hammer, (1977). Since then, many detailed

volcanic histories have been obtained from Greenland and Antarctic ice cores as well as cores from ice caps in Canada and alpine glaciers (e.g. Palais et al., 1990; Legrand and Delmas, 1987; Delmas et al., 1992; Ferris et al., 2011; Cole-Dai et al., 2000; Cole-Dai et al., 1997; Thompson et al., 2002; Palmer et al., 2001; Stenni et al., 2002; Yalcin et al., 2003; Traufetter et al., 2004). One of the most important aspects of volcanic records is they provide useful stratigraphic tie points. By matching volcanic events across multiple sites, a common timescale can be achieved which allows comparisons of ice core data across sites on regional or global scales. By bringing together many volcanic records it is possible to estimate the atmospheric sulphate loadings associated with paleovolcanic events. Gao et al., (2008) and Crowley and Unterman, (2012) have produced global volcanic forcing indexes that can be included in climate models to simulate the effects of volcanism on the climate system.

For a volcanic signature to be recorded in an ice core, the sulphur emissions must be transported to the ice core site. Large-scale stratospheric tropical eruptions have a greater effect on global climate as they have a global-scale radiative effect when compared to eruptions closer to the poles where deposition is restricted to one hemisphere (Robock, 2000). Meridional transport from the mid latitudes brings volcanic aerosols to the Antarctic. Transport to the Antarctic can be delayed from 6-24 months depending on meteorological features such as the position of the east-west wind belts around the equator blocking poleward movement out of the tropics during the east phase of the quasi-biennial oscillation (QBO), and the formation of the circumpolar vortex during winter, which stops incursion of the stratospheric aerosol to the Antarctic (McCormick et al., 1995; Zielinski, 2000). Volcanic aerosol is transported from the stratosphere to the troposphere through gravitational sedimentation, downward air movement (subsidence) and episodic mixing of tropospheric and stratospheric air masses through tropopause folds (McCormick et al., 1995). Once in the troposphere aerosols are deposited by rain out or gravitational settling.

In addition to preserving volcanic sulphate aerosols, ice cores may also contain deposits of volcanic ash or tephra produced during the eruption. Whilst most rock and ash particles are deposited locally, fine tephra particles can be

transported considerable distances, and chemical analysis of these tephra shards has been used in ice cores from Antarctica and Greenland to identify eruption sources (Dunbar et al., 2003; Lavigne et al., 2013; Narcisi et al., 2012; Palais et al., 1990; Zielinski et al., 1997).

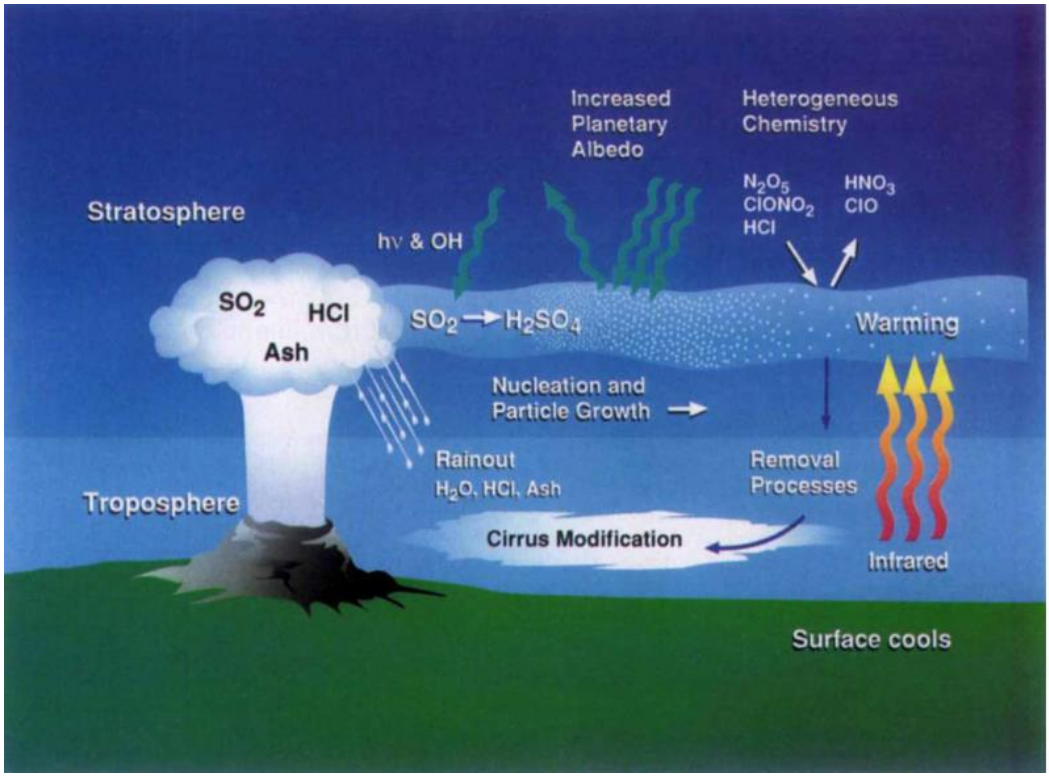

Figure 1.6 – Effect of volcanism on climate. Volcanic eruptions inject ash, sulphur rich gases, water vapour and hydrochloric acid (HCl) in to the atmosphere. Ash and HCl typically rains out quickly, whereas sulphur rich gases react with water vapour to form sulphuric acid (H_2SO_4) and may remain in the atmosphere from months to years. The H_2SO_4 aerosols following an eruption reflect incoming solar radiation, and absorb outgoing surface radiation, leading to both surface cooling and atmospheric warming. Volcanic aerosols are removed from the stratosphere through gravitational settling and mixing at the troposphere boundary layer and rained out from the troposphere. (Figure from McCormick et al., 1995).

1.9.2 Previous studies of volcanism using Law Dome ice cores

Preliminary work to identify volcanic eruptions in the DSS ice core record was subsequently expanded upon by Palmer et al., (2001), who used an accurately dated, continuous $nssSO_4^{2-}$ record covering 1995-1301 CE to identify and characterise volcanic signatures. This study expands upon this earlier work by significantly extending the volcanic record to the Holocene (12,000 years before

CE 2000) and by revisiting the dating of and calculation of volcanic sulphate flux calculations by Palmer et al., (2001; 2002).

1.10 Deposition mechanisms for trace ion species

The transfer of aerosols from the atmosphere to the ice is a critical phase in the development of a glaciochemical record. Aerosol deposition to the ice occurs via three mechanisms; wet, dry and fog deposition (Bergin et al., 1995; Davidson et al., 1996; Legrand and Mayewski, 1997).

1.10.1 Wet Deposition

Wet deposition processes include precipitation and scavenging by blowing snow (Legrand and Mayewski, 1997). The removal of aerosols by precipitation occurs by three mechanisms – nucleation, in cloud (rain out) and below cloud (wash out) scavenging (Davidson et al., 1996). Deposition by nucleation occurs when the aerosol particles act as condensation sites aiding the formation of ice crystals. The ice crystals aggregate into larger snow crystals and eventually precipitate out as snow or rain (Davidson et al., 1996). In cloud scavenging occurs where aerosols collide with the cloud water (in-cloud ice crystals and water droplets). These particle collisions that occur as the snow moves through the air effectively scavenge or "wash out" the atmosphere of particles. This wash out can occur from snowfall or from blowing surface snow (Davidson et al., 1996; Legrand and Mayewski, 1997).

1.10.2 Fog deposition

Fog deposition occurs where liquid water is present at the surface. The water droplets within the fog condense on particles in the atmosphere, thereby capturing other aerosols in a process like in-cloud scavenging (Davidson et al., 1996). The larger size of the water droplets enhances the rate of sedimentation compared to that of dry deposition of the same particles, while chemical reactions can take place in the liquid phase that can change the chemistry (Bergin et al., 1995).

1.10.3 Dry Deposition

Dry deposition describes a group of processes that deposit particles through direct interaction between the atmosphere and snow surface (Legrand and Mayewski, 1997). Unlike wet and fog deposition, which occur only under certain meteorological conditions, dry deposition is a continuous process. Deposition occurs through a variety of ways; impaction, interception, Brownian diffusion, sedimentation and gas sorption (Cunningham and Waddington, 1993; Davidson et al., 1996). The dry depositional mechanism may be enhanced by "wind pumping" or ventilation, caused by a pressure differential between air in the firn layer and wind moving over the surface. The causes air to circulate through the pore spaces of the firn, depositing particles in the snow (Cunningham and Waddington, 1993; Harder et al., 2000; Waddington et al., 1996).

Dry deposition is a continuous process independent of snow accumulation and occurs at all sites, but is a more dominant mode of deposition at inland sites with low accumulation rates (Harder et al., 2000). Previous studies of coastal locations like Law Dome have shown wet deposition to be dominant (Kreutz et al., 2000), with Wolff et al., (1998) finding that only 5-10% of aerosols are dry deposited. The concentrations of ions within the snow depend not only on the atmospheric concentration, but the meteorological conditions (i.e. presence or absence of fog or storms), winds, surface roughness, and the chemical nature of the aerosols (Bergin et al., 1995). Ventilation is the effect of airflow moving through interstitial pore spaces of snow and firn, and can affect the top several meters of firn (Neumann and Waddington, 2004). Ventilation may enhance dry deposition of aerosols in firn (Colbeck, 1989; Cunningham and Waddington, 1993; Harder et al., 2000).

1.11 Post-depositional processes

Changes to the trace chemistry record can take place after aerosol deposition to the ice sheet. These changes can alter or destroy the chemistry record of an ice core. Post-depositional processes include melt, diffusion, sublimation, reworking of surface snow, thermal and photochemical reactions.

If a site becomes sufficiently warm that surface snow melts, water may percolate down through the firn layers disrupting the annual layering of older ice. Meltwater elutes ionic species – preferentially sulphate and nitrates, but all species can be affected - which can cause the loss of annual ion deposits (Davies et al., 1982). The migration of glaciochemical signals in upper firn layers via diffusion processes can lead to a smoothing of isotope and chemical signals. Diffusion is not confined to the near surface; MSA is known to diffuse through solid ice as well as firn (Roberts et al., 2009; Smith et al., 2004) where MSA migrates along grain boundaries from summer to winter ice layers forming a stable salt with the sea salt cations. This process appears to be enhanced at low accumulation sites (Curran et al., 2003) however unlike isotopes or peroxide, the peak in concentration of MSA remains clearly defined (Pasteur and Mulvaney, 2000). Chemical reactions between volatile species (including nitrate and sulphate) can also take place altering chemistry records; and nitrate may undergo photolytic breakdown in the near surface (Bertler et al., 2005; Wolff, 1996). Water vapour sublimation causes a loss of snow mass and concentrates the remaining trace chemistry in surface snow. Water vapour sublimation is most significant at windy sites with low accumulation rates (Wolff et al., 1998). The sublimation process can affect the isotope records and cause the re-release of particles to the air (Pomeroy and Jones, 1996).

Wind can have an important impact on ice core records. Wind-driven ablation can completely remove snowfall events from the record at a sampling site (Petit et al., 1982). Redistribution of surface snow and the formation of small ridge-like features called sastrugi can disrupt annual layering. Strong winds entrain snow particles, which skip across the ice surface in a process known as saltation. Saltating particles transport snow (and its associated chemistry) to new sites and blowing snow can scavenge aerosols from the lower troposphere (Pomeroy and Jones, 1996; Wolff et al., 1998).

Wind-driven ventilation may alter the chemistry record. Air filtered through porous firn can introduce new aerosols, and may also re-entrain already deposited particles, changing the chemistry record (Colbeck, 1989; Legrand and

Mayewski, 1997; Waddington et al., 1996). It may also carry atmospheric water vapour into firn, where it mixes with existing pore-space vapour, affecting isotope records preserved by enhancing sublimation and diffusion (Albert, 2002). The influence of air circulation reduces with depth from the surface. Snow burial to depths below which ventilation is a major influence takes longer at low accumulation sites; therefore they may experience greater post depositional changes.

1.12 The Holocene epoch

The Holocene is the most recent period of Earth history including the present day. The start of the Holocene has been defined as the end of the Younger Dryas (Greenland Stadial 1), dated 11,700 b2k with a maximum error of 99 years (Walker et al., 2009). This timing was based on abrupt changes in deuterium excess values and more gradual changes in $\delta^{18}O$, dust and chemistry concentration and annual layer thickness in the Greenland NGRIP ice core (Walker et al., 2009).

1.12.1 Holocene climate optima

Holocene climate has been considered a period of relative stability, with no major abrupt climate variations as those seen during the cold glacial (deMenocal and Bond, 1997). However, detailed studies have revealed significant climate multi-decadal to multi-millennial fluctuations during the Holocene.

A series of warming and cooling events have occurred in the Antarctic during the Holocene. The warming events are referred to as climatic optimums. Antarctic water isotope studies have indicated a widespread early Holocene climatic optimum between 11,550 – 9,050 b2k (Masson et al., 2000) with warming of 0.2 - 2.5°C, depending on location. A suggested mechanism for this was a weakening of global oceanic heat transport. The Atlantic meridional overturning circulation (AMOC) carries heat from SH surface waters north where it cools, sinks and is returned south at depth as North Atlantic Deep Water (NADW). A stronger AMOC results in cooling in the South Atlantic and warming in the North Atlantic. The reverse is true of a weaker AMOC (van Ommen, 2015).

The climatic optimum is followed by a minimum around 8,050 b2k, thought to have been induced by a strengthening of oceanic circulation in line with the end of the NH cold event around 8,150 b2k (Masson et al., 2000). Regional climate optima have also been defined in the Ross Sea sector (8,050-6,050 b2k) and a weak event in East Antarctica 6,050 – 3050 b2k (Masson et al., 2000).

More recent climate fluctuations include the warm Medieval Climate Anomaly (MCA) and a cool period known as the Little Ice Age (LIA) (Mann et al., 2009). The expression of the MCA and LIA were highly regional, with no globally synchronous warm or cool periods that can be used to define them (PAGES Consortium, 2013) In Antarctica, there is no clear consensus on timing of these events. Orsi et al., (2012) found WAIS divide (West Antarctica) was colder than the last 1000 year average between 1300 – 1800 CE, while Etheridge et al., (1996) suggest 1550-1800 CE were colder at Law Dome, East Antarctica based on CO_2 mixing ratios. Glacial retreat and advance at Rothera Point (West Antarctica) about 990 CE and 1280 CE respectively correspond closely to the MCA and LIA as reported in the NH (Guglielmin et al., 2015).

1.12.2 Abrupt cooling in the early Holocene

There is evidence for an abrupt cooling event in the early Holocene around 8,150 b2k (Alley et al., 1997a; Thomas et al., 2007). This event (commonly referred to as the 8.2 kiloyear event) was a hemispheric climate perturbation in which atmospheric methane concentrations decreased by ~80 ppb, corresponding to a 15±5% reduction in methane gas emissions (Kobashi et al., 2007). The event was characterized by an abrupt climate shift from normal Holocene conditions to colder, windier and drier conditions. Greenland temperatures were up to 6°C cooler during the 160.5 year cold period (Alley et al., 1997a; Thomas et al., 2007). It is thought to have resulted from the collapse of the Northern Hemisphere Agassiz and Laurentide ice sheets (Wagner et al., 2013) where meltwater pulses affected circulation and cooled sea surface temperatures in the North Atlantic (Ellison et al., 2006; von Grafenstein et al., 1998). Consequently the event has been most prominent in Greenland ice cores (Alley and Ágústsdóttir, 2005). The event has been detected in the methane

records from EDC (Antarctica) ice cores by Spahni et al., (2003) and Law Dome (van Ommen et al., 2007).

1.12.3 Sea ice extent

Sea ice is an important component of ocean-atmosphere dynamics. Efforts has been made to reconstruct past Antarctic sea ice extent at the Last Glacial Maximum (e.g. CLIMAP, 1981; Crosta et al., 1998; Gersonde, 2003; Gersonde et al., 2005). Reconstructions suggest the winter sea ice field expanded to 39 x 10^6 km^2, close to a 100% increase on present sea ice extent of 19 x 10^6 km^2 (Gersonde et al., 2005). Large uncertainties still exist around summer sea ice extent. The earlier sedimentology-based CLIMAP reconstruction suggests a small summer sea ice retreat. The diatom-based Gersonde et al., (2005; 2003) and Crosta et al., (1998) reconstructions argue for continued large annual retreat, with a small increase in summer sea ice extent at the LGM relative to today.

Holocene changes to sea ice extent around Antarctica are not fully understood or quantified. Few long sea ice proxies exist covering the entire Holocene epoch. Sea ice reconstructions in the region around DSS are limited. The diatom-based sea ice reconstruction from marine sediment core SO136-111 (56°S, 160°E) indicates it was largely ice free by 14,000 b2k. A reconstruction from sediment core E27-23 (59°S, 155°E) shows only small amounts of sporadic winter sea ice during the Holocene (Ferry et al., 2015). High resolution sea ice presence reconstructions from marine sediment cores off the Dronning Maud Land (DML) coast are available from TN057-13PC4 (53°S, 005°E) and TN057-17PC1 (50°S, 006°E) (Divine et al., 2010; Nielsen et al., 2004). These reconstructions based on diatom assemblages found that for the last 10,000 years the winter sea ice extent varied mainly between 51-53°S in that sector. The early Holocene climate optimum corresponded with a period of reduced seasonal sea ice cover along the DML coast. During this time the winter ice edge retreated south of 53°S, before readvancing during the mid-Holocene (Divine et al., 2010).

1.12.4 Westerly wind patterns

Antarctica is encircled by a belt of zonal winds known as the southern westerly winds (SWW). These winds are an important control on Southern Hemisphere and global climate. Their strength and position influences upwelling in surface waters and ocean currents, formation of the polar vortex, precipitation distribution and sea ice formation (Anderson et al., 2009; Bromwich, 1988; Carleton, 1989; Enomoto and Ohmura, 1990; Kwok and Comiso, 2002; Toggweiler et al., 2006; Wallace and Hobbs, 2006; Yuan et al., 1999). Since these processes affect changes in source and transport of aerosols to the ice sheet, it follows that changes in the behaviour of the SWW belt will imprint in the chemistry record preserved in Antarctic ice cores. Holocene changes to the SWW belt are still a subject of much debate as to their sign and magnitude and changes may not be uniform around the Southern Hemisphere (Knudson et al., 2011; Kohfeld et al., 2013), with the onset of ENSO activity driving increased zonal asymmetry in the last 6,000 years (Fletcher and Moreno, 2011, 2012). Wind driven movement of sea ice opens ice-free water closer to the Antarctic coast (Holland and Kwok, 2012) which may cool and enable further sea ice production. Stronger or a more westerly wind belt may have led to greater sea ice production and moving it further away from the coast.

Chapter 2 – Law Dome ice cores

2.1 Dome Summit South ice cores

Four separate ice cores have been used in this study [Table 2.1]. Cores drilled after DSSmain are close to this original DSS site but have been spaced so as to retrieve only fresh, undisturbed ice each time. This study will focus primarily on results from the DSSmain ice core. DSSmain is 1196 m long and drilled to bedrock across 5 seasons between 1988 and 1993 and the oldest ice dates approximately to 88 ka. The upper 117 m of DSSmain was drilled using a thermal drill, before an electromechanical drill was put in place for the remaining deeper ice. The upper 117 m of DSSmain was found unsuitable for trace ion analysis due to micro fractures and the possibility of contamination, therefore two subsequent ice cores DSS97 and DSS99 were drilled to cover the recent era. The upper 117 m of DSSmain was analysed for a continuous isotope record. The DSS record has been updated to 2012 by the shallow firn core DSS1213, drilled in 2012/13 season and covering the period 1989 – 2012. Prior to DSS1213, a series of short cores ~6-10 m length had previously been used to update the record to 2009 (Plummer et al., 2012). After drilling, cores were logged with notes taken on breaks and stratigraphy, cut in to ~1 m core sections and sealed in polyethylene bags whilst kept at -18°C before being transported back to Hobart for processing.

2.2 Ice core sampling preparation

Ice core sections were prepared for sampling at -18°C wearing polyethylene gloves to avoid contamination. Each core section was examined and information such as exact length, breaks and any other physical features (e.g. wind crusts) noted. Core sections were first halved lengthways using a vertical bandsaw. From one half a 35 mm x 35 mm piece of ice was cut along the length of the ice core yielding a chemistry "stick" which was used for trace ion chemistry. Other pieces were used for $\delta^{18}O$ and peroxide analysis or returned storage. Each chemistry stick was sealed in a polyethylene bag until ready for further processing.

2.2.1 Decontamination of the chemistry stick

The 35 mm x 35 mm chemistry stick for trace ion measurements requires careful preparation to decontaminate the ice samples and prevent recontamination before analysis. This was achieved by removing the outermost 3-5 mm of ice from the chemistry stick using a stainless steel microtome blade under a laminar flow hood blowing filtered air over the ice. This procedure was carried out at -18°C, with operators wearing double shoulder-length polythene gloves and a facemask to guard against aerosol contamination. All surfaces in contact with the ice were thoroughly pre-cleaned using reagent grade isopropyl alcohol and deionised water (DI). Samples were taken at between 25 and 50 mm intervals along each chemistry stick using the microtome blade to separate individual samples in to sterile accuvettes. To ascertain if any contamination to the ice occurred during processing, a "blank" stick cut from frozen DI water (resistivity 18.2 MΩ·cm) was sampled using the same procedure as for the chemistry stick.

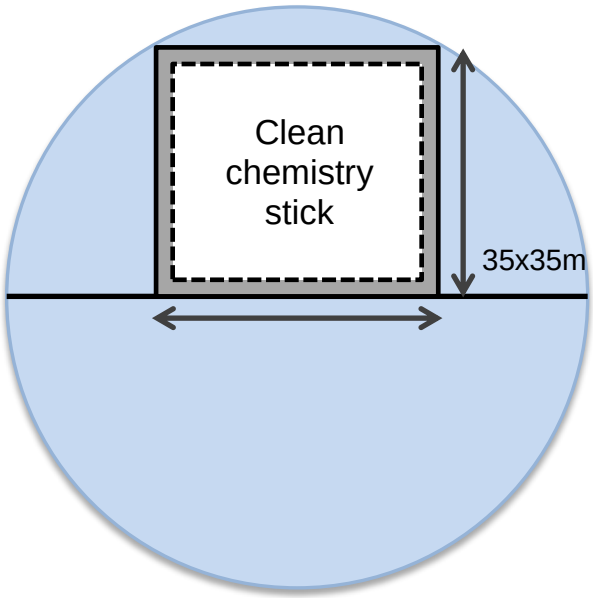

Figure 2.1 – Core cross section. An end-on view of a typical ice core cross section. The chemistry "stick" is taken from the central 35mm x 35mm section along the length of each core using a bandsaw. Grey shaded area is the 3-5mm of ice manually removed in the decontamination process using a microtome blade under a laminar flow bench, leaving the central clean portion. Each metre-long decontaminated stick is sampled into the desired resolution and placed in a sterile accuvette to be analysed.

Table 2.1 – Details of ice cores used in the Law Dome composite record.

Core Name	Location	Date Drilled	Period covered	Depth
DSS1213	66° 46’21”S 112° 48’19”E	2013	2012 - 1989	29 m
DSS97	66° 46’38”S 112° 48’41”E	1997	1988 - 1890	240 m
DSS99	66° 46’14”S 112° 48’25”E	2000	1889 - 1842	125 m
DSSmain	66° 46’11”S 112° 48’25”E	1988 - 1993	1841 CE - ~100 ka	1196 m

2.2.2 Sample resolution

The sampling resolution affects the data resolution obtained from the ice core. Choice of sampling resolution balances analysis time with desired data resolution and the practicalities of obtaining that resolution. For annual dating of an ice core using the chemistry record, the ice core must be sampled at sufficient resolution to resolve seasonality – usually 8-10 samples minimum per year. This presents a challenge where layers are thin due to low annual snowfall and flow thinning of ice layers as a certain sample volume is required for each analysis. With thinning layers, the ice must be sampled progressively more finely to maintain the 8-10 samples needed for identification of seasonality, leading to sample volumes too small for analysis.

At DSS a 50 mm sample resolution maintains an average of 12 samples per year (up to 60 samples per year in near-surface firn) for cores DSS1213, DSS99, DSS97 and DSSmain to a depth of 402 m (1300 CE). Beyond 402 m layer thinning due to ice flow required finer sampling to maintain an annual data resolution. The DSSmain core was sampled at 30 mm to a depth of 578 m (979 CE) then 25 mm to 852.668 m (333 BCE). Below this depth the sample sizes would have yielded insufficient volume for the discrete analysis techniques used to retain a clear annual resolution dataset. Larger sample sizes were used to give an annual or multi-annual resolution through the Holocene and earlier.

2.3 Trace ion analysis

Analysis of polar snow and ice faces a number of challenges, including low concentrations, small sample volumes and large sample numbers for high-resolution studies (Curran and Palmer, 2001). Ion chromatography (IC) methods have been widely applied to the measurement of trace ion concentrations in firn and ice with detection limits in the order of parts per billion (Buck et al., 1992; Curran and Palmer, 2001; Huber et al., 2001).

2.3.1 Law Dome trace ion analysis history

Previous studies of trace ion chemistry at the DSS site have used data from ice cores DSS99, DSS97 and part of DSSmain (e.g. Curran et al., 1998; Palmer et al., 2001). DSS99 and DSS97 were analysed using IC according to the methods of Curran and Palmer, (2001). DSSmain from 117 m to 401 m was analysed using the methods of Buck et al., (1992) at the University of New Hampshire prior to 2001. Sections of DSSmain from 401 – 819 m and 1006 – 1190 m were analysed using the methods of Curran and Palmer, (2001) during the intervening period. The gap between 819 – 1006 m (187 m of ice) was analysed in this study. This new data has been combined with existing data to present a full Holocene trace ion record from DSS for Cl^-, Na^+, SO_4^{2-} and MSA^-.

2.3.2 Ion chromatography methods for this work

Analysis of samples was conducted using suppressed ion chromatography methods modified from Curran and Palmer, (2001). The method used by Curran and Palmer was derived for a Dionex DX-500 IC using premixed sodium tetraborate (anion) and sulphuric acid (cation) eluents. Samples analysed in this study used a Dionex ICS-3000 IC with potassium hydroxide (anion) and MSA (cation) eluents supplied by automatic eluent generator cartridges. The IonPac AS14 separation column used by Curran and Palmer was replaced by an IonPac AS18 column. The use of eluent generator cartridges reduces the likelihood of eluent mixing errors or contamination, while the AS18 column gives better separation of MSA and chloride peaks (Roberts et al., 2009). Analysis runs were 21 minutes, which allowed adequate separation of MSA from interfering peaks and for sulphate to be eluted in a single analysis run. Capturing all ions of interest in a single run saves preparation and analysis time whilst making good use of limited sample volumes from ice cores. The analysis methods are summarised below.

2.3.2.1 Anion analysis method

Anions (MSA^-, Cl^-, NO_3^-, SO_4^{2-}) were eluted with potassium hydroxide (KOH) with a 3-stage concentration gradient. The initial concentration ramps from 5 mM to 23 mM from time 0 to 7.5 minutes, then is reduced to 15 mM by 9 minutes where it is held constant until 15 minutes, before further reduction to 5 mM by the end of the run (21 minutes). Flow rate was 0.420 ml/min. The sample volume was 5 ml, which was injected through a TAC-2 4 mm pre-concentrator column. Anions were separated by an IonPac AS18 guard and analytical column set before passing through an anion self-regenerating suppressor (ASRS-II) with a 16 mA current prior to measurement by the conductivity cell.

2.3.2.2 Cation analysis method

Cations (Na^+, Mg^{2+} and Ca^{2+}) were eluted with an MSA eluent at a concentration of 14.0 mM with a flow rate of 0.250 ml/min. Samples were injected from the automated sampler and stored in a 250 μL loop until 6 minutes when they were injected in to the separation columns. The cation species separated in 15 minutes with separation by IonPac CS12A guard and analytical columns. A cation self-regenerating suppressor (CSRS) with current set at 19 mA was used to increase sensitivity before the sample entered the conductivity detector cell. Although the run time was 15 minutes, only one sample is injected every 21 minutes to align the anion and cation systems.

2.3.3 Sample loading

Ice samples were thawed in their accuvettes 2-3 hours prior to analysis. Sample loading was performed under a laminar airflow hood, with all surfaces and equipment within pre-cleaned thoroughly with isopropyl alcohol and DI water (resistivity >18 Ω·cm) before use. Polyethylene gloves were worn at all times. A 6.2 mL aliquot was drawn off from each sample accuvette (including the blank ice samples) and transferred to IC vials, which were capped and placed in the automated sampler. Any samples with less than 6.2 mL in volume were diluted with DI water, and the dilution accounted for when calculating the final

concentration. A primary standard containing known concentrations of all ions of interest was diluted in to six working calibration standards. A full calibration was loaded at the start of each analysis sequence and approximately every 2 m of ice thereafter. A small calibration of one high and one low working standard were run between full sets. To assess contamination during the loading phase and ensure no carry-over, blank samples of DI water were also loaded before and after each standards set.

Following analysis, chromatographs were examined to make sure peaks were correctly identified and the peak area of each ion was recorded (example chromatograms in appendix A1). A calibration curve was derived from the working standards run by plotting the peak area against the known sample concentrations for each ion [Figure 2.2]. The equation for the line (slope and intercept) was used to calculate the concentration of the ice core samples. In the event of the instrument not fully injecting a sample, the remaining sample portion was weighed and a correction applied. Concentrations are expressed in this work as micro-equivalents per litre (μEq/L).

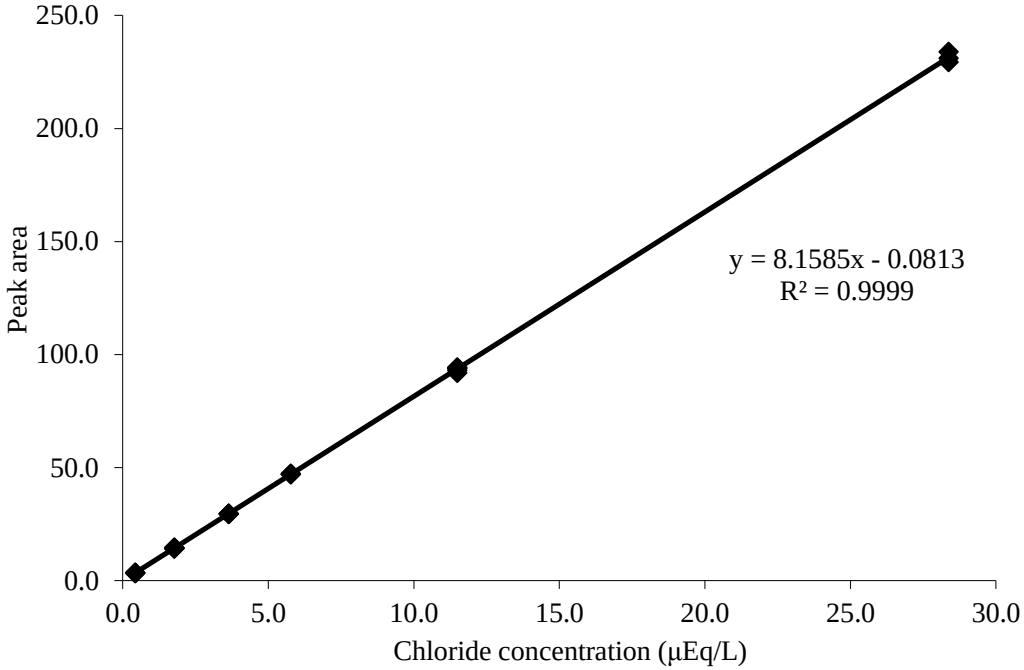

Figure 2.2 – Example calibration curve. This is an example calibration curve for the chloride ion. Each point represents the measured peak area of a working standard relative to its known concentration. By using the equation for the line, the peak values measured for each ice sample can be calculated as a concentration.

2.3.4 Calibration range and analytical limits

The range of the calibration curve for each ionic species is defined by the lowest and highest working standard concentrations and is shown in Table 2.2. Sample data is expected to fall within this range for each species. The lowest concentration standard is also the limit of quantitation (LoQ) which is defined as the lowest concentration at which the analyte can not only be reliably detected but at which some predefined goals for bias and imprecision are met (Armbruster and Pry, 2008). The LoQ chosen was half the mean annual low concentration for each species and lies well above the detection limits of the analysis method as defined by Curran and Palmer (2001). Unusual events (e.g. storm events, volcanic eruptions) may lead to some samples exceeding the upper bounds of the calibration curve. These values should be treated with caution, however the linear nature of the calibrations minimises the potential error introduced.

Table 2.2 – Detection limit and calibration range for ions used in this study.

Ionic Species	**MSA^-**	**Cl^-**	**NO_3^-**	**SO_4^{2-}**	**Na^+**	**Mg^{2+}**	**Ca^{2+}**
Detection Limit[1]	0.001	0.006	0.005	0.008	0.01	0.04	0.02
Lower Calibration	0.006	0.452	0.063	0.056	0.34	0.06	0.11
Upper Calibration	0.442	29.673	4.146	3.696	22.31	4.15	7.36
Range in DSS ice cores[2]	0.012-0.221	0.90-10.22	0.13-0.50	0.11-1.2	0.70-8.75	0.12-1.2	0.22-0.62

[1] – from Curran and Palmer (2001). [2] – Curran et al., (1998). Concentrations in μEq/L. Range determined from mean high and low concentrations for each species over 28 seasonal cycles.

2.4 Analysis results

A section of existing DSSmain ice from 818 to 1006 m has been analysed and the results are shown in Figure 2.3. This section is dated from 2,140 – 4,453 b2k (dating methods are covered in section 3.4). The data from this analysis has been used to compile the DSS Holocene chemistry record examined in chapter 4. Sample resolution decreased from 25 mm to 50 mm at 849.68 m to maintain sufficient sample volume. Analysis of this data forms part of Australian Antarctic Division project AAS 4061 HiREACH and the full dataset is available from the Australian Antarctic Division Datacentre.

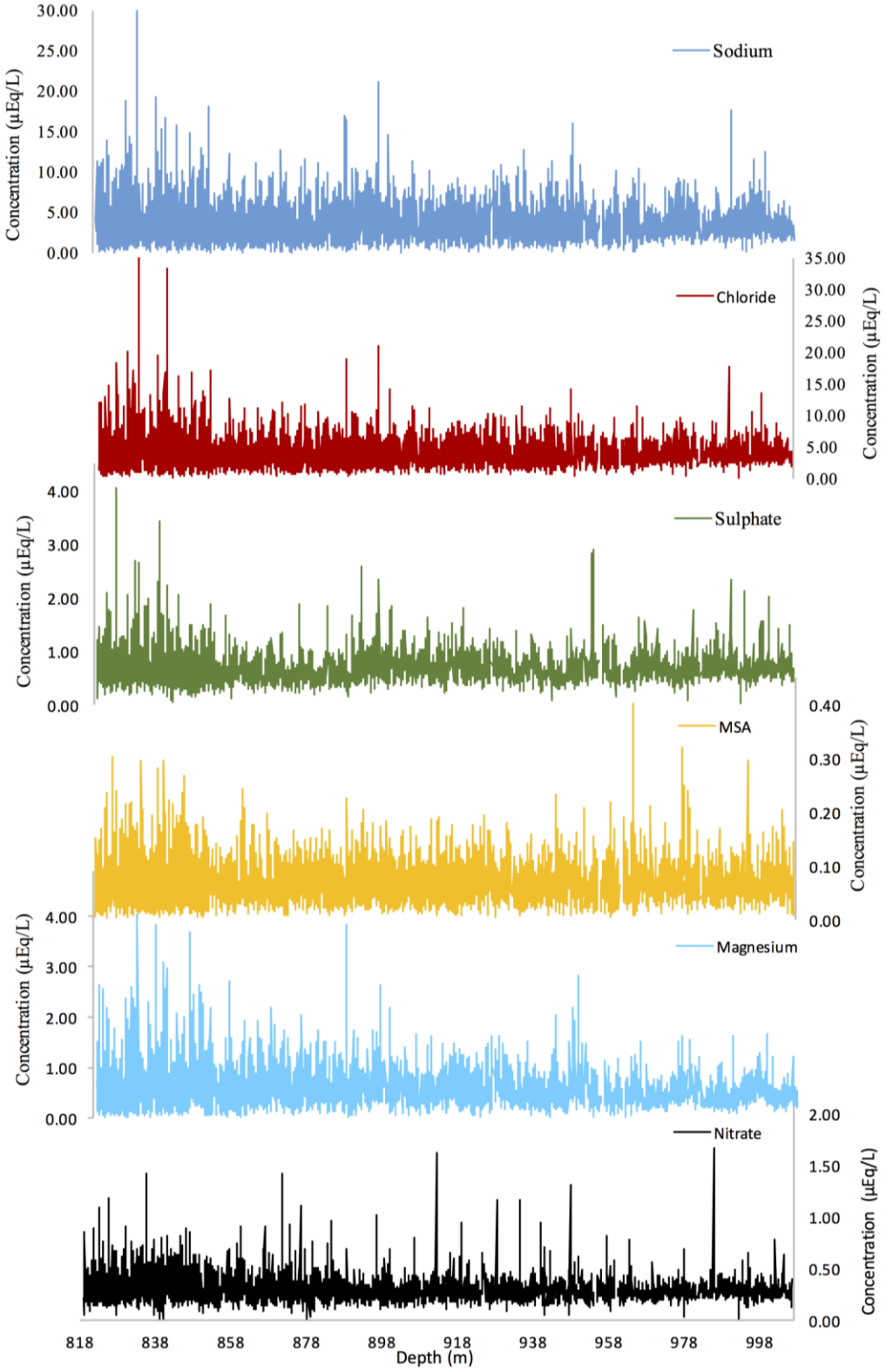

Figure 2.3 – Trace ion analysis acquired in this work. Depth in the DSSmain ice core. At 849.68 m depth sample resolution changed from 25 mm to 50 mm. Analysis covers the date range 2,140 – 4,453 b2k. Magnesium and nitrate were used to resolve annual layer counting ambiguities only and are not discussed in detail in this work.

2.4.1 Method comparison

Comparisons of earlier analysis methods of Curran & Palmer (2001) and Buck et al., (1994) were comprehensively discussed by Palmer (2002) showing there was no statistically significant difference between the two methods. To assess whether there are significant differences between the methods described in section 2.3.2 and those of Curran & Palmer (2001), a 4 m section of DSS ice was re-analysed. With the exception of MSA, mean values for the two datasets are within the uncertainty bounds of each other [Table 2.3]. MSA values are lower in the reanalysis due to time in storage. Uncertainty reported as the standard error of the mean.

Table 2.3 – Analysis methods comparison. The mean concentration (µEq/L) for ionic species across two analysis methods from 4 m of DSS ice. Analysis was performed using the methods described in this work (section 2.3.2) and the previously used methods of Curran & Palmer (2001). MSA concentrations are lower compared to previous analysis due to losses in storage.

Method	MSA	Cl^-	NO_3^-	SO_4^{2-}	Na^+	Mg^{2+}	Ca^{2+}
This work	0.06±0.01	4.59±0.51	0.28±0.02	0.72±0.05	4.26±0.42	0.92±0.11	0.24±0.06
Curran & Palmer	0.09±0.01	5.27±0.53	0.28±0.02	0.80±0.04	4.15±0.42	1.00±0.10	0.21±0.05

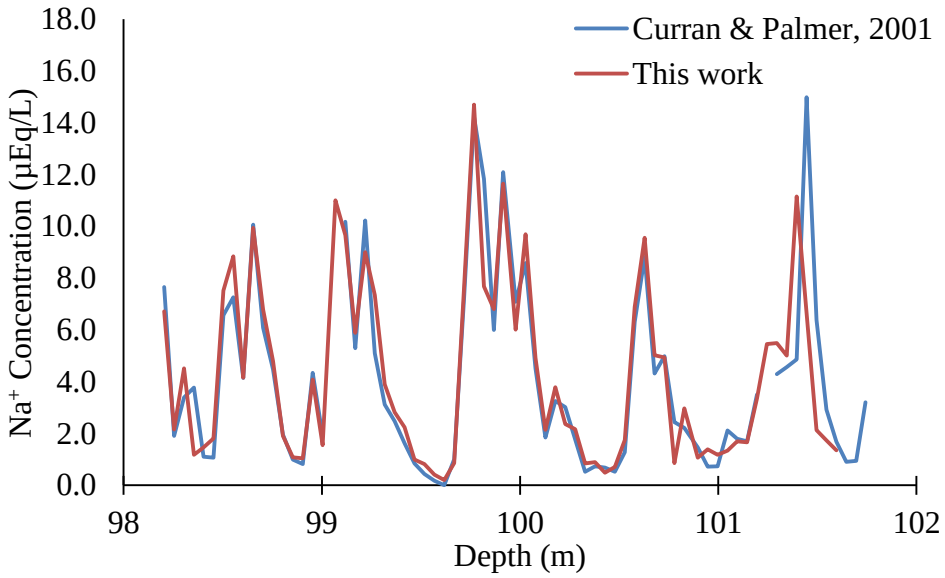

Figure 2.4 – Comparison of analytical methods.

2.4.2 Issues affecting magnesium and calcium analysis

The precipitation of magnesium and calcium hydroxides on suppressor membranes leads to a reduction in sensitivity for these species over the life of the suppressor. A loss of sensitivity is an issue because the lower calibration limit is close to the detection limit of these species [Table 2.2]. This issue was prevalent with earlier generation suppressors but has been substantially addressed with recent advances and techniques in suppressor regeneration. DSSmain analysis has spanned several generations of suppressor types that introduce greater uncertainty into the records of these species. Analysis of existing DSSmain ice has shown it to have been contaminated by calcium carbonate from storage in a concrete floored warehouse. Owing to these issues, the Holocene records of these two species will not be discussed in detail.

2.5 Isotope analysis

Existing oxygen isotope and deuterium data ($\delta^{18}O$ and δD respectively) from DSS ice cores was used in this study for the purposes of ice core dating (see Chapter 3 for details of dating) therefore a brief summary of the analysis method follows. Ice cores were sampled at 10 – 50 mm resolution. For $\delta^{18}O$ measurements, 0.4 mL subsamples were equilibrated with CO_2 at 25°C with a VG Isoprep-18 equilibration bench. The oxygen isotope ratio of equilibrated CO_2 was measured on a VG Isogas SIRA mass spectrometer at the Central Science Laboratory, University of Tasmania. The $\delta^{18}O$ values are expressed as per mil (‰) and relative to the Vienna Standard Mean Oceanic Water (VSMOW) standard. The standard deviation of $\delta^{18}O$ values for repeated measurements of laboratory reference water samples was less than 0.07 ‰. For δD measurements melted ice samples were analysed using a high-temperature elemental analyser (EA) interfaced with a continuous flow isotope ratio mass spectrometer (IRMS). Sample volumes of 0.3-0.5 µL were injected through a heated port and vaporised. For δD a reduction system was used, with the water vapour reacting with chromium powder in a quartz reaction tube at 1050°C to generate hydrogen gas. Under a helium carrier gas, reactant gases were separated through a gas chromatograph column before entering the IRMS. Three internal laboratory

standards were calibrated against International Atomic Energy Agency (IAEA) water standards VSMOW, Greenland Ice Sheet Precipitation (GISP) and Standard Light Antarctic Precipitation (SLAP). Measured isotope analysis results are reported relative to VSMOW. Internal laboratory standards were analysed periodically throughout sample analysis runs to calibrate the instrument. The known standards values were compared with the measured instrument values, and the equation describing this relationship used to calculate the ice sample values. The standard deviation of the δD values for repeated measurements of laboratory reference water samples was less than 0.5 ‰.

2.6 Hydrogen peroxide analysis

Previously analysed hydrogen peroxide (peroxide) data was used where available to assist the identification and dating of annual layers in Chapter 3. Analysis was made using a commercial diffraction grating type fluorescence detector and fluorimetric analysis method (van Ommen and Morgan, 1996). Discrete ice samples with a minimum 3 mL volume were melted and brought to room temperature immediately prior to analysis. The instrument was calibrated using standards of known concentration of hydrogen peroxide.

2.7 Conclusion

Previous chemistry analysis on Law Dome ice cores by Curran et al., (1998) and Palmer et al., (2001) has been built upon in this work. The 700 years of annually dated chemistry from Palmer et al., (2001) has been extended with new analysis to 333 BCE. The chemistry analysis methods have been updated to reflect new instruments and components to achieve a high quality chemistry record, with equal or better detection limits. Beyond the layer counted section new chemistry analysis on existing DSSmain ice has given a continuous chemistry record down to 4,453 b2k. Combining this new analysis with existing data a full Holocene record has been compiled from DSS for the first time.

Chapter 3 - Ice core dating

Ice core data is of little value if a reliable chronology is not first established. Well-dated records inform us about the timing of climate events and are essential when comparing data with other paleoclimate records.

Ice cores can be essentially dated by three methods:

- Counting of annual layers.
- Identifying distinctive reference horizons (i.e. volcanic eruptions or climate events) in the ice core and other independent well-dated records and transferring the date across to the ice core.
- Deriving a depth-age relationship by modelling of accumulation rates and ice flow patterns.

The method chosen will vary according the individual characteristics of the core such as depth, accumulation rate and data available. Usually these methods are used in conjunction; for example, layer counting is only possible in the upper part of an ice core; therefore a timescale derived from accumulation modelling is necessary to date the deeper ice. However, the accumulation rates determined from layer counting are essential for accurate modelling of deep ice. Reference horizons may be used to date records or check the dating error of a timescale. A discussion of the different dating methods will be followed by a detailed account of how the DSS record was dated.

3.1 Annual layer counting

Annual layer counting (ALC) represents the most accurate method to produce an ice core chronology (Winstrup et al., 2012). Annually varying physical and chemical properties of snowfall to the ice sheet result in a layering or stratification of the ice. By identifying the layers it is possible to derive a timescale by counting back from the top of the ice core. There are many seasonally varying parameters

that can be used to date an ice core and it is best practice to make use of multiple parameters to produce the most accurate and robust timescale.

3.1.1 Visual inspection

ALC by visual inspection of the ice is one of the most straightforward methods of dating an ice core. Owing to seasonal differences in atmospheric conditions (i.e. radiative fluxes, wind) summer snow deposits are coarser in texture than winter snow resulting in a visible seasonal banding which can be counted by trained observers (Alley et al., 1997b). Impurities in the ice like continental dust cause visibly cloudy layers to develop which also aid in counting (e.g. Svensson et al., 2008). ALC of visible layers has been employed in Antarctica (e.g. Taylor et al., 2004) and extensively in Greenland (e.g. Alley et al., 1997; Gow et al., 1997; Meese et al., 1997; Rasmussen et al., 2006).

3.1.2 Electrical properties of ice

The electrical properties of ice have been used to date ice cores both by ALC and use of reference horizons. Primarily two methods have been employed: DC electrical conductivity measurements (ECM) and dielectric profiling (DEP). Both methods have the advantage to be quick to deploy with a high resolution of 1-3 mm (Hammer, 1980; Moore, 1993; Moore and Maeno, 1991). ECM measures the DC conductivity of ice. The core is cut and two electrodes with a potential difference of 1000 - 2000 volts are dragged across a freshly cut surface. The resulting microampere current reflects the hydrogen ion [H^+] concentration in the ice (Hammer, 1980; Wolff et al., 1997). This makes ECM useful for detecting volcanic layers in ice. The DEP method measures an ice core's AC capacitance and conductance and responds to ammonium and Cl^- ions as well as acid [H^+] ions (Moore et al., 1992, 1989; Moore and Paren, 1987; Wolff et al., 1997), making it potentially useful for detecting seasonality as well as volcanic layers (Moore et al., 1992; Oerter et al., 2000).

ECM and DEP methods are easy to deploy and an ice core timescale can be quickly produced from the data. However, there are some potential issues with

electrical conductivity data that can affect the interpretation of the record; different operators, electrode setups, variable core geometries and changes in temperature all have the potential to affect results. However, if these are controlled repeatable, quantitative results can be obtained (Wolff et al., 1997).

3.1.3 Isotopes

The isotopic ratios of the stable isotopes of oxygen and hydrogen ($\delta^{18}O$ and δD) in an ice core vary in response to solar input (Dansgaard, 1964). Seasonal changes in solar energy input result in changes to the isotopic composition of precipitation. This is observed as a cyclical response within the isotope ratio signal of an ice core (see section 1.7 for more detail). This cyclical response is used to determine annual layers and has been used extensively to date ice cores by ALC (e.g. Cole-Dai et al., 1997; Ferris et al., 2011; Palmer et al., 2001; Sigl et al., 2013; Taylor et al., 2004; Vinther et al., 2006). Because isotopes can be related well to the summer temperature maximum at a site, the summer isotope peak can be a very accurate horizon (e.g. van Ommen and Morgan, 1997). Diffusion of the signal however results in gradual smoothing of the cycles with increasing depth, broadening the peaks and making dating more difficult.

3.1.4 Hydrogen peroxide

Although peroxide offers one of the clearest seasonal cycles, the peroxide signal suffers from the smoothing effects of diffusion like the water isotopes (Sigg and Neftel, 1988). Additionally, peroxide is sensitive to melt, photolytic breakdown and dust inputs that can destroy the peroxide signal (Neftel et al., 1986).

3.1.5 Trace ion chemistry

Seasonal variations in trace chemistry species have been used to define annual horizons in ice cores (e.g. Cole-Dai et al., 1997; Ferris et al., 2011; Palmer et al., 2001; Sigl et al., 2013; Taylor et al., 2004; Traufetter et al., 2004; Vinther et al., 2006). A wide variety of trace ions have been used for annual dating, but common

ionic species include Cl^-, Na^+, Mg^{2+}, Ca^{2+}, K^+ (sea salts), MSA, NO_3^-, SO_4^{2-} and NH_4^+. In addition to these measured species, calculated species $nssSO_4^{2-}$ and SO_4^{2-}/Cl^- ratio exhibit clear seasonal patterns that assist with dating.

Sea salts are at their highest concentrations during winter, which makes their signal useful for establishing evidence of a year cycle. We expect high concentrations of sea salts to interleave with the summer peaking species. At Law Dome the sea salt signal is associated with cyclonic systems over the Southern Ocean that cross Law Dome (Bromwich, 1988; Curran et al., 1998).

The MSA signal in ice cores has a well-defined peak during summer only during the upper most part of the core. The post-depositional movement of MSA precludes it being used to define the timing of summer at depth. However, as the peak remains well defined even after it has moved it is still useful for determining the presence or absence of a summer season. MSA deposition is usually out of phase with respect to sea salts; however MSA and sea salt co-deposition can occur in late spring and early autumn at Law Dome. This may represent occasional long-range transport events introducing MSA from mid-latitude sources rather than being sourced from melting sea ice (Curran et al., 2003).

The nitrate signal can be confusing to interpret due to post depositional changes, however it is a summer-peaking species and has been used to date records in conjunction with other chemistry species (e.g. Kreutz et al., 1997). Ammonium (NH_4^+) has an annual response that has been used to date ice cores (e.g. Rasmussen et al., 2006). The main natural, annually varying sources are wildfires and emissions from soil and vegetation and from bacterial decomposition of excreta, which increases during summer (Fuhrer et al., 1996). Ammonium was not measured at Law Dome.

The $nssSO_4^{2-}$ record is a calculated dataset that shows a strong seasonal cycle. It has well defined peaks that correspond to the summer increase in biogenic sulphate. The SO_4^{2-}/Cl^- ratio is also used to define seasonal cycles. Sulphate has many sources, however the two dominant sources are biogenic and seawater derived. The seawater-derived component is highest during winter, whilst the

biogenic peaks during the summer. Sea salt sulphate and chloride share the same source (seawater) therefore the ratio between these species remains relatively constant during winter. During summer, the dominant sulphate source changes from seawater derived to biogenic. The result is a large increase in the measured sulphate in summer without a chloride increase. This provides a clearly defined summer peak in the SO_4^{2-}/Cl^- ratio. During periods of volcanic activity the winter SO_4^{2-}/Cl^- ratio can be elevated but it is still lower than the summer peak. Together with $nssSO_4^{2-}$, isotopes and peroxide, it is one of the clearest summer indicators.

3.1.6 Annual Layer Counting challenges

ALC is subject to accumulating age uncertainty due to the presence of ambiguous annual layers. When layers are not clearly defined the potential for errors by misidentification of a year or missing a year cycle entirely increases. Factors giving rise to increasing uncertainty are reduced resolution, a single or few dating parameters used, or favouring an existing interpretation based on prior knowledge. Environmental factors such as variations in the amplitude of seasonal signals, post-depositional processes and changes in annual ice accumulation can lead to a confused and ambiguous signal in the record, making interpretation of annual layers difficult. The potential for error in identifying years can be mitigated and some ambiguities resolved by comparing a number of different seasonal markers rather than relying on one seasonal tracer.

Resolution is a significant factor in the interpretation of annual records. The ice core must be sampled at 8-12 samples per annual cycle or better to determine annual layers. At low accumulation sites ALC is not feasible because insufficient snowfall occurs to record and preserve the annual cycle; diffusion smooths annual signals and post-depositional processes disturb or completely remove some annual layers (Petit et al., 1982). Examples of Antarctic sites where ALC could not be performed include EPICA Dome C (2.84 cm yr^{-1}) Dome Fuji (2.99 cm yr^{-1}) and Vostok (2.00 cm yr^{-1}), (Parrenin et al., 2007; Petit et al., 1999), which are considerably lower than the 68 cm yr^{-1} annual accumulation recorded at DSS.

Ice masses are not stationary and the weight of the overlying ice mass compresses and displaces the layers outward [Figure 3.1]. This has the effect of stretching out or thinning the layers through plastic deformation of ice, therefore determining annual layers in ice becomes progressively more difficult with increasing depth. Areas with greater lateral ice flow speeds have a higher deformation and greater disturbance to the annual layering. Beyond the point at which annual layers cannot be reliably counted other methods must be used to produce a timescale.

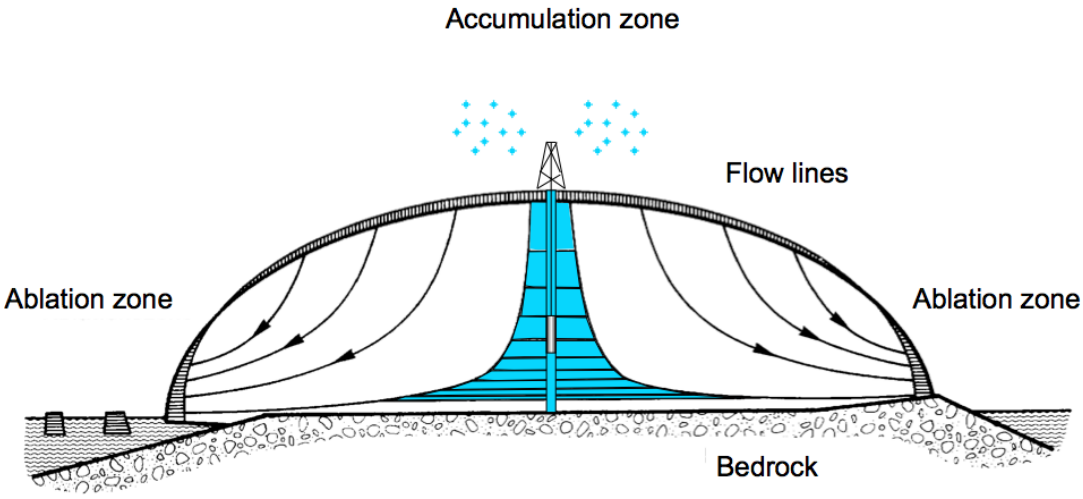

Figure 3.1 – Cross section of an ice sheet. Snow accumulates on a dome, and the weight of the overlying ice pushes downward and outward along the flow lines, stretching and thinning the deeper ice layers. Outward flowing ice mass is lost (ablated) at the margins due to melting or iceberg calving.

3.1.7 Importance of dating independence

An independently dated record is one dated without reference to external influences (e.g. reference horizons or prior knowledge of the date which a volcanic horizon is expected to lie). Independent records are important because they inform on the dating of events rather than the events informing on the dating of the ice core. A circular argument can occur when the date of a volcanic horizon is constrained by prior knowledge, then used as evidence for timescale accuracy. The Law Dome ice core record is an independent record during the layer counted period.

3.2 Reference horizons

Reference horizons (age ties or tie points) are a key component in ice core record dating and synthesis. Sudden, major climate and atmospheric perturbations can leave a distinctive imprint on climate records, including those of ice cores. Horizons identified in an ice core can be found in other dated, independent records (e.g. other ice cores, tree ring data, historical documents) which then allows the core to be dated absolutely. Absolutely dated horizons provide an opportunity to verify the accuracy of and give an estimate of dating error in the ice core chronology by comparing the expected date with the actual date of the modelling or layer counting (e.g. Sigl et al., 2015), and depth-age models may be adjusted based on the discrepancies. This is particularly useful in situations where ALC cannot be reliably performed to check and constrain age models based on accumulation estimates and flow thinning calculations. Additionally, accumulation estimates can be made for time periods between reference horizons, which can be factored into timescale reconstructions (e.g. Ren et al., 2010).

Another key aspect of reference horizons is that they can be used to provide a relatively dated record by synchronising records from different locations. Data from a single ice core is only representative of local or regional spatial scale; therefore it is often necessary for climate studies to bring together multiple records from the region of interest (Steig et al., 2005). Large volcanic eruptions are one of the most common reference horizons due to their abrupt signatures giving precise dating points. Volcanic events appear as sharp peaks in measured sulphate and/or ice core conductivity and have been used extensively to date and synchronise cores (e.g. Parrenin et al., 2012; Ruth et al., 2007; Severi et al., 2007; Sigl et al., 2013). However other distinctive events have also been used such as abrupt cooling at 8,150 b2k (e.g. Vinther et al., 2006), fallout from nuclear bomb tests (Steig et al., 2005) and radiometric ages (Aciego et al., 2011).

There are challenges to overcome before being able to use reference horizons for dating and synchronisation of records. Each horizon identified must be unambiguous across multiple ice cores or proxy climate records. It can take

considerable time and care to thoroughly validate each reference horizon to make certain the correct horizon has been identified across multiple records. This is particularly important with increasing age as the further back in time the fewer unambiguous reference horizons are available and the dating uncertainties attached to them are greater. Reference horizons also rely on the assumption that climate events occur and are recorded contemporaneously across regions.

3.3 Modelling

For the climate record of an ice core to be of use it must be dated. When ALC cannot be reliably employed, modelling of the ice sheet properties may be the only way to provide a timescale. The Dansgaard-Johnsen (1969) flow model was originally developed for Camp Century (Greenland) ice cores and has been widely applied to ice core timescales (e.g. Casey et al., 2014; Svensson et al., 2006; Takata et al., 2004; Veres et al., 2013). The model assumes that the vertical strain rate (rate of deformation of the ice) and lateral flow velocity are constant from the surface to a certain depth, beyond which it decreases at a linear rate with increasing depth to 0 at bedrock (Dansgaard and Johnsen, 1969). The lateral flow is derived from borehole measurements and studying the structure of the ice crystals in the ice core (e.g. Glen, 1955; Morgan et al., 1998). The Dansgaard-Johnsen model is a relatively simple way of producing an ice core timescale, however application of the model requires assumptions about the steady-state nature of the system. Variability in strain rate from changes in ice sheet geometry need to be understood and accounted for (Paterson, 1994). Changes in accumulation rate for example change the ice sheet mass balance and strain rates, therefore variability in accumulation rate through time is an important site factor to understand. Reference horizons can be used to check against the model output and inform on whether the steady state condition is satisfied. The bedrock topology is important to understand as zones of enhanced flow distortion and deformation in the ice around rough surfaces can complicate the dating (Morgan et al., 1997).

3.4 Dating of the DSS ice cores

The DSS record has been dated using a combination of annual layer counting, stratigraphic markers and accumulation modelling techniques to produce a single timescale. This chapter details how the DSS chronology through the Holocene was put together and is split into two sections – one detailing the annual layer counting and the other detailing the modelling based on accumulation estimates and stratigraphic tie points with other records. The ALC period uses calendar years denoted by CE or BCE for Common Era/Before the Common Era. For longer time periods the term "years before 2000 CE" (denoted by b2k) is used.

3.4.1 Annual Layer Counting at DSS

ALC at DSS between 1995 – 1300 CE was previously completed by Palmer et al., (2001). That work has been verified here by revisiting that layer counting, and expanded upon using newly acquired chemistry data from the existing DSSmain core and the recently drilled DSS1213 core. The layer counting presently covers the period 2012 CE – 333 BCE.

Years were defined based on seasonal variations in the chemical stratigraphy. Year horizons were defined using $\delta^{18}O$ records where possible. The $\delta^{18}O$ record has a peak that corresponds with the average local temperature maximum of January 10th (van Ommen and Morgan, 1997). The summer signal was verified using other summer-peaking indicators, primarily the $nssSO_4^{2-}$ and SO_4^{2-}/Cl^- ratio, though NO_3^- was also used. MSA was used to verify a summer cycle had occurred, but not for the timing due to its movement in the ice. The winter-peaking sea salt species were useful for determining that a winter cycle occurred between the summer-peaking species, and for determining whether peaks in the isotope records were associated with summer (i.e. low sea salts) or an intrusion of warm, moist air outside of summer (i.e. high sea salts and an isotope peak). A number of summer and winter species provide evidence for a year and having multiple lines of evidence increases the robustness of the dating scheme by reducing the number of ambiguous years within the record. Where no

isotope data was available, the nssSO_4^{2-} record was used to define the summer. In this study 2345 annual horizons were identified, starting with 2012 CE, and the oldest horizon dated 333+13/-7 BCE, corresponding to 852.668 m depth in the DSSmain core. The derivation of the error estimate and the ambiguous horizons are detailed in section 3.4.1.1.

The layer counting re-examined the existing published DSS record (Palmer et al., 2001) to assess the consistency of the identification and counting of annual year horizons. The identification of individual years was consistent with the existing DSS record and the dating in this study agreeing without error until 1818 CE. Dates previously published for the DSS record older than 1818 have a 1-year dating error due to a damaged section of core. This adjustment was made after synchronizing the $\delta^{18}O$ record of a new mid-length core retrieved from the DSS site in 2005 to the existing DSSmain ice core across the period in question.

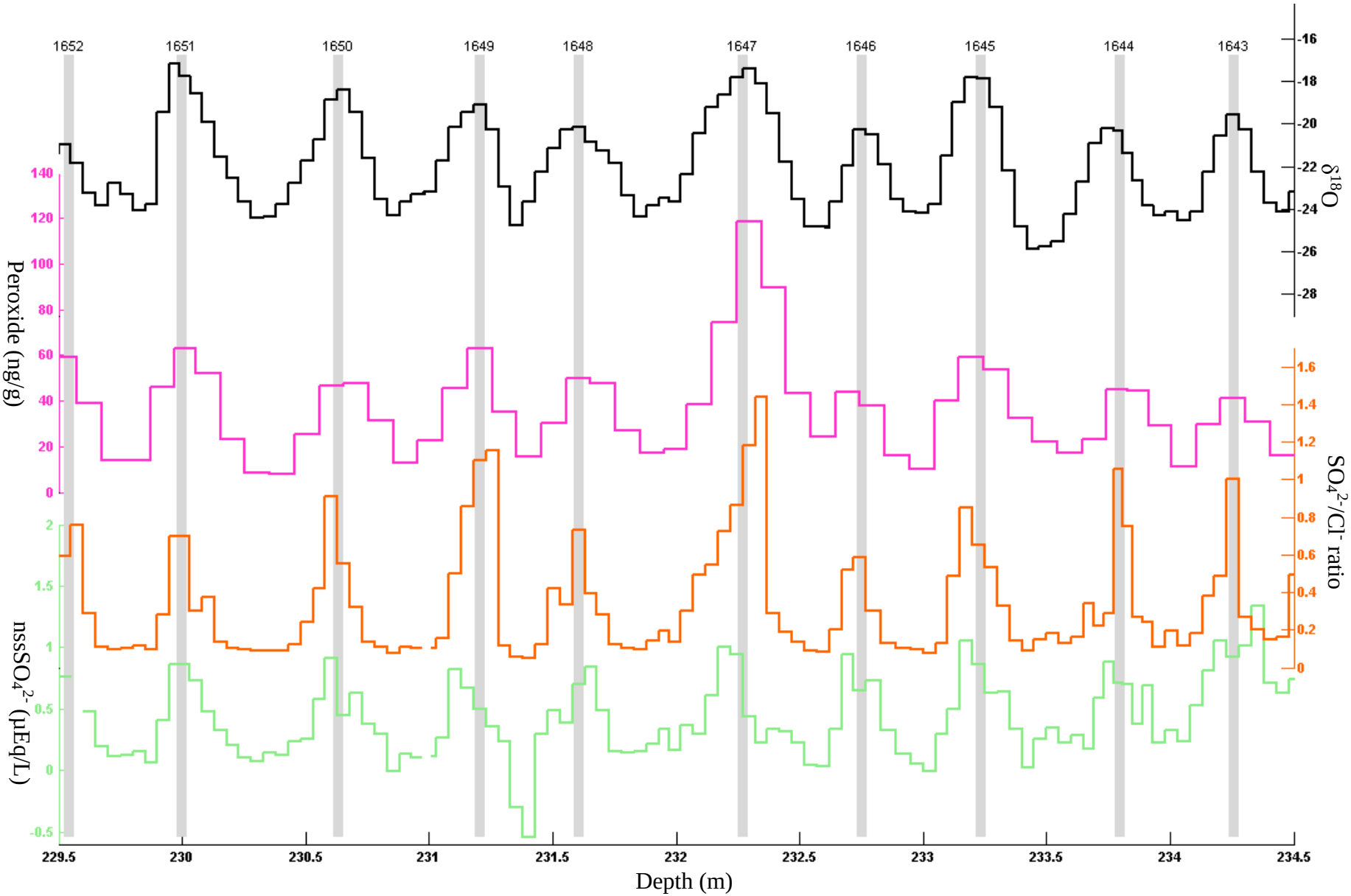

Figure 3.2a - Summer peaking chemistry. Seasonality in DSSmain. Grey bars mark summer horizons. Year CE above grey bar.

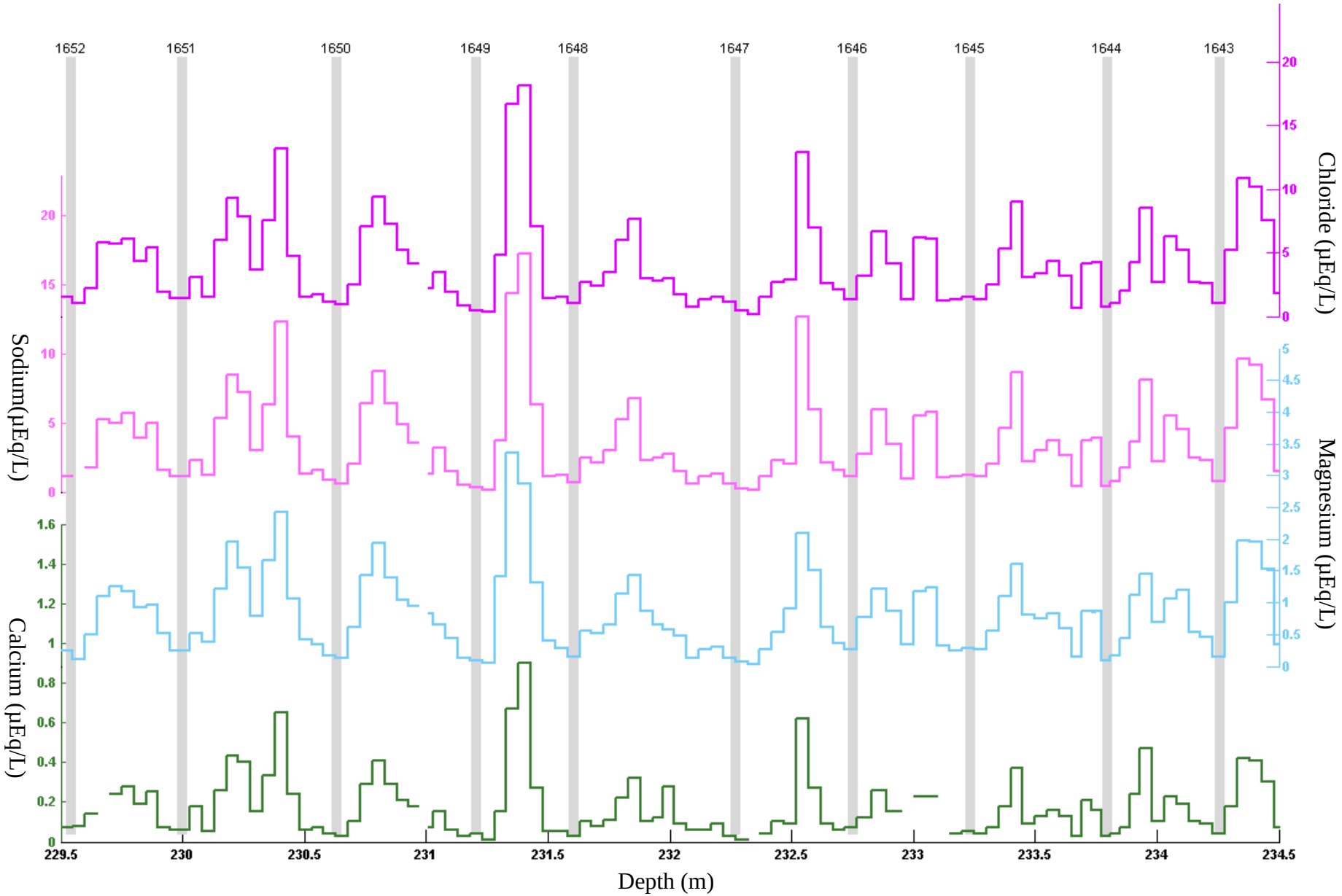

Figure 3.2b - Winter peaking chemistry. Seasonality in DSSMain. Grey bars mark summer horizons. Year CE above grey bar.

3.4.1.1 Uncertainties in the layer counted timescale

Not all ambiguities in the record could be resolved. The following is a list of ambiguous horizons in the DSS record and how they impact the error estimate of the record. Each ambiguous horizon adds +1 or -1 year to the cumulative error in the timescale depending on whether the horizon is counted or not counted, respectively. +1 – all horizons older than the ambiguous horizon are potentially 1 year younger than the timescale dates (i.e. a year was counted when it should not have been). Alternatively, -1 – all horizons older than the ambiguous horizon are potentially 1 year older than the timescale dates (i.e. years were missed).

1805 CE

1806 CE was considered an ambiguous horizon in dating of the Palmer et al., (2001) DSS record. There were signs of a summer/winter cycle in the trace chemistry record that was not supported by $\delta^{18}O$ data, thus it was not counted as a year, but led to an age error of -1 prior to 1806. The correction to dates prior 1818 CE from the Palmer et al., (2001) work makes this horizon now 1805 CE. Using data from another Law Dome ice core drilled subsequently this can be ruled out as a dating error. Peroxide data from that core through this section shows clear, unambiguous seasonal cycles that rule out the presence of a year, and thus there is no counting error. This data was not available at the time of publishing the 2000 year volcanic record (Plummer et al., 2012), therefore this represents an improvement to the error estimates in that work. It does not change the dates given for volcanic events.

1774 CE

The year 1774 was counted in this study and the previous work of Palmer et al., (2001) as 1775. Isotope data through this section has a clearly defined, but smaller amplitude peak than surrounding years. Peroxide data does have a peak, but it forms part of a shoulder with the preceding year so is not clear. Trace chemistry suggests this is a year as it has low chloride as expected in a summer, whilst summer markers SO_4^{2-}/Cl^- and $nssSO_4^{2-}$ have nicely defined peak. Therefore, this has been counted as a year, giving a dating error of 1774 +1.

717 – 716 CE

There was a slight shoulder to the $\delta^{18}O$ signal preceding the 716 horizon. The chemistry shows a small drop in chloride and a small rise in our summer markers corresponding with the $\delta^{18}O$. However, the chemistry suggests a small intrusion of a warmer air mass during winter rather than a year. The feature is isolated and small scale relative to the signature of surrounding years therefore this was not counted a year in the timescale, but counted as an uncertainty. The timescale error is a 717±1 at this point.

713 – 712 CE

This is similar to 717-716. Here, the $\delta^{18}O$ signal has a double peak before the 712 CE summer horizon. The term double peak is used to describe a period when two distinct peaks can be identified, but the drop between peaks doesn't return to the winter values surrounding it. The first peak has weak chemistry support for a year, and is likely a warm air intrusion. The second peak is clearly defined as a year by chemistry. The first $\delta^{18}O$ peak was not counted a year, but counted as an uncertainty. The timescale error is 712 +1/-2 at this point.

712 – 711 CE

There is a peak in $\delta^{18}O$ between these horizons. This is not supported as a year horizon by chloride or $nssSO_4^{2-}$ chemistry, but SO_4^{2-}/Cl^- does have a corresponding signal, therefore this was not counted a year, but counted as an uncertainty. The timescale error is 711 +1/-3 at this point.

589 – 588 CE

There is a double peak about the 588 CE horizon in $\delta^{18}O$. Sea salts concentrations associated with the first $\delta^{18}O$ peak are low. The sea salt concentration increased coinciding with a brief dip in $\delta^{18}O$ before returning to summer concentrations in time with the second $\delta^{18}O$ peak. The SO_4^{2-}/Cl^- ratio and $nssSO_4^{2-}$ records behave similarly, suggesting the start of summer coincides with the first $\delta^{18}O$ and a storm system may have moved across during the summer. This was not counted a year, but counted as an uncertainty. The timescale error is 588 +1/-4 at this point.

504 – 503 CE

There is a $\delta^{18}O$ peak between these two horizons. There is weak chemistry evidence supporting this as a summer horizon. A temporary drop in chloride concentrations, and a slight elevation of SO_4^{2-}/Cl^- ratio, however the $nssSO_4^{2-}$ signal shows no response consistent with a summer season. This was not counted as a year, but counted as an uncertainty. The timescale error is 503 +1/-5 at this point.

453 CE

The $\delta^{18}O$ peak between the surrounding horizons is closely spaced but distinct. The chemistry record is unclear, but suggests a year with a drop in chloride and peaks in SO_4^{2-}/Cl^- ratio and $nssSO_4^{2-}$ signal. These peaks are not clearly defined from the preceding year as they do not return completely to winter values. This was counted as a year horizon. The timescale error is 453 +2/-5 at this point.

338 – 337 CE

There is a small, but distinct $\delta^{18}O$ peak between these two horizons. Chloride and SO_4^{2-}/Cl^- ratio do not support a year, however the $nssSO_4^{2-}$ record does show a peak. This was not counted as a year, but counted as an uncertainty. The timescale error is 337 +2/-6 at this point.

299 CE

The $\delta^{18}O$ record has a small peak. The sea salt record and SO_4^{2-}/Cl^- ratio both show clear signs of a year, however the $nssSO_4^{2-}$ record does not. This was counted as a year. The timescale error is 299 +3/-6 at this point.

121 CE

No $\delta^{18}O$ data is available. Chemistry data is unclear. The chloride signal has a momentary spike (1 sample) but otherwise shows low concentrations consistent with summer. The SO_4^{2-}/Cl^- and $nssSO_4^{2-}$ records both show a small peak. Nitrate, which may also be used as a summer indicator, shows a peak. This was counted as a year. The timescale error is 121 CE +4/-6 at this point.

37 BCE

There is no $\delta^{18}O$ data available through this period. There is a small section of missing chemistry through this period, however the chemistry does appear to be starting to rise towards a summer value in the $nssSO_4^{2-}$ and nitrate records. The SO_4^{2-}/Cl^- ratio is unclear. The gap between horizons if no year were present during this period would be unusually large, but not implausible therefore it has been counted as a year. The timescale error is 37 BCE +5/-6 at this point.

47 BCE

There is no $\delta^{18}O$ data available through this period. The chemistry suggests a brief summer storm may have occurred bringing elevated sea salts. It is one sample and would suggest an unusually brief annual cycle if it were representative of a winter. Nitrate levels do not return to winter values. This has been counted as a year. The timescale error is 47 BCE +6/-6 at this point.

61 BCE

There is a small chemistry gap in this section. The $\delta^{18}O$ data clearly indicates the presence of a year. This has been counted as a year. The timescale error is 61 BCE +7/-6 at this point.

75 BCE

The chemistry in this section is unclear due to small gaps in the continuity, but it would be an unusually large year without a year between the 74 and 76 BCE horizons, therefore this has been counted as a year. The timescale error is 75 BCE +8/-6 at this point.

85 BCE

There is a chemistry gap across the likely summer of 84 BCE. The chemistry either side is indicative of winter with elevated sea salts and low summer markers. For this to be a winter it would be unusually long therefore a summer horizon was placed between the winters. The distance peak to peak between the 84 and 86 BCE horizons also suggests a likely year. The timescale error is 85 BCE +9/-6 at this point.

135 BCE

There is a gap in the cation chemistry record through the probable summer period. The summer horizon has been placed based peroxide measurements and average year spacing of the surrounding years. The timescale error is 135 BCE +9/-6 at this point.

207 and 208 BCE

These two horizons have been placed based on average spacing of surrounding horizons throughout a chemistry gap. The timescale error is 208 BCE +12/-6 at this point.

285 – 286 BCE

There is a shoulder peak in the isotope data between these two years. The isotope peak is associated with a rise in sea salts, which suggests this is a spring air mass intrusion. This was not counted as a year. The timescale error is 286 BCE +12/-7 at this point.

313 BCE

This summer horizon has been placed based on the average year spacing of the surrounding years. The timescale error is 313 BCE +13/-7 at this point.

3.4.2 Comparison with other layer-counted Antarctic timescales

There are presently only four Antarctic sites that have layer counted timescales beyond 1000 years; Law Dome (this study), West Antarctic Ice Sheet (WAIS) Divide (Sigl et al., 2013) Dronning Maud Land (DML) (Traufetter et al., 2004) and South Pole (Ferris et al., 2011). Ice cores capable of annual or sub-annual dating are crucial for understanding high-frequency climate modes (e.g. SAM, ENSO) beyond the instrumental period. With few long records the importance of each is heightened, and the spatial distribution (Figure 3.2) highlights how critical Law Dome is in representing the Indian Ocean sector of East Antarctica. The accuracy of the DSS record at the end of the ALC period is 333 BCE +13/-7 years which compares favourably with timescale errors reported for other cores at similar ages, summarised in Table 3.1.

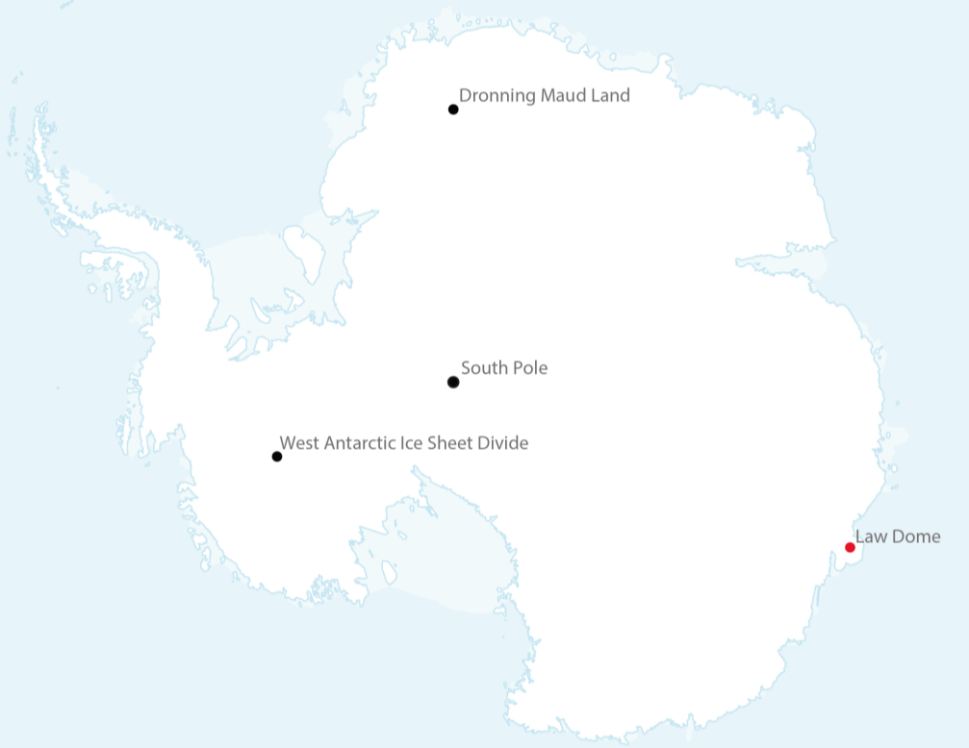

Figure 3.3 – Distribution of long layer counted Antarctic ice cores.

Sigl et al., (2015) have tested ice core chronologies with independent age markers. They compared two carbon-dated ^{14}C enrichment events in tree wood between 774-775 CE and 993-994 CE with beryllium-10 (^{10}Be) events recorded in ice cores. ^{10}Be is a proxy for solar activity and cosmic ray intensity (Bard et al., 2000; McCracken et al., 2004) and it is postulated that the cause of the ^{14}C enrichment produced an excess of ^{10}Be through interaction of high-energy particles with the atmosphere (Sigl et al., 2015). This independent test using data from Greenland (NGRIP and NEEM-2011-S1) and Antarctic (WAIS divide) found the ages of the ^{10}Be maxima are 768 CE revealing a 7-year offset in ice core chronologies ~1000 years and older. Whilst ^{10}Be measurements have not been made on the DSSmain core to identify this event, the close agreement with the WAIS Divide (Sigl et al., 2013) and NGRIP volcanic records suggests that the DSS timescale may be offset to a similar degree. Further evidence from tree ring dating using frost rings is also suggestive of an approximate 7 year offset in DSS, NGRIP, WDC06A and NEEM-2011-S1 dates from around 900 CE and older (Baillie and McAneney, 2015).

Table 3.1 – Timescale uncertainty at layer counted Antarctic sites.

Site	Dating
Law Dome (DSS)[1]	333 BCE +13/-7
WAIS divide (WDC06A)[2]	426 BCE ±12
DML (B32)[3]	165 CE ±25
South Pole (SP04)[4]	176 CE ±20

[1]This study. [2]Sigl et al., 2013. [3]Traufetter et al., 2004. [4]Ferris et al., 2011.

3.5 Modelling

The timescale beyond the 333 BCE was derived from a combination of layer counting and age ties to other Antarctic records, with ages interpolated between these using a Dansgaard-Johnsen flow model (van Ommen et al., 2004). Ties to other records were established through changes in methane concentrations, the relative changes in dust concentration and changes in the $\delta^{18}O$ records. Offsets between model age and ties were used to infer accumulation changes. The original timescale has subsequently been updated, benefitting from a longer layer counted record, the addition of volcanic tie constraints in the late Holocene and the 8,150 b2k methane event, and improved dating for the gas and dust ties previously used. Details on the volcanic, gas and dust ties through to the LGM follows.

3.5.1 Volcanic synchronisation

The DSS record was synchronised to the AICC2012 timescale by matching of the volcanic signatures identified in the SO_4^{2-} record through the late Holocene to the EPICA Dome C (EDC) EDC99 core DEP (Parrenin et al., 2012) on the AICC2012 timescale. The AICC2012 timescale is a multi-parameter, multi-site chronology developed from four Antarctic ice cores and is virtually identical to the layer counted GICC05 timescale for the last 60,200 years (Veres et al., 2013). Only volcanic events in the AICC2012 timescale were used to constrain the dating for the model. The full list of volcanic events identified beyond 23 BCE is listed in Appendix A2. Reliable matching of events was not possible during the early Holocene due to a discontinuous sulphate record from

poor DSS core quality; however further age constraints for the model were established from using perturbations in the gas and dust records from Law Dome.

3.5.2 Gas ties

The DSS ice core has been previously analysed for methane gas concentrations. Abrupt changes in methane concentrations recorded in the DSS methane record have been used as a further dating constraint for the age model. The abrupt Holocene methane event (discussed in section 1.12.2) has been used as a tie point during the Holocene. The DSS methane record was matched with the GISP2 methane record on the GICC05 timescale. Ice dates for the tie points are 8,178 and 8,270 b2k for the onset and termination respectively (Roberts et al., in prep.). Further methane perturbations associated with abrupt cooling during the Younger Dryas and Older Dryas stadials, and warming during the Bølling-Allerød interstadial and transitions between these climate events has been used to synchronise Law Dome to the GICC05 timescale (Pedro et al., 2011).

The accuracy of the methane gas synchronisation technique is limited by the offset between the age of the ice and the age at which the trapped gas bubbles in the ice core are sealed off from contact with the atmosphere during transformation from snow to ice – referred to as the Δage. Higher accumulation sites like Law Dome have more accurately constrained Δages than low accumulation sites because trapped gas bubbles are sealed off from the atmosphere more quickly (Pedro et al., 2011; Spahni et al., 2003). The gas Δage uncertainty attached to the timing of the Holocene methane event at Law Dome is 30 years, which is in addition to the event date uncertainty.

3.5.3 Dust ties

Large changes in dust concentration (measured by particle counts) have been used to synchronise DSS to other ice cores. Previous studies defined dust-age tie points at DSS by matching to the Byrd (Antarctica) ice core which was tied to the GRIP (Greenland) ice core for dating (van Ommen et al., 2004). Dust-age tie points have subsequently been updated by matching the DSS dust record

to the better resolved EDC dust record (Lambert et al., 2008) on the improved AICC2012 timescale.

Table 3.2 – Model tie points from the LGM to 2332 b2k.

DSS Depth (m)	Age (b2k)	Type	Timescale	Uncertainty (years)	Δage uncertainty (years)
852.69	2332	ALC	-	+13/-7	
868.16	2440	Volcanic	AICC2012	20	
949.32	3375	Volcanic	AICC2012	20	
951.98	3423	Volcanic	AICC2012	20	
952.60	3435	Volcanic	AICC2012	20	
966.49	3674	Volcanic	AICC2012	20	
970.31	3735	Volcanic	AICC2012	20	
987.43	4055	Volcanic	AICC2012	20	
1101.14[a]	8178	Methane	GICC05	30	31
1101.77[a]	8270	Methane	GICC05	30	30
1108.64[b]	9333	Isotope	GICC05	150	29
1121.29[b]	11,681	Methane	GICC05	75	33
1125.19[b]	12,819	Methane	GICC05	102	50
1129.04[b]	14,687	Methane	GICC05	30	43
1130.90[a]	16,630	Dust	AICC2012	328	
1132.22[a]	18,618	Dust	AICC2012	328	

[a] – Roberts et al., in prep. [b] – Matched in Pedro et al., 2011. Type refers to the climate feature matched – volcanic event, methane gas or isotopic changes, or signatures in dust concentration. The DSSmain record has been locked to either AICC2012 or GICC05 timescales.

3.6 Summary

The layer counted Law Dome DSS record is one of the most detailed and accurately dated Antarctic ice core records. The DSS ice cores have been layer counted to an age of 333 BCE with an error estimate of +13/-7, where the 333 BCE horizon may be a maximum of 13 years older or 7 years younger than the date reported. This gives an age range estimate for the 333 BCE horizon of 319-

340 BCE, corresponding to a depth of 852.688 m in the DSSmain ice core. Layer counting ceased at this depth because the ability to reliably distinguish annual cycles diminished.

The accurate annual dating of this record has been essential to the refinement of volcanic dating in the most recent 2000 years (chapter 5) which in turn refines modelling of the climate impact of volcanism during the same period by providing accurate dating and estimates of sulphur gas emissions that are responsible for climate forcing following eruptions. The dating has allowed the development of new millennial-length reconstructions of ENSO and South Eastern Australia rainfall patterns beyond the instrumental period (Tozer et al., 2015; Vance et al., 2015, 2013) as well as establishing an accurate accumulation history for Law Dome (Roberts et al., 2015) and has enabled Law Dome data to be contributed to a 2000 year Antarctic temperature reconstruction (PAGES 2k Consortium, 2013). Beyond the layer counting a timescale was developed using a Dansgaard-Johnsen flow model fit between tie points to investigate changes at the site in the Holocene.

Chapter 4 – Holocene trace ion chemistry records

The aim of this chapter is to investigate the influence of local and regional processes on the Law Dome DSS trace chemistry record for the Holocene. The chemistry records of sodium (sea salt), sulphate and MSA will be investigated together with accumulation data to establish timing and magnitude of changes in the DSS record. By comparing DSS with other Antarctic ice cores and data from marine sediment records it is possible to explore links between local (e.g. aerosol depositional regime changes, local ice sheet retreat) and regional features (e.g. sea surface temperature, sea ice presence).

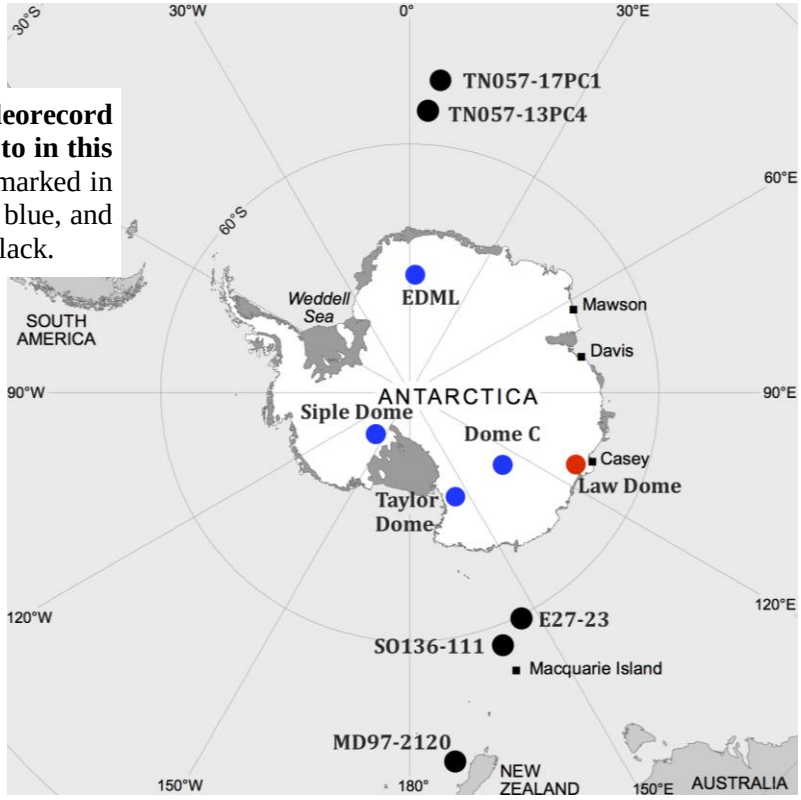

Figure 4.1 – Paleorecord locations referred to in this study. Law Dome marked in red, other ice cores blue, and sediment cores as black.

4.1 DSS trace chemistry records

The full Law Dome sea salt record is shown in Figure 4.2. The Holocene is highlighted in grey, defined in this study as 12,000 b2k to present, where b2k is years before 2000 CE. The apparent increase in sea salt concentrations during the late Holocene is partially a product of sample resolution. In the early Holocene, temporal resolution is approximately 20-30 years per sample, increasing to >20 samples per year at the top of the record. The seasonality associated with chemistry species tends to be smoothed with decreasing resolution. Therefore, all further data in this chapter will be presented as 100-year averages, which maintains a minimum of 3 samples per average.

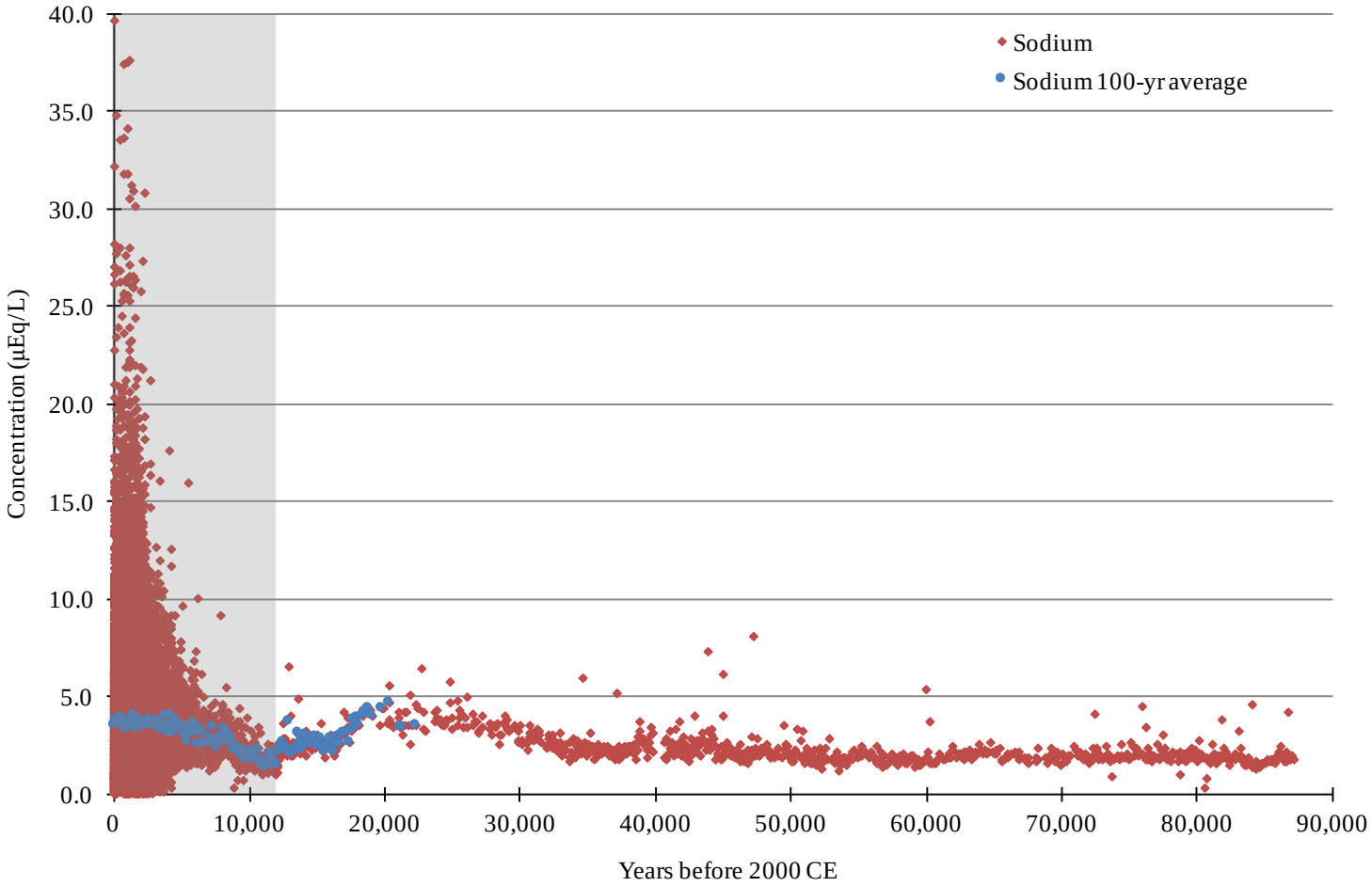

Figure 4.2 – Full DSS sodium record. Sodium concentration (µEq/L) record at full resolution (red) and 100-yr averages (blue), maintaining a minimum of 3 samples. Grey shading defines the Holocene (12,000 to present) which is the focus of this study. Oldest age is 87,212 b2k.

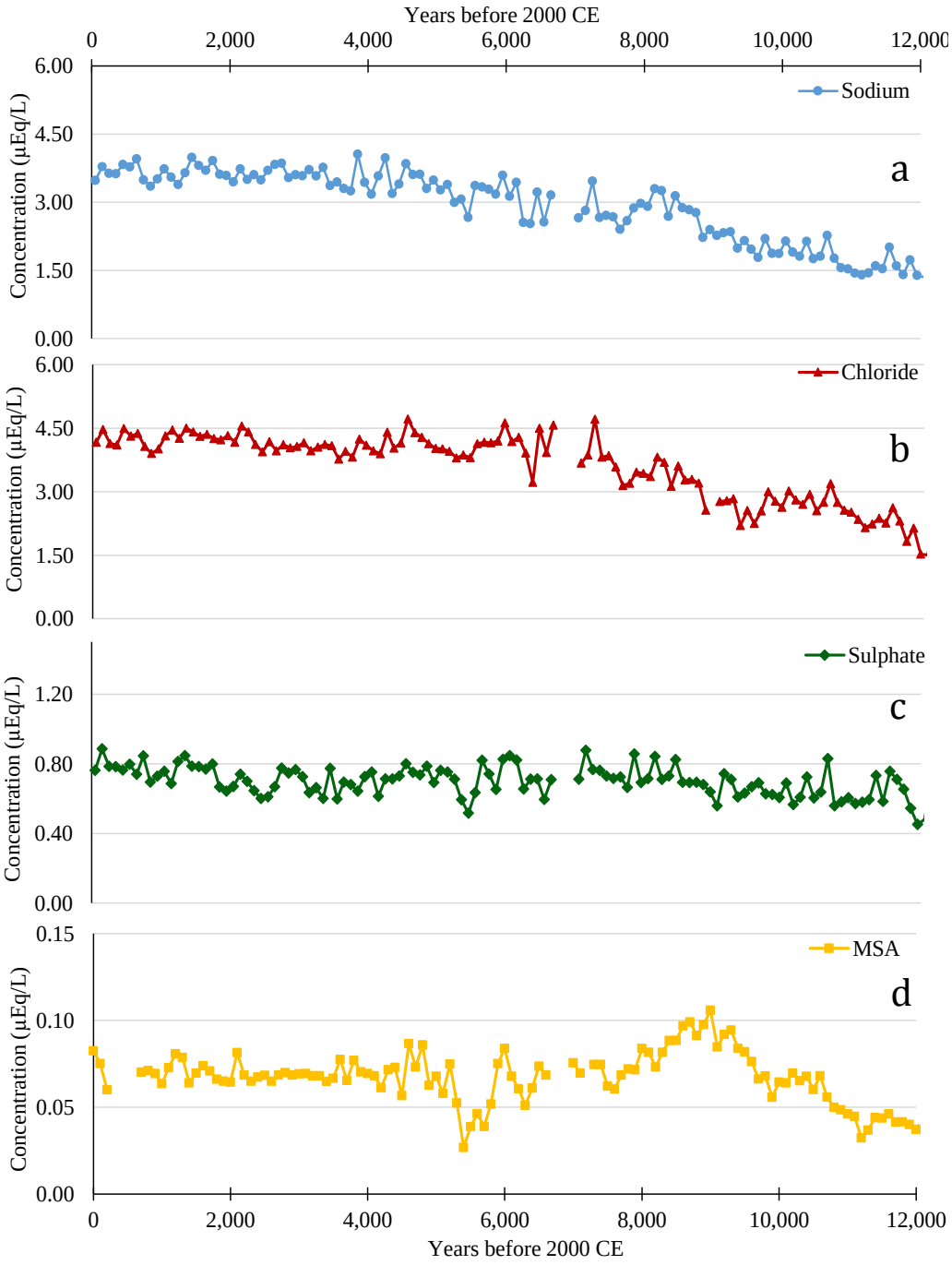

Figure 4.3 – DSS Holocene chemistry records. a) – Sodium, **b**) – Chloride, **c**) – Sulphate, **d**) – MSA. All species reported as concentrations in µEq/L and presented as 100-year averages.

4.2 Holocene sea salt and sulphate chemistry record

The chloride and sodium (sea salt) records co-vary with only small differences between the chemical species [Figure 4.3a, b]. Sodium concentrations range from 1.39±0.15 to 4.06±0.44 µEq/L and the mean Holocene concentration is 2.93 µEq/L. Chloride concentrations range from 1.53±0.14 to 4.55±0.43 µEq/L, and have a mean concentration of 3.55 µEq/L. The lowest concentrations for both species are at the beginning of the Holocene, while the highest values are recorded in the late Holocene. The mean Cl^-/Na^+ ratio for the Holocene is 1.21±0.06, close to the 28 year Cl^-/Na^+ ratio of 1.18±0.02 reported by Curran et al., (1998) and remains within error of the seawater ratio of 1.17 (Broecker and Peng, 1982) throughout the Holocene. Average concentrations of sulphate through the Holocene are shown in [Figure 4.3c]. The sulphate record has an average concentration of 0.70 µEq/L, and ranges from 0.45±0.05 to 0.89±0.06 µEq/L. The highest Holocene concentrations are from the modern era. Sulphate concentrations show only minor variation at the site throughout the Holocene, with a slight increase evident around 9,000 b2k. A more significant rise is seen from 3,250 b2k, where concentrations increase from 0.63±0.04 to the modern average 0.89 µEq/L (~40%).

4.2.1 Holocene MSA record

The record of MSA [Figure 4.3d] shows a 100% increase in concentrations between the early Holocene low and a peak concentration at 9,000 b2k. A stable Holocene pattern for MSA is established from 7,950 b2k to present, with the exception of the mid Holocene perturbation from 5,100 – 5,650 b2k. The lowest Holocene concentrations of MSA are recorded during this period at 5,250 b2k.

Interpretation of the MSA record is complex. MSA production is predicated on precursor species, most of which today is produced by a few key Antarctic algae species and therefore does not directly reflect changes in primary productivity (Saltzman et al., 2006). MSA is sensitive to post depositional movement and losses. The rate of atmospheric readmission of MSA from firn

decreases with increasing accumulation rate. At snow accumulation rates of 100 kg m^{-2} a^{-1} or greater post depositional loss is insignificant (Weller et al., 2004). Law Dome accumulation did not reach this threshold until ~14,612 b2k (van Ommen et al., 2004).

Formation of the relatively stable MSA occurs via oxidation of DMS by OH^- in the atmosphere and the yield of this reaction is inversely related to temperature (Arsene et al., 1999; Bates et al., 1992). Warmer temperatures and increased atmospheric moisture associated with the early Holocene optimum may have favoured MSA production leading to the peak observed in the record at 9,000 b2k, however the peak timing is approximately 660 years after the isotope maximum [Figure 4.4]. The MSA record from Siple Dome also has a delayed response to warming at the start of the Holocene, but the delay there was considerably longer, over several kiloyears (Saltzman et al., 2006).

An additional source of uncertainty is the stability of the MSA record in the ice core during storage. MSA is known to migrate from ice during storage (Roberts et al., 2009; Smith et al., 2004). Much of the deep DSS ice record has been stored without melt and re-freeze techniques being applied to preserve MSA. This limits the quantitative analysis that can be applied to the MSA record without further investigating the MSA storage effects, which is beyond the scope of this project. However, qualitative assessments of MSA changes can still be made.

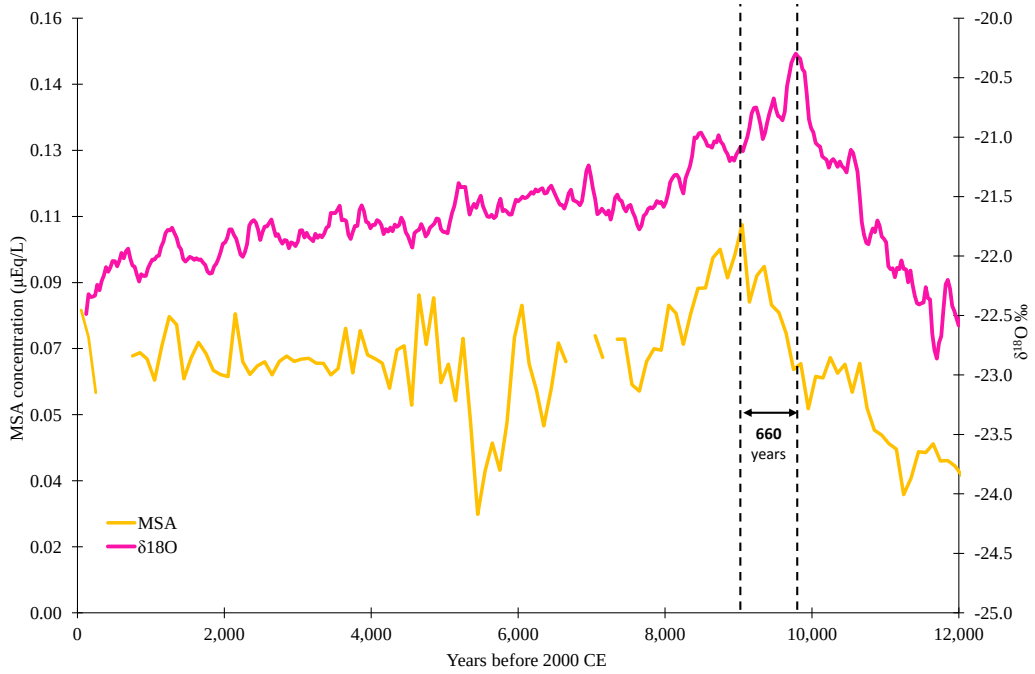

Figure 4.4 – The DSS MSA and isotope ($\delta^{18}O$) record for the Holocene. Data presented as 100 year averages. The dashed lines pass through the respective peaks. There is a 660-year offset between the atmospheric temperature optimum and MSA.

4.2.2 Continental dust input

To estimate the continental source of Ca^{2+}, which can be used as a proxy for continental dust, non-sea salt calcium ($nssCa^{2+}$) is calculated according to the following formula.

$$nssCa^{2+} = \frac{R_t}{R_t - R_m}(Ca^{2+} - R_m Na^{+}) \qquad \textbf{Equation 3}$$

R_m is 0.038 or the Ca^{2+}/Na^{+} sea water ratio, which is well defined globally, and $R_t \approx 1.78$, the average crustal ratio which varies depending upon source material, but has only minimal effect on $nssCa^{2+}$ calculation (Röthlisberger et al., 2002b). It should be noted that $nssCa^{2+}$ only represents part of the total dust content in the ice, with insoluble particulate dust also present, however $nssCa^{2+}$ is thought to essentially follow the same patterns as the insoluble dust record (Fischer et al., 2007b).

The $nssCa^{2+}$ record from Law Dome [Figure 4.5] shows similar features to other Antarctic records, with elevated dust levels at the LGM, and generally low concentrations throughout the Holocene. The DSS $nssCa^{2+}$ record is however highly variable due to the exceptionally low level of Ca^{2+} ions which were close

to the detection limits of the instrument. The record from 0 - 6,150 b2k has been affected by dust contamination from storage in a warehouse with a concrete floor, and is considered unrepresentative of Holocene dust at the site (see section 2.4.2 for further details). Average nssCa^{2+} concentrations during the period 12,000-6,150 b2k were low (0.10±0.02 µEq/L), in agreement with the generally low values reported in other Antarctic records throughout the Holocene (e.g. Fischer et al., 2007b; Lambert et al., 2012; Röthlisberger et al., 2002b). On account of the issues affecting the DSS Ca^{2+} record only, it will not be featured in further discussions.

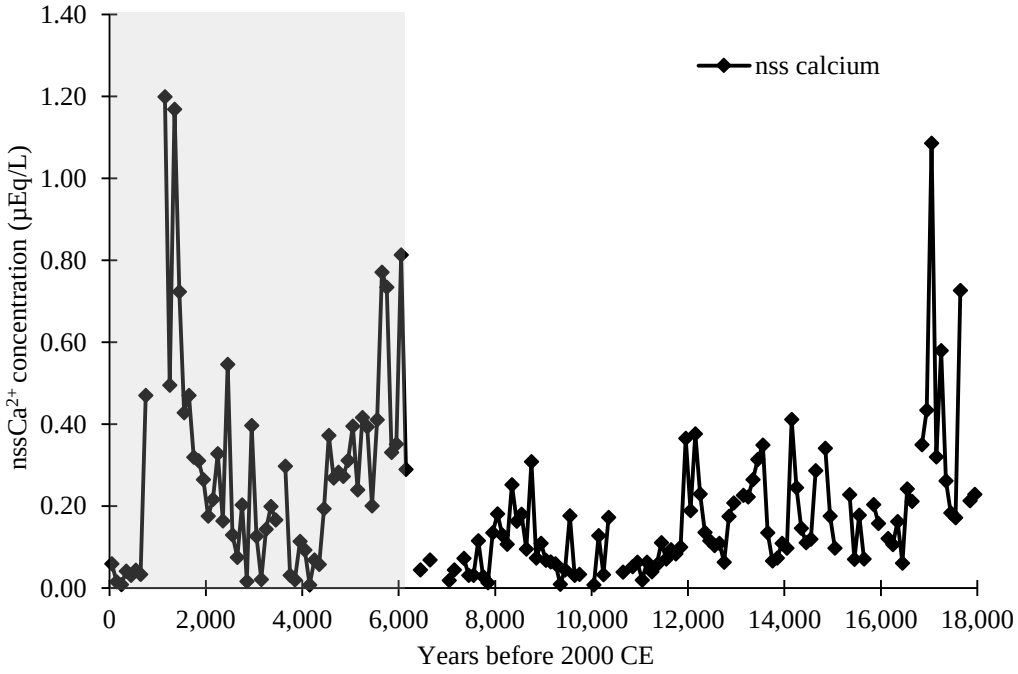

Figure 4.5 – The DSS nssCa^{2+} record. nssCa^{2+} concentration averages 0.55 µEq/L at the LGM (18,000 b2k), with average Holocene values of 0.1 µEq/L. The grey shaded area reflects calcium carbonate contamination from storage in a concrete floored building rather than changes to continental dust sources.

4.3 Consideration of flux versus concentration

The choice whether to use a concentration or flux for irreversibly deposited species is largely determined by the dominant mode of aerosol deposition. Low accumulation sites are dominated by dry deposition, while wet deposition dominates at high accumulation sites. Under a wet deposited regime, sea salt concentration changes are not expected to result from changes to snow

accumulation rate. Under a dry deposition regime concentration will vary with accumulation, leading to high concentrations under low accumulation scenarios such as the LGM that are not necessarily representative of source changes. As such a flux rather than a concentration in ice is expected to provide a better estimate of change to atmospheric chemistry loads (Legrand, 1987). Aerosol deposition fluxes are derived by multiplying ice core concentrations by the mean annual snow accumulation rate. A flux can be significantly affected by errors in accumulation estimates and is only closely related to the atmospheric aerosol load for chemistry dominated by dry deposition (Mayewski and Legrand, 1990; Udisti et al., 2004). A concentration however is a precise measurement of the chemical constituent of the ice, therefore a concentration is a better choice for wet-deposited sites. The required snow accumulation necessary for wet deposition to be the dominant mode is debated, however Wolff et al., (2006) suggest that at 0.109 ma^{-1} ice equivalent or greater, wet deposition dominates.

4.4 Law Dome depositional regime

Under today's climate regime DSS has a high accumulation rate (0.687 ma^{-1} ice equivalent) where sea salts are essentially wet deposited (Roberts et al., 2015; van Ommen et al., 2004). Law Dome has an east-west snow accumulation gradient (Morgan et al., 1997). The DE08 ice core 8 km east of DSS has an accumulation of 1.2 ma^{-1} ice equivalent, while core w10k is 10 km west of DSS and has an accumulation rate of 0.42 ma^{-1} ice equivalent. There is no detectable change in mean annual sea salt concentrations with varying accumulation rate across Law Dome in ice cores (Plummer, 2009). The DSS snow accumulation rate beyond the layer counted period is estimated at tie points used in the construction of the timescale. The LGM accumulation rate is estimated at 0.050 ma^{-1} ice equivalent with a possible error of 50-200% (van Ommen et al., 2004). DSS snow accumulation increased steadily through the deglaciation period reaching 0.244 ma^{-1} ice equivalent in the early Holocene. A rapid increase in snow accumulation between 12,000 and ~7,000 b2k is observed (180% increase), by which time the present day mean accumulation rate of 0.687 ma^{-1} ice equivalent was reached.

From the LGM to 12,000 b2k the concentration of sea salts decreased with increasing accumulation [Figure 4.6], indicative of a dry-deposition dominated system. At 12,000 b2k the lowest 100-year mean sea salt concentrations in the entire record (1.35 μEq/L) are reported before increasing. The 0.244 ma^{-1} ice equivalent accumulation rate exceeds the threshold suggested by Wolff et al., (2006) for wet deposition dominance. The sodium flux record for DSS [Figure 4.7] increases from with the concentration increase from 12,000 b2k, suggesting that contribution of wet deposition is increasing at DSS, but does not become dominant until between 7,000 and 10,000 b2k. The DSS accumulation record has only been estimated between discrete tie points used in the timescale reconstruction, therefore large uncertainties exist on timing of this change. Estimating accumulation rate from the relationship between temperature and saturation vapour pressure – where it is assumed that accumulation rate at the time of deposition varies with saturation vapour pressure – works well for inland sites dominated by diamond dust precipitation, but not at coastal sites where there is a transport limit on accumulation rather a thermodynamic one (Steig et al., 2000; van Ommen et al., 2004).

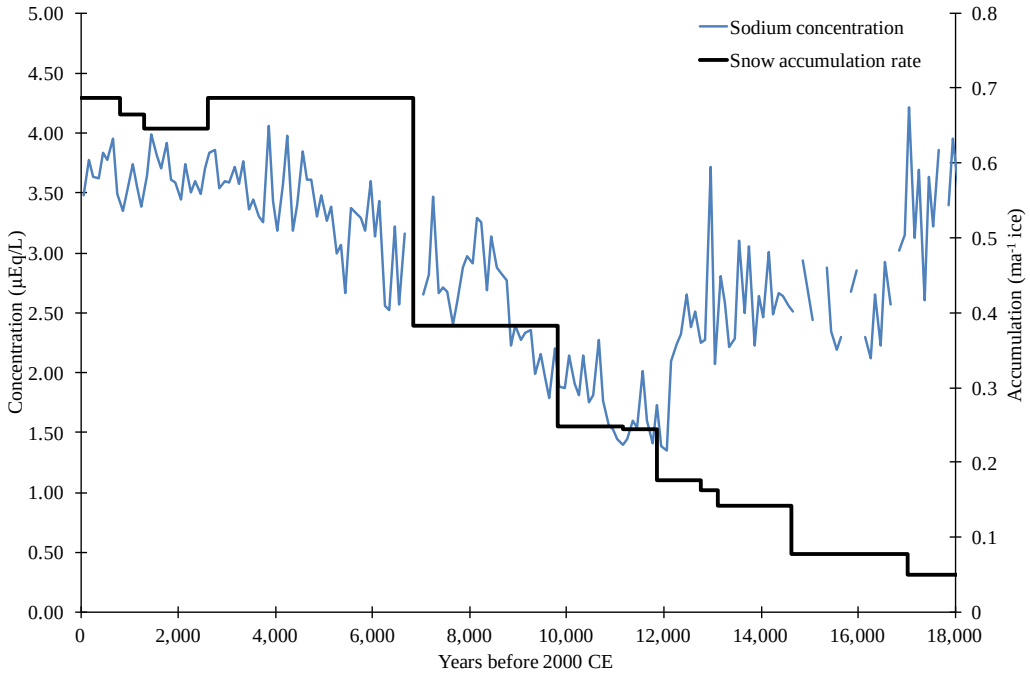

Figure 4.6 – DSS Sodium concentration and snow accumulation rate for the since the LGM. Na^+ concentration in blue, and the black line is estimated annual accumulation rate in metres of ice. The accumulation rate is estimated only at discrete points in the Holocene, leading to a stepwise pattern in the accumulation record (van Ommen et al., 2004).

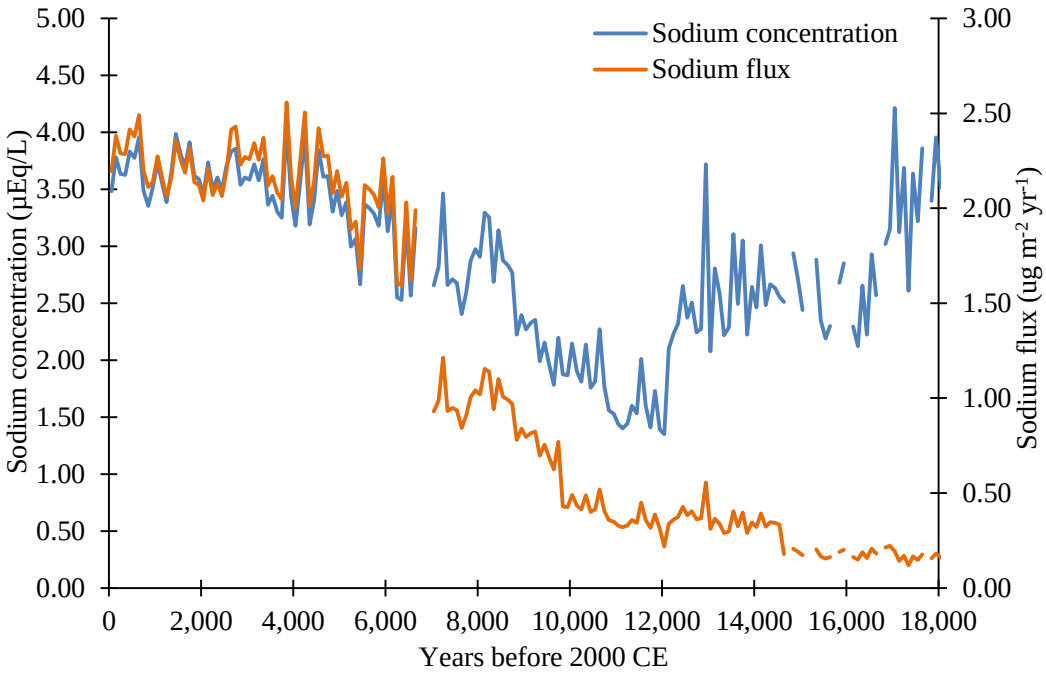

Figure 4.7 – Sodium concentration and flux records for DSS since the LGM. The use of a flux record accounts for the rise in measured concentrations due to changes in snow accumulation rate. The snow accumulation record at DSS is estimated from tie points used to construct the DSS chronology and hence the stepped nature of the record. The change at approximately 7,000 b2k is exaggerated by the step change in accumulation rate.

4.5 Regional comparison of sea salt concentrations

To examine regional changes in aerosol deposition, the sodium records of EPICA Dome C (EDC) (Wolff et al., 2006) EPICA Dronning Maud Land (EDML) and DSS sites are compared. EDC is located approximately 1000 km inland from Law Dome on the polar plateau at 3,233 m elevation. The EDML ice core was drilled at Kohnen Station in the interior of Dronning Maud Land, at 2,882 m elevation (Fischer et al., 2007a). Comparison of EDC and DSS [Figure 4.8a] show some clear similarities, particularly from the LGM to beginning of the Holocene. Concentrations at the LGM were similar at both sites, however EDC has a more marked decline in concentrations in the late termination. Concentrations at DSS increase 25% between 12,000 and 9,000 b2k. EDC concentrations change less than 2%. This pattern of change is also evident at EDML [Figure 4.8b]. Both the inland records show the abrupt increase observed in DSS between 9,000 and 8,000 b2k – 38% at DSS, 30% at EDC and EDML (shaded area, Figure 4.8). After this time, DSS continues to increase, with present

concentration levels reached at 5,000 b2k, representing a 117% increase from 12,000 b2k. The two inland sites show little difference, or a decline at EDML in the mid Holocene. From 3,000 b2k the two inland sites record concentration increases of approximately 20%. The increase in sea salts observed at DSS between 12 – 9,000 b2k was not evident at the inland locations, inferring a local control at DSS. Law Dome was up to 40 km further inland relative to the coast at the LGM, however was believed to have reached its present configuration by around 8,000 b2k (Goodwin and Zweck, 2000). A 40 km relative change to Law Dome is unlikely to have significantly affected sea salt deposition at either EDC or EDML, but could have significant ramifications for the coastal Law Dome.

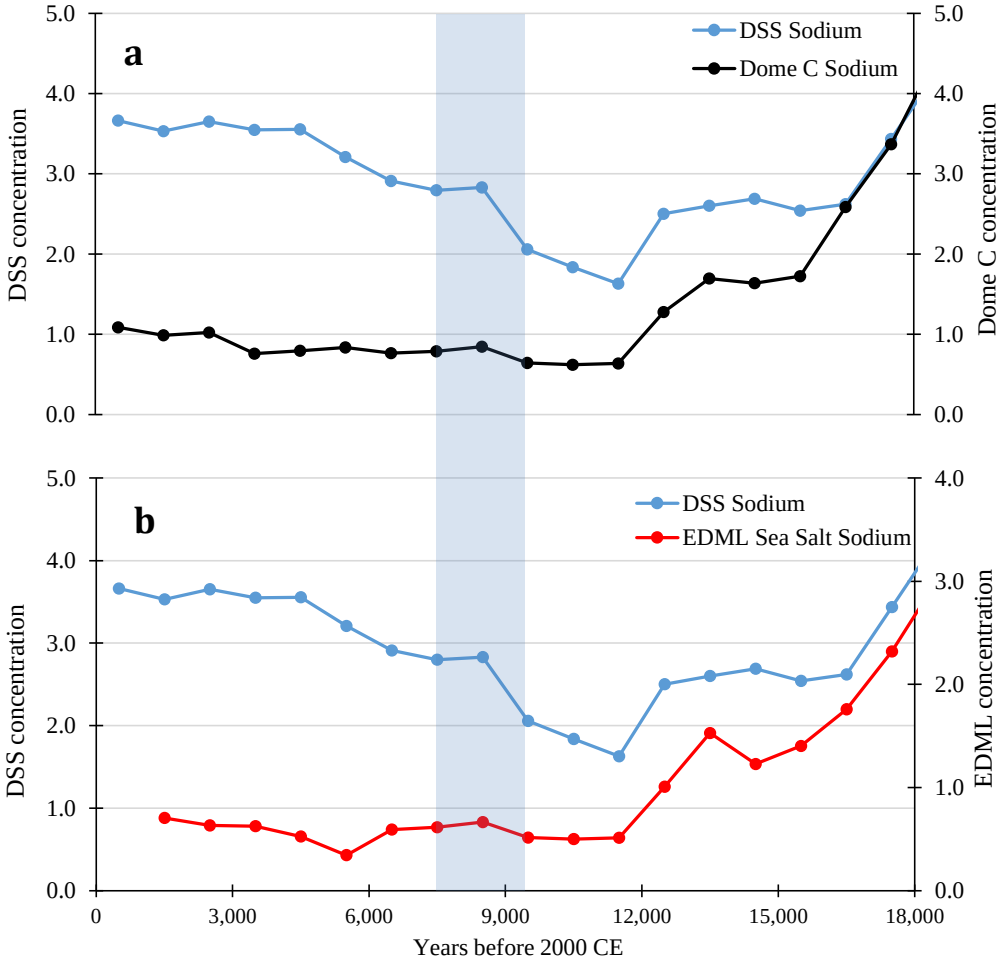

Figure 4.8 – Law Dome compared with EDC sodium (a) and EDML (b) sea salt sodium records. Concentration (µEq/L) data presented on millennial scale for clarity. All sites display similar a pattern pre-Holocene. DSS increases in concentration by 25% and the two inland sites do not from 12-9,000 b2k. This is attributed to local changes to Law Dome. The increase from 9,500-5,000 b2k is potentially the effect of changes to the southern westerly wind belt or cyclonicity affecting coastal DSS more than inland sites. Blue shading 7,500 – 9,500 b2k highlights the abrupt increase apparent across all three sites.

4.6 Changes in transport mechanisms

Sea salt aerosol formation is closely linked to cyclonic activity, where higher surface wind speeds allow for more efficient sea salt aerosol formation. Sea salt aerosols are transported and mainly wet deposited along the storm track (Fischer, 2004; Fischer and Mieding, 2005). Therefore, sea salt and snow deposition are linked to the frequency of cyclonic activity and their ability to cross the coast. DSS sea salt deposition under present day conditions is strongly linked to the strength of the Antarctic High, and its influence on the latitudinal position of the storms in the circumpolar trough. When the Antarctic High is stronger, cyclones track north of the ice edge over open water, increasing DSS sea salt loads (Souney et al., 2002). Long-term trends in sea salts may respond to other factors such as cyclonic frequency and intensity, mean position of the storm track and how far inland they are able to penetrate.

Global circulation models have been used to investigate cyclonic activity at the LGM (Genthon & Krinner, 1998), suggesting a reduction in cyclonic activity around east Antarctica, with the greatest reduction off the Wilkes Land and Terre Adelie coasts (up to 50%). They also reported an average mean sea level pressure (MSLP) rise around Antarctica at the same time, indicative of a less active circumpolar trough, which could decrease the intrusion of marine air masses inland. PMIP2 simulations of Holocene climate using 5 coupled ocean-atmosphere models support a weakened circumpolar trough at the LGM, accompanied by a weaker Southern Annular Mode (SAM) signal (Kim et al., 2014). A coupled atmosphere-ocean-sea ice model forced primarily by insolation changes identified similar trends, where the circumpolar trough strengthened from 9,000 b2k, accompanied by a small increase in westerly wind speeds (Renssen et al., 2005). This offers a mechanism through which increased aerosols and precipitation may be delivered to Law Dome. Changes in the relative position and strength of the mean zonal wind band across the Southern Ocean are also expected to impact aerosol transport and deposition.

Curran et al. (1998) suggested sea salt aerosols at DSS may be sourced from the Southern Ocean between Macquarie Island and DSS. A relationship

between Macquarie Island winds and DSS sea salts might indicate a Holocene shift in wind patterns. The time-averaged (100 years) DSS record has been correlated with mean zonal wind anomalies over Macquarie Island (54°S). The correlations are made using a Gaussian kernel method with bootstrapping resampling to derive the probability density function and uncertainty bounds [upper and lower bounds in brackets] at the 95% confidence limit (Roberts et al., 2016). This technique does not require the datasets to be matched pairs on the same timescale. The correlation shows a moderate inverse trend (r= -0.66 [-0.78 : -0.62]) with Law Dome sea salts (i.e. higher wind speed over Macquarie Island results in lower sea salts and vice versa) [Figure 4.9]. The inverse nature may be explained by sea salts being sourced over the open ocean between Law Dome and Macquarie Island (as proposed by Curran et al., 1998) where stronger winds over Macquarie Island are likely associated with a more northern southern westerly wind (SWW) belt. There is evidence of southward displacement and increased speed of the mean zonal SWW from proxy records from Campbell Island, south of New Zealand (McGlone et al., 2010) and Chile (e.g. Lamy et al., 2010) and CO_2 records in the Southern Ocean, with wind driven upwelling concurrent with rising CO_2 levels in the Holocene (Anderson et al., 2009; Hodgson and Sime, 2010).

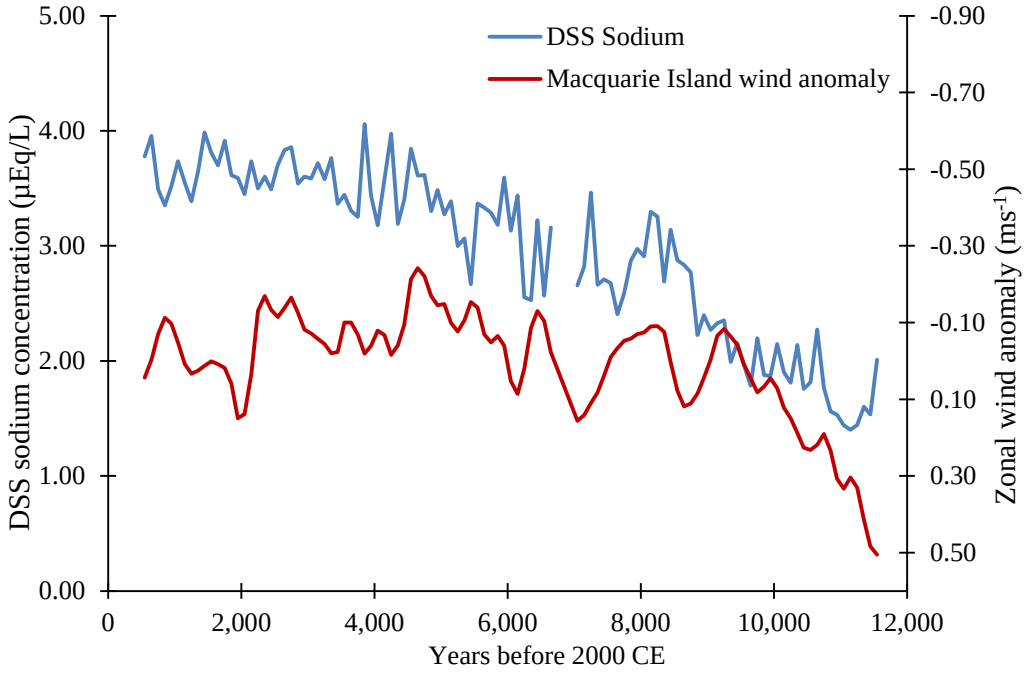

Figure 4.9 – Macquarie Island wind anomaly and sea salts. The DSS sea salt record has been compared with CCSM3 reconstructions of Holocene surface wind anomaly over Macquarie Island. Anomaly calculated with respect to the last 500 years and shown on an inverted axis.

The role of sea ice also needs to be considered since winter sea ice was greatly expanded at the LGM. Souney et al., (2002) found increased DSS sea salt concentrations were associated with displacement of the circumpolar trough north of the sea ice margin. A reduction in sea ice extent increases the amount of open water as a sea salt source to DSS. The modern sea ice edge is a region of enhanced cyclogenesis as a zone of increased baroclinic instability driven by meridional air temperature gradients and radiation balance (Schlosser et al., 2011). The centre of cyclogenesis may have moved closer to the coast with contracting sea ice extent in the early Holocene. However, relationships between cyclonic activity and the sea ice are uncertain over long time scales (Simmonds, 1996).

DSS was a mainly dry depositional site at the LGM until 12,000 b2k. During the transition, snow accumulation increased in association with increasing atmospheric moisture. From 12,000 b2k DSS appears to be under increasing wet depositional dominance based on sea salt concentrations increasing with rising accumulation rate. Comparisons with inland ice core sites EDC and EDML suggest they co-varied until 12,000 b2k. Between 12,000 and 9,000 b2k, local changes in Law Dome structure through ice sheet retreat likely influenced the DSS sea salt records through changes in distance to source. The 30% increase in sea salt concentrations recorded at EDC, EDML and DSS between 9-8,000 b2k appears to represent a regional feature, which may be associated with increased air mass intrusions inland. The ability for cyclones to move inland has been related to the strength of the Antarctic High (Souney et al., 2004), but increased cyclogenesis and contraction of the westerly wind belt with the shrinking ice sheet could also increase penetration. DSS today receives most of its snowfall from cyclonic systems bringing wet deposited aerosols (Bromwich, 1988; Curran et al., 1998; Souney et al., 2002). An increase in cyclonic activity beginning 8-7,000 b2k suggests this is when the present, essentially fully wet deposited regime began. This is supported by the flux data showing a lower flux component in the early Holocene compared to the mid-late Holocene as well as paleo-modelling suggesting an increase in cyclonic activity (Krinner and Genthon, 1998; Renssen et al., 2005) and potential southward migration or strengthening of the westerly winds (Kim et al., 2012; Varma et al., 2012).

4.7 Evidence of ice sheet changes in the DSS chemistry record

Changes to the chemistry record at Law Dome reflect changes in the source, transport and deposition of aerosols. One process that should be considered is how physical changes to Law Dome may have varied over time and how that affected the chemistry record. Coastal areas are particularly sensitive to changes in distance from the source. Sea salt concentration in ice cores decreases as a non-linear function with increasing distance from source and elevation (Benassai et al., 2005). Transects across the relatively flat Ronne-Filchner ice shelf showed that sea salt concentrations decrease by up to 30% over 100 km moving inland from the coast (Minikin et al., 1994). Suzuki et al., (2002) identified a decrease of 50% over 100 km and 600 m of elevation inland of the Princess Elizabeth Coast and Kärkäs et al., (2005) similarly identified a 64% decrease 100 km inland in western Dronning Maud Land. Significant changes in the position of DSS relative to the coast are expected to impact on its sea salt record.

Law Dome is currently located 110 km inland from the coast of Wilkes Land, however modelled paleo-reconstructions of the ice margin off Law Dome have indicated it likely extended 40-65 km further than present, and the dome elevation was estimated to be 300 m higher than the 1370 m elevation at the time of that study, with a seaward migration of the summit approximately 25 km at the LGM (Goodwin and Zweck, 2000). The timing of the glaciation and subsequent ice retreat remains poorly constrained in this region (Mackintosh et al., 2014). The clearest evidence for the timing of the ice sheet retreat in the Wilkes Land sector is from the Windmill Islands, approximately 15 km from the present coast. Goodwin and Zweck, (2000) showed ice thickness over the Islands thinned from a maximum of 990 m at 13,000 b2k to being ice free by ~8,000 b2k using a model of glacio-isostasy derived from glacial moraine dating evidence. Using biological marker evidence from marine flora assemblages it is suggested the deglaciation of the outermost Windmill Islands started much later around 10,750 b2k and took about 2000 years (Hodgson et al., 2003)**.** Evidence from penguin colonies (Emslie and Woehler, 2005) and lake sediment diatom assemblages (Roberts et al., 2004) demonstrate the Windmill Islands were at least substantially deglaciated by 9,000

years, and the period between 9,000 and 8,180 b2k was a transitional time where melt, isostastic uplift and sea level were closely balanced. (Roberts et al., 2004).

The ratio of SO_4^{2-}/Na^+ has been investigated [Figure 4.10] and from 12,000 b2k the ratio begins to transition from the steady pre-Holocene value of 0.38 towards the 0.23 value of today. The change represents an increase in sea salt contribution, with the ratio moving towards the seawater ratio without substantial change to SO_4^{2-} input. The ratio is unaffected by the use of a flux or concentration; therefore, it depicts a real change in Na^+ transport to the site. The steady decline in the ratio is interrupted at ~8,000 b2k, coincident with an increase in sea salt concentrations, though interpretation through this part of the record is hindered by gaps in the record due to poor ice core quality. The SO_4^{2-}/Na^+ ratio continues to decline with increasing sea salt until 3,250 b2k where rising SO_4^{2-} relative to sea salt drives a recent increase in the ratio.

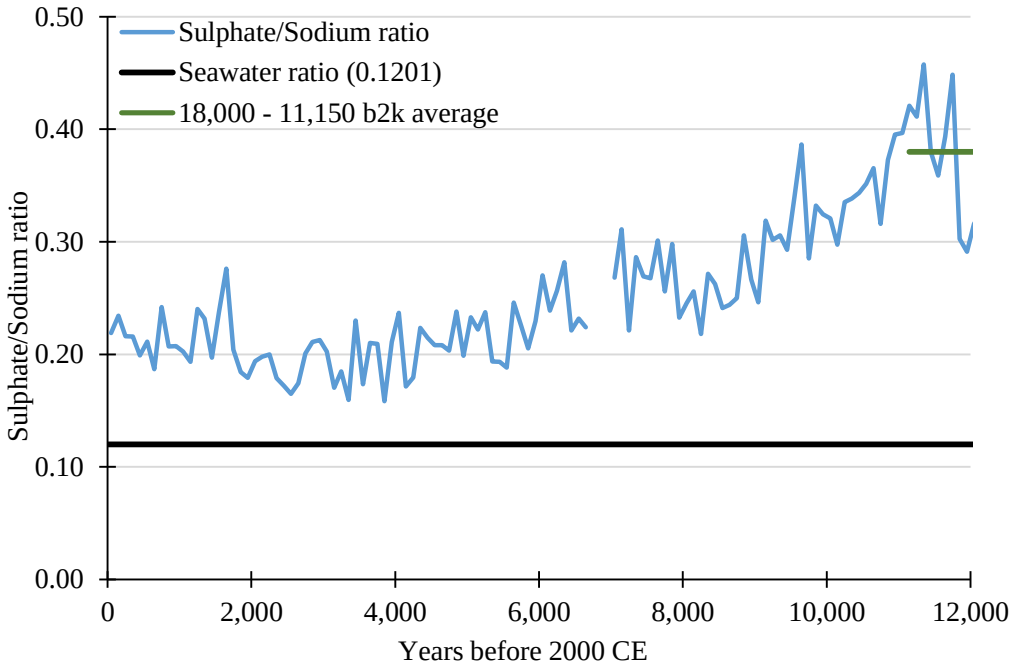

Figure 4.10 – Holocene sulphate/sodium ratio at DSS. The ratio (blue line) decreases with increasing sodium concentration in the early Holocene, bringing it closer to the seawater ratio (black line). The change at ~8,000 b2k is an increase in sulphate, possibly associated with increased cyclonic activity at the site. The LGM to Holocene average (green line) is 0.38. The present day average is 0.23, driven by an increase in total sulphate concentration since 3,250 b2k.

The SO_4^{2-}/Na^+ ratio varies from coastal to inland regions under present day conditions [Figure 4.11]. Sites close to the coast have an average ratio approaching or below the seawater ratio (0.1201) due to frost flower or sea ice formation induced fractionation. Moving inland, with increasing distance from source and elevation, sites are progressively affected by dropout of larger sea salt particles, increasing SO_4^{2-} concentrations relative to seawater ratio, hence higher SO_4^{2-}/Na^+ values. This is expected because the fractionated aerosol source is only detectable in larger sea salt particles (Udisti et al., 2012).

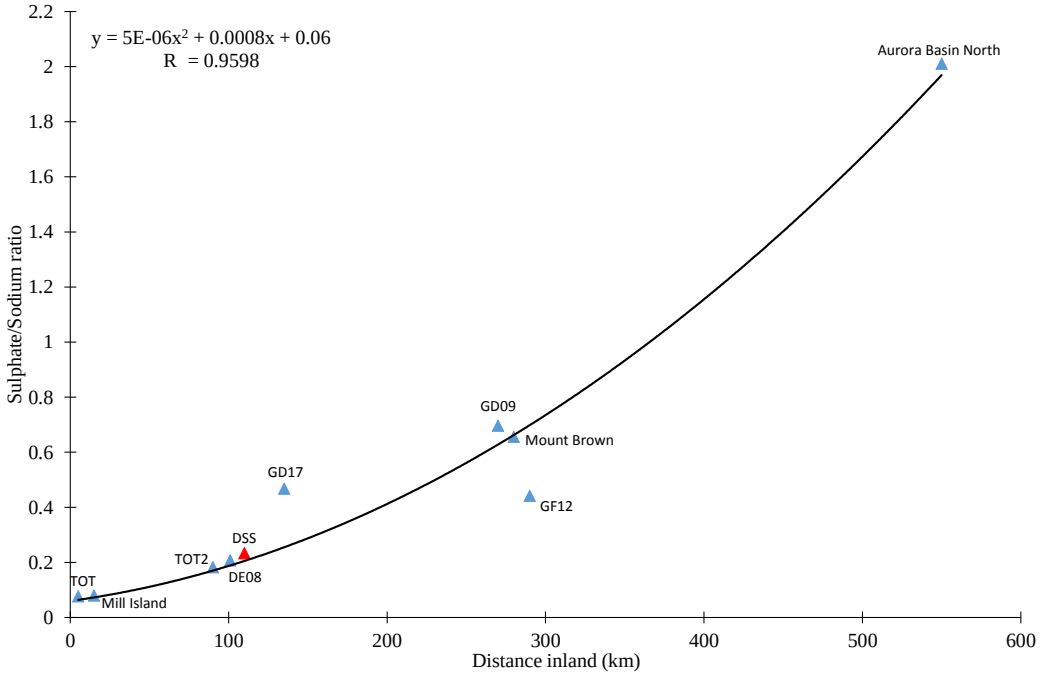

Figure 4.11 – Sulphate/sodium ratio change moving inland. Triangles represent ice core sites. The ratio increases exponentially with distance from the coast. DSS is in red. TOT and TOT2 data are from the lower and upper sections of the Totten Glacier respectively. Mill Island is a small island located north of the Bunger Hills. DE08 is located 8 km east of DSS. GD17 and GD09 are located 200 and 270 km inland of Wilkes Land respectively. GF12 is located 290 km inland from the Bunger Hills region. Mount Brown is located 280 km inland in the Vestfold Hills area. Aurora Basin North is located 550 km inland. A map of these ice core locations is provided in appendix A5.

During the LGM, the DSS site was up to 40 km further inland and 300 m higher elevation relative to today's setting, therefore we would expect the SO_4^{2-}/Na^+ ratio to be higher during this period, with an excess in SO_4^{2-} relative to Na^+. The change in ratio suggests DSS began behaving more like the coastal site it is today. This may be driven by changes in ice sheet geometry and distance from the coast, and enhanced transport efficiency through increased wind activity

carrying sea salts further inland. The SO_4^{2-} record does not increase independently of the sea salt record until ~3,000 b2k so the change is unlikely related to an increase in $nssSO_4^{2-}$. This is supported by studies at EDC and EDML ice core sites showing little evidence for $nssSO_4^{2-}$ changes in the Holocene (Kaufmann et al., 2010). The relationship between SO_4^{2-} and Na^+ can be further explored through $nssSO_4^{2-}$. At DSS today $nssSO_4^{2-}$ accounts for 60% of total sulphate. By assuming this relationship remains constant, the Na^+ record was reconstructed from total SO_4^{2-} by rearranging the calculation of $nssSO_4^{2-}$ (equation 1) to solve for Na^+. This overestimated the actual measured Na^+ concentration from 7,500 b2k and older. By increasing the proportion of $nssSO_4^{2-}$ to 75% of total SO_4^{2-}, the reconstruction more closely approximated the measured Na^+ for the early Holocene [Figure 4.12]. This does not imply greater primary production, but is consistent with DSS being more inland, with less sea salt reaching the site and a lesser contribution of sea salt SO_4^{2-} to the total SO_4^{2-} budget.

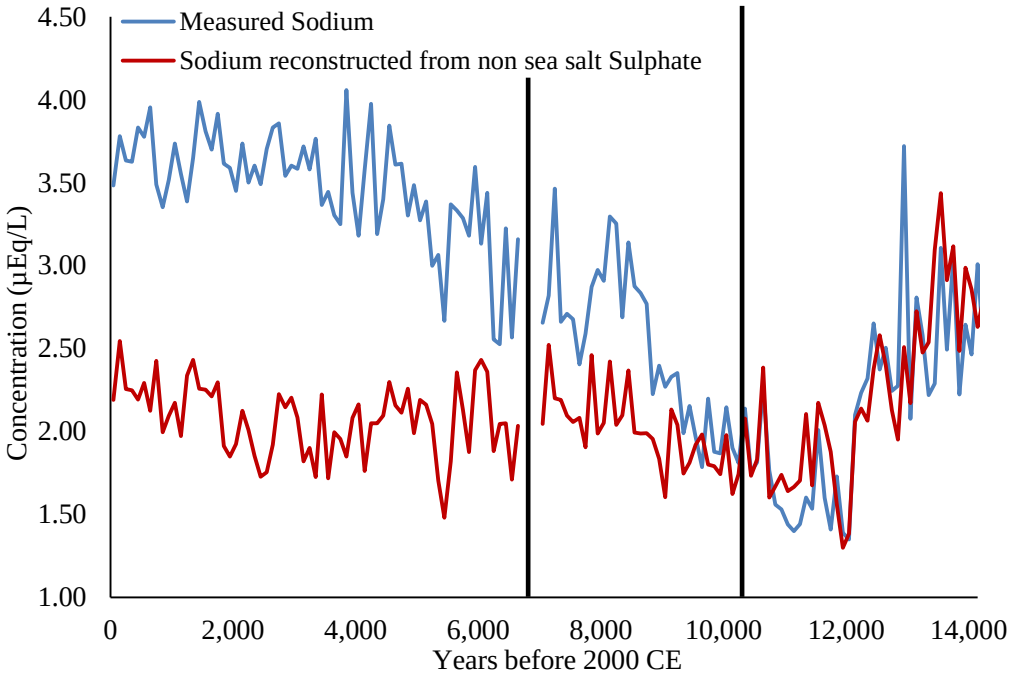

Figure 4.12 – Sodium reconstructed from nssSO4 record. The blue line represents the measured sodium concentration. The red line is reconstructed sodium assuming a constant 75% of total sulphate is $nssSO_4^{2-}$. Under present day conditions 60% of total sulphate is $nssSO_4^{2-}$ at DSS. The black bars indicate a transitional period (10,400-7,500 b2k) during which the regime changed. From 7,500 b2k to present the sodium record is better reconstructed using the modern ratio where 60% of total SO_4^{2-} is $nssSO_4^{2-}$. The relatively steady state of SO_4^{2-} through the Holocene suggests the change was driven by increased sodium levels at DSS.

With increased winter sea ice extent from the LGM to the early Holocene it is likely a greater sea salt fractionation occurred rather than less as might be assumed, however, the distance from the source is also greater so a smaller amount of the extra sea salt reaches the site (Röthlisberger et al., 2008). The reconstructed Na^+ record with 75% $nssSO_4^{2-}$ of total SO_4^{2-} begins to underestimate the measured concentrations from 10,400 b2k. This implies the amount of $nssSO_4^{2-}$ to SO_4^{2-} decreased from this time onward, with present day conditions beginning at 7,500 b2k. The period between 10,400 and 7,500 b2k was transitional, and broadly associated with glaciological changes to Law Dome. The exact timing of the transition to the modern setting is quite broad from this reconstruction. The timing window could be narrowed using seasonal data to determine the fractionation change more precisely and reduce uncertainty around the actual contribution of $nssSO_4^{2-}$ to SO_4^{2-}.

4.8 DSS sea salt and reconstructions of sea surface temperature

We have compared the DSS records of sea salt concentration to sea surface temperature (SST) records from several deep sea sediment core locations around Antarctica and the sub Antarctic [Figure 4.1] and correlations are reported using the methods of Roberts et al., (2016) described previously.

There is a strong inverse correlation between the TN057-13PC4 (13PC4) SST reconstruction (Hodell et al., 2001) and DSS sea salts ($r= -0.76$ [$-0.80 : -0.74$]). 13PC4 is a high resolution (20-50 years per sample) marine sediment core located 53°S, 005°E off the Dronning Maud Land coast. SST was estimated by comparing sample diatom assemblages to modern day assemblages in a process known as the Modern Analogue Technique (Hodell et al., 2001). 13PC4 sits south of the present day position of the Antarctic Polar Front (APF), around the edge of the current sea ice boundary. In contrast to 13PC4, SST reconstructions from TN057-17PC1 marine sediment core (Nielsen et al., 2004) nearby (50°S, 006°E) have no significant correlation with DSS sea salts. 17PC1 lies around the northernmost possible extent of the APF. The SST record from TN057-17 warms quite markedly in the last ~1,500 years [Figure 4.13b]. Nielsen et al., (2004) suggested this may result from missing a few centimetres from the core top.

Divine et al., (2010) propose the SST estimation technique used may have overestimated the modern SST. Correlation with the DSS sea salt record for the Holocene if this strong warming signal is omitted is still weak (r= -0.34 [-0.52 : -0.21]) but significant at the 95% confidence level.

In the southwest Pacific Ocean sector, lower resolution (500-700 years per sample) SST reconstructions exist from marine sediment core SO136-111, located 45°S, 174°E (Ferry et al., 2015). Correlation with this SST reconstruction is weak (r= -0.38 [-0.68 : -0.26]). An SST reconstruction from MD97-2120 off the New Zealand south coast with similar resolution (Pahnke et al., 2003) has a moderate negative correlation r= -0.44 [-0.69 : -0.37] with DSS. The uncertainty bounds on correlations with the low resolution records are large therefore it is difficult to be unequivocal in interpretation, but the correlations are persistent and significant at the 95% confidence level. The strength of this relationship may be enhanced closer to the continent or by proximity to atmospheric features (e.g. polar front).

A mechanism explaining the regional relationship between SST and DSS sea salt concentrations involves wind driven heat transport over the Southern Ocean. Lower SSTs are associated with increased speed of the prevailing winds through transfer of latent and sensible heat fluxes from the sea surface (Wallace et al., 1990). This relationship is considered indicative of atmospheric forcing on the ocean (Frankignoul, 1985) where higher wind speeds increases heat transfer from the ocean to the atmosphere (Cayan, 1992). Studies of the increasing surface westerlies under current climate regimes show enhanced generation of northward Ekman drift currents which lower SST by divergence-driven upwelling in surface waters (Hall and Visbeck, 2004). Increasing the strength of westerlies and/or a southward contraction of the mean zonal wind belt in to the source area for Law Dome would result in depressed SSTs and greater production of sea salt aerosol. An increase in cyclonic activity since the LGM as suggested by (Krinner and Genthon, 1998; Renssen et al., 2005) would also increase sea salt aerosol production. The Antarctic Circumpolar Current (ACC) is influenced partially by the strength of the westerly winds (Allison et al., 2010; Rintoul et al., 2001; Trenberth et al., 1990) which offers a mechanism linking sea salt production and

SST across regional scales. Enhanced sea ice production and transport from the Weddell Gyre in response to westerly wind intensification has been proposed by Divine et al., (2010). The strength of the present day Weddell Gyre responds positively to wind forcing (Wang et al., 2012). TN057-13PC4 is close to the Weddell Gyre and ACC boundaries, so may be more sensitive to variations in these ocean features than cores further north. A relationship with SST would suggest the open ocean is an important source for aerosols to Law Dome throughout the Holocene. Increased latent heat flux transfer results in more atmospheric moisture, providing a further mechanism for increased accumulation observed at Law Dome during the early Holocene.

Table 4.1 – DSS sodium concentration and SST reconstruction correlations.

Site Name	Correlation [95% uncertainty bounds]	Location
TN057-13[a]	r= -0.76 [-0.80 : -0.74]	53°S, 005°E
TN057-17[b]	r= -0.34 [-0.52 : -0.21]*	50°S, 006°E
MD97-2120[c]	r= -0.44 [-0.69 : -0.37]	56°S, 160°E
SO136-111[d]	r= -0.38 [-0.68 : -0.26]	45°S, 174°E

[a] – (Divine et al., 2010) [b] – (Nielsen et al., 2004) [c] – (Pahnke et al., 2003) [d] – (Ferry et al., 2015)

* - correlation without anomalous warming in the SST reconstruction (see text for discussion).

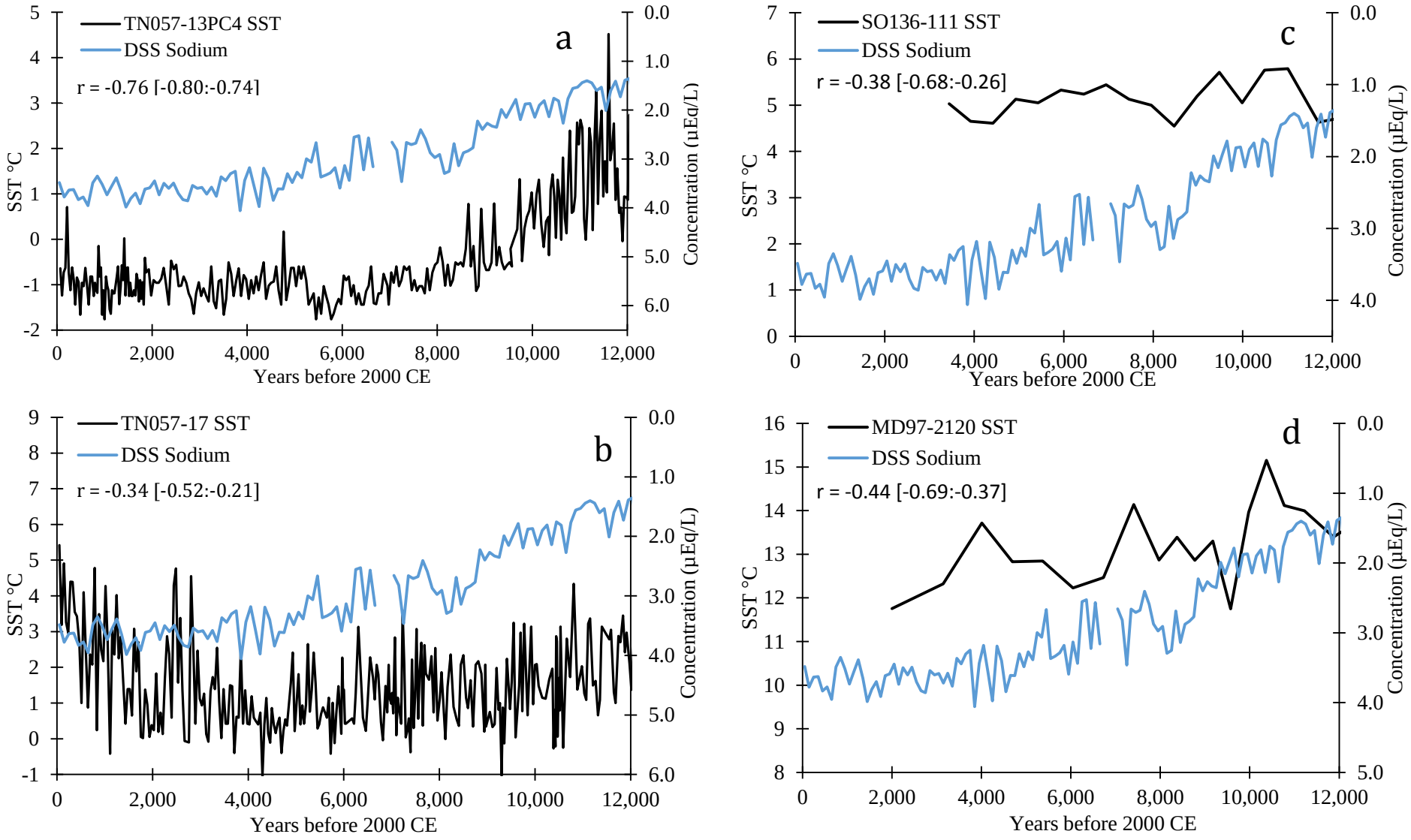

Figure 4.13 – Sea surface temperature and DSS sea salt concentrations. The DSS sea salt record has an inverse correlation with marine sediment core SST reconstructions around the Southern Ocean. Sodium concentration (inverted axis) blue line. SST reconstruction in black. Correlations are as shown in Table 4.1.

4.9 Sea ice presence and DSS sea salts

Sea ice extent reconstructions through the Holocene to the LGM would be a valuable addition to our understanding of Holocene climate changes, with the radiative forcing of sea ice extent expected to be important for ice sheet retreat (Wallace and Hobbs, 2006). It is proposed that sea ice is a source of sea salt to the Antarctic continent, and that this could be used as a proxy for ice extent (Fischer et al., 2007a; Wolff et al., 2003). On short time scales sea salts have been shown to respond primarily to meteorological conditions rather than sea ice extent, but long term trends may be tracked through ice cores (Levine et al., 2014)

Past sea ice reconstructions are largely restricted to selected time slices such as the LGM (Röthlisberger et al., 2010). There have been extensive efforts to reconstruct Antarctic sea ice conditions at the LGM using diatom assemblages from marine sediment cores as proxies (e.g. CLIMAP, 1981; Crosta et al., 1998; Gersonde, 2003). These studies have demonstrated winter sea ice extended out considerably further than present day conditions. Constraining the summer sea ice extent at the LGM has proven more difficult due to poor microfossil preservation, however Gersonde et al., (2005) reconstructed summer sea ice extent in the Law Dome region, the results of which suggest a significant seasonal melt was occurring at the LGM.

Few Holocene-length records of Antarctic sea ice exist. The DSS sea salt record has been compared with two high resolution reconstructions from marine sediment records TN057-13PC4 and TN057-17PC1, located off the Dronning Maud Land coast. These cores are located close the modern sea ice edge, making them sensitive to changes in ice extent. A positive correlation ($r = 0.66$ [0.62 : 0.78]) is found with the TN057-13PC4 (53°S, 005°E) winter sea ice reconstruction (Divine et al., 2010). The correlation between the more northerly reconstruction from TN057-17PC1 (50°S, 006°E) (Nielsen et al., 2004) is weak $r = 0.37$ [0.10 : 0.57]. The sea ice extent record of 17PC1 shows often low (<0.5 months/year) or no ice coverage which may make it less sensitive to sea ice changes. Sea salt concentrations might be expected to increase since sea ice is considered a source of sea salt. However, considering the relationship between

SST and sea salts at DSS and the possible control SST may have on sea ice formation, it is difficult to interpret the DSS record as a sea ice extent proxy. The sea ice presence record from SO136-111 is largely ice free by 14,000 b2k therefore is not be considered. The E27-23 reconstruction is also generally ice free, showing only sporadic winter sea ice during the Holocene (Ferry et al., 2015) and no significant correlation in the Holocene is found with DSS sea salts.

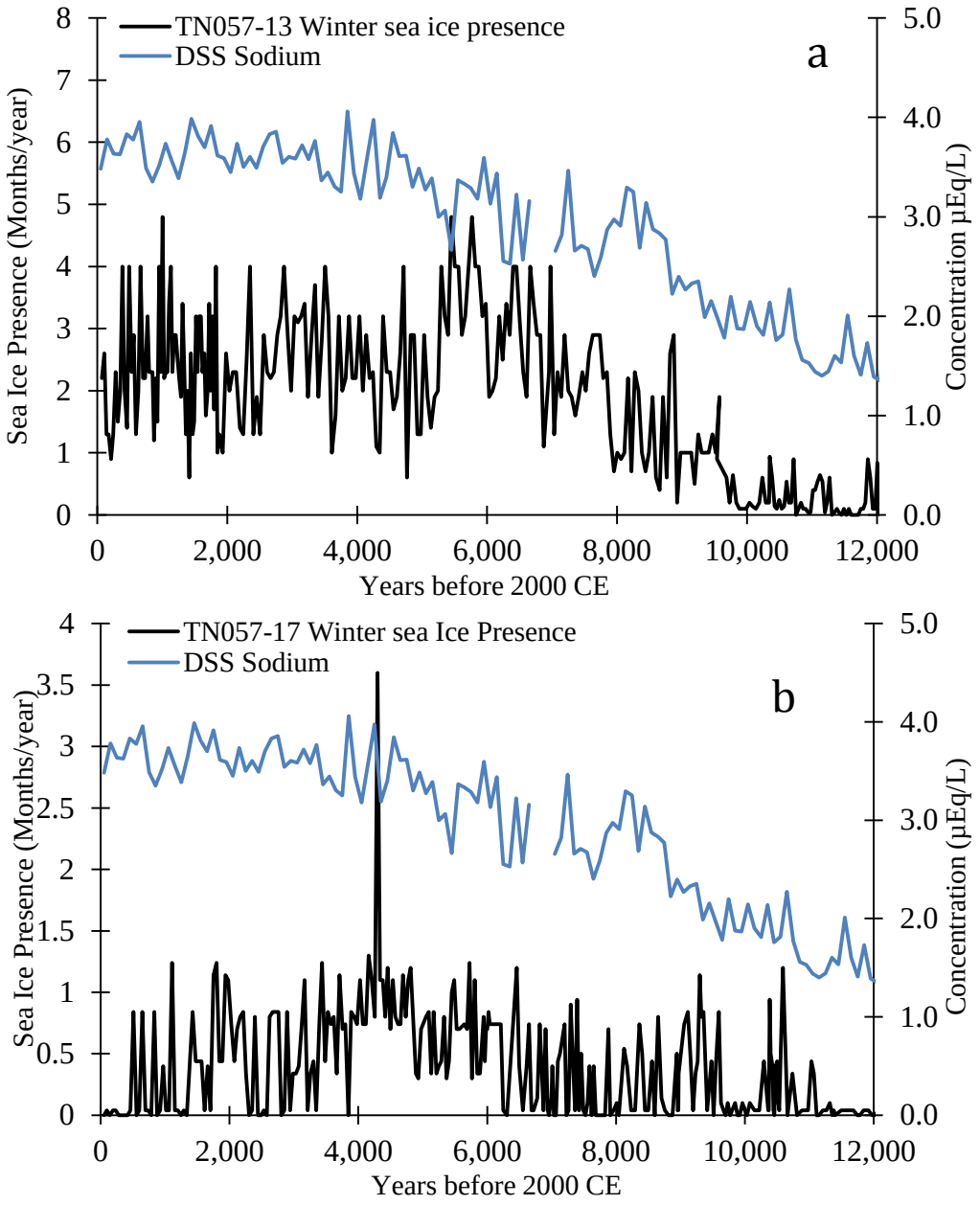

Figure 4.14 – Sea ice presence and DSS sea salt concentrations. A positive relationship exists between sodium concentration (blue line) and sea ice presence reconstructed from marine sediment cores (**a**) TN057-13 and (**b**) TN047-17 (black line). TN057-17 is the further north of the two, hence less sea ice presence.

4.10 MSA relationship with sea ice and sea surface temperature

Correlation between the MSA and SST reconstructions do not show a clear response, and no significant correlations exist between MSA and SST records [Figure 4.14a]. The MSA record does decrease in line with cooling evident in the SST record of TN057-13 around 5,250 b2k. The sea ice presence correlation is negative for TN057-13 r= -0.41 [-0.65 : -0.27] [Figure 4.14b]. Correlation with TN057-17 was weak, but also negative r= -0.19 [-0.43 : -0.15].

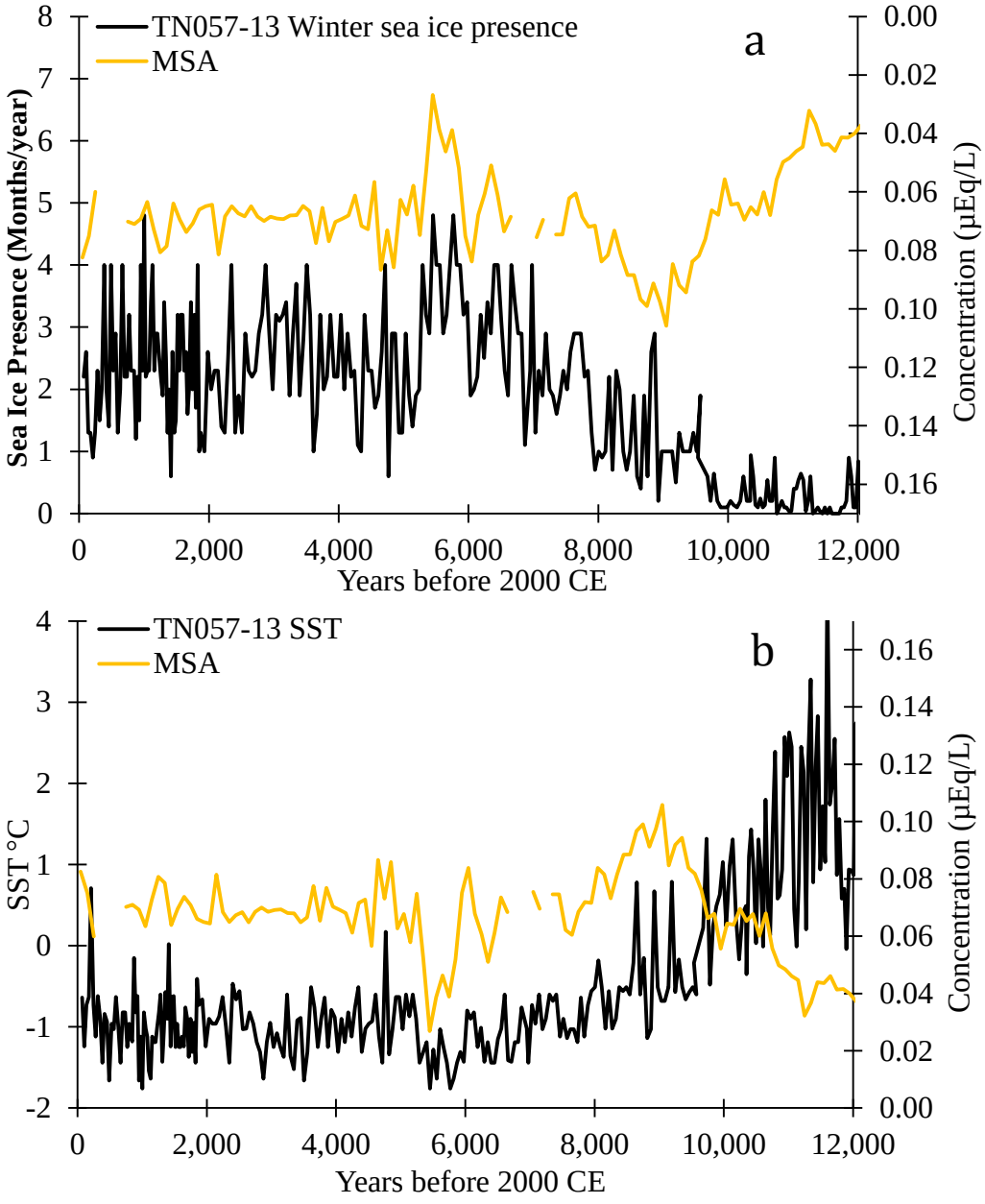

Figure 4.15 – MSA and TN057-13 sea ice and SST reconstructions. MSA (yellow) compared with records of sea ice presence (months/year) (**a**), and SST °C (**b**). MSA on an inverted axis in (a). The SST cooling evident 5-6,000 b2k is a period of decreased MSA concentration and increased sea ice presence.

The relationship between MSA, SST and sea ice is complex and is related to many factors including sea ice extent, open water in summer, phytoplankton activity and species, nutrient availability and atmospheric transfer and oxidation processes. Under present day conditions, MSA correlations with sea ice extent vary between locations (e.g. Abram et al., 2013). However, there is no clear relationship between MSA concentration and sea ice presence or SST evident in this study on 100 year timescales. The 100 year mean MSA concentration may not respond to sea ice extent and SST conditions in the same manner as interannual variability as described by Abram et al., (2013) or Curran et al., (2003). There is not enough independent evidence from the data currently available to understand what the DSS MSA data is informing us of regarding sea ice extent and SST, combined with the uncertainties from MSA analysis on stored ice, means further assessment is beyond the scope of this study.

4.11 Orbital forcing and sea level rise

Variations in Earth's orbital parameters change the amount and distribution of solar insolation across the planet. Solar insolation is the average intensity of the incident solar radiation affecting the Earth's surface (Mellor, 1997). The DSS sea salt record has been compared with Southern Hemisphere summer insolation [Figure 4.15] (Berger and Loutre, 1991) and a strong positive correlation r= 0.87 [0.86 : 0.92] is found. The correlation suggests sea salt transport to DSS could be related to insolation driven processes. Many climate processes have been linked to insolation changes; formation and strength of atmospheric structure, equator to pole thermal gradient, oceanic heat transport, winds, glacial melt and sea ice production (Abelmann et al., 2006; Chiang and Bitz, 2005; Clark et al., 2009; Clement et al., 1999; Denis et al., 2010; Lambeck and Chappell, 2001; McGee et al., 2014; Moy et al., 2002; Smith et al., 2011). The mechanisms behind the linkage are not clear. Solar-forced GCM simulations suggest insolation may impart control on westerly winds patterns and cyclonicity around Antarctica (e.g Genthon & Krinner, 1998; Renssen et al., 2005). Changes in winds around the Antarctic could affect sea salt aerosol transport, particularly to coastal regions.

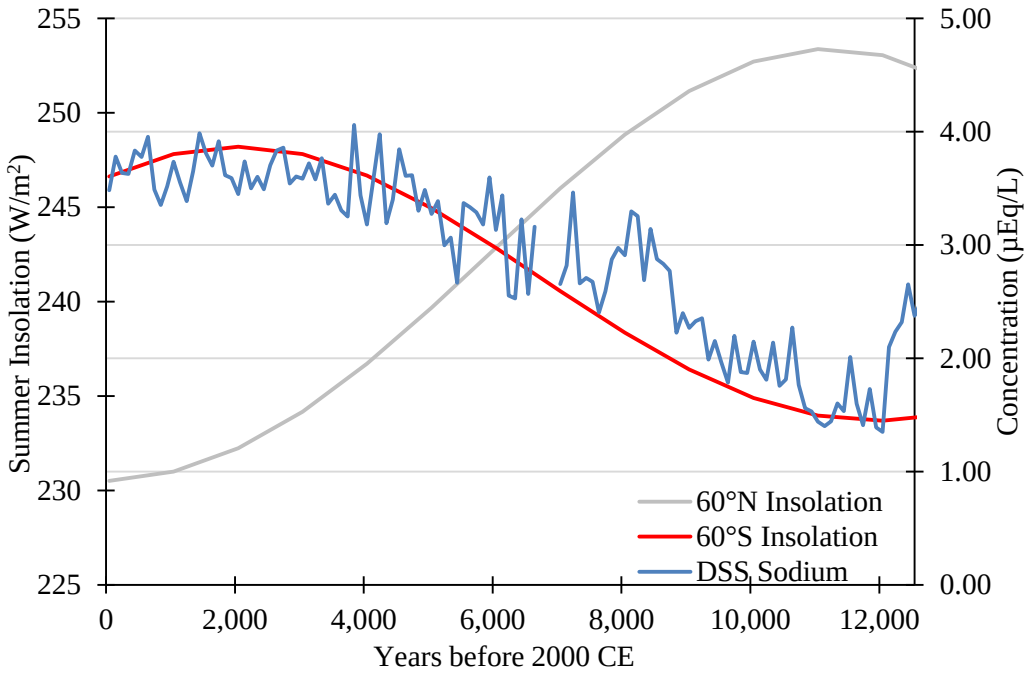

Figure 4.16 – DSS sea salt and mean summer solar insolation during the Holocene. The sea salt (sodium) record (blue line) is strongly correlated with Southern Hemisphere summer insolation (red line) – r= 0.87 [0.86 : 0.92] $p<0.05$. Insolation data from Berger and Loutre (1991).

There was a rapid rise in global sea level between 11,750-7,050 b2k (Smith et al., 2011). Comparison of DSS Na^+ with Holocene sea level rise (Lambeck et al., 2002) [Figure 4.17] shows broad agreement between the two records. This is not unexpected since insolation driven changes, enhanced by sea level rise feedback destabilising and thinning coastal ice streams, are considered key drivers of ice sheet melting (Smith et al., 2011). The centennial scale variability observed in the sea salt record cannot be readily explained through sea level rise. The major sea level rise occurred in the early Holocene between 11,750 and 7,050 b2k, while sea salt concentrations continued to rise for a further 2,000 years. These two factors suggest other processes exert greater control on sea salt concentrations at DSS.

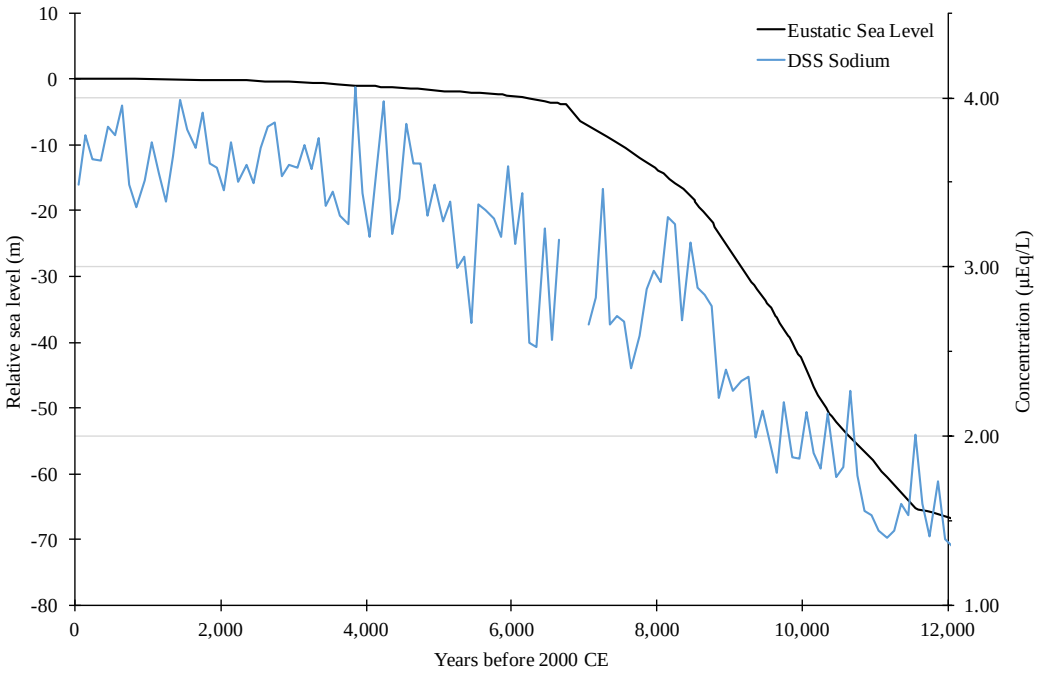

Figure 4.17 – Holocene sea level rise and sodium concentration. Eustatic sea level curve from Lambeck et al., (2002) in black. DSS sodium in blue. The early Holocene rapid sea level rise occurs between 11,750 – 7050 b2k. The increase in sodium begins at 12,000, ending ~5,000 b2k.

4.12 5,600 – 5,100 b2k abrupt changes in the DSS record.

A mid Holocene perturbation of the climate system between 5,100 and 5,650 b2k is observed in the DSS MSA record, with the lowest concentration values at 5,250 b2k. The lowest MSA and sulphate concentrations in the Holocene are observed during this time. A smaller decline in sea salt concentrations is also evident, but excursions of similar magnitude are present elsewhere in the record. A sharp decline is observed in the EDML sea salt Na^+ record at 5,750 b2k (Fischer et al., 2007a) and in the MSA record at Siple Dome approximately 5,950 b2k (Saltzman et al., 2006). The climate reconstructions from TN057-13 and TN057-17 marine sediment cores show a period of cooler SST and sea ice expansion at this time, suggesting this is a regional feature. This timing also coincides with the abrupt termination of the African Humid Period. The early-mid Holocene was a humid period for North Africa and the Sahara, however, by 5,000 b2k the regime had shifted to an arid, dry climate. The termination of the moist air over North Africa has been linked with solar insolation changes and feedbacks associated with sea ice expansion in the Atlantic sector (de Menocal, 2015; Hodell et al., 2001). Whether these abrupt

phenomena recorded in ice cores and marine sediment cores are related to African Humid Period requires further investigation for confirmation.

4.13 Summary

The Holocene record of chemistry shows marked changes in sea salt concentration reflecting the broader reorganisation of both Holocene climate modes, and changes to the depositional mode to Law Dome, ultimately driven by insolation changes. Sea salt concentrations declined with increasing accumulation through the LGM-Holocene transitional period as expected under a dry-depositional regime. From 12,000 b2k the sea salt concentrations began to increase with increasing accumulation, suggesting that wet deposition became the dominant depositional mode. The sodium flux and concentration records co-vary from 12,000 b2k supporting this assertion.

The SO_4^{2-}/Na^+ ratio has changed from 0.38 at 12,000 b2k to 0.23 today. Interpretation of the ratio suggests that an excess of sulphate relative to the seawater ratio of sodium existed in the early Holocene. The ratio was steady from the LGM until 12,000 b2k, when sodium deposition increased relative to sulphate. The ratio today varies as a function of distance to the coast and altitude, with a higher ratio moving inland as larger sea salt particles drop out depleting the sea salt record. A first order interpretation is that 12,000 b2k was the point at which the ice sheet around Law Dome began to contract and thus more sea salt was able to be deposited at the site as it became closer to the source. Similarities in the sea salt records of DSS, EDC and EDML suggest a common sea salt depositional pattern between the sites existed until the early Holocene. The small change in DSS site parameters to a more coastal site is unlikely to affect either inland site, but may have drastically increased the sea salt deposition at DSS through decreased particle dropout with reduced distance to the coast.

From 8,000 b2k, sea salt concentrations continued to rise at a steady rate and have stabilised since 5,000 b2k. The inverse correlation observed with SST reconstructions is consistent with either increased average wind over the Southern Ocean and/or shifting of the source region for DSS aerosols. Increased

atmospheric moisture content relative to the LGM and increased cyclonic activity have been proposed for the early Holocene, and the increase in sea salt and snow accumulation at DSS is consistent with this. The relationship between SST and Law Dome sea salts is a regional feature, seen in sediment core SST reconstructions around the continent and as far north as southern New Zealand. This relationship is not fully explored, but established relationships between the ACC and westerly winds may explain the regional linkages.

The sea salt-sea ice presence relationship is less definitive as few records are available in the vicinity of Law Dome. The correlation with the TN057 marine sediment proxy records of sea ice presence may suggest that sea ice extent varied on regional scales around the EAIS, however the possibility that sea ice extent is responding to SST changes cannot be discounted. Sea salt particle dropout from the atmosphere increases as a function of distance and elevation, therefore as Law Dome became more coastal and lower elevation and an increase in sea salt concentrations would be expected. Glaciological studies indicate that the present Law Dome configuration was reached by approximately 8,000 b2k, while the sea salt-SST relationship persists beyond this period of local reorganisation. This may be evidence for a southerly contraction of storm tracks or an increase in cyclonic activity or intensity around Law Dome.

With exception of an anomaly around 5,250 b2k, MSA concentrations are lowest in the early Holocene and peak at 9,000 b2k before returning to modern day levels shortly after 8,000 b2k. The peak at 9,000 b2k shows the highest concentrations recorded in the Holocene. There is no consistent relationship between MSA, SST and sea ice presence on a Holocene-length timescale evident in this study. Formation of MSA is highly variable, responding to many factors including DMS production, flux to the atmosphere, oxidation in the atmosphere and post depositional movement and readmission to the atmosphere. MSA preservation may be more sensitive to post-depositional effects than sea salts as it is more volatile, hence it may not be appropriately preserved until a higher accumulation threshold is reached. The complicated nature of MSA production makes it highly variable, coupled with uncertainties over the analysis of ice cores

in long term storage makes it difficult to assess MSA and make definitive conclusions here.

Chapter 5 – 2000-year volcanic history from the Law Dome ice core record.

5.1 Abstract.

Volcanic eruptions are an important cause of natural climate variability. In order to improve the accuracy of climate models, precise dating and magnitude of the climatic effects of past volcanism are necessary. Here we present a 2000-year record of Southern Hemisphere volcanism recorded in ice cores from the high accumulation Law Dome site, East Antarctica. The ice cores were analysed for a suite of chemistry signals and are independently dated via annual layer counting, with 11 ambiguous years at 23 BCE, which has presently the lowest error of all published long Antarctic ice cores. Independently dated records are important to avoid circular dating where volcanic signatures are assigned a date from some external information rather than using the date it is found in the ice core. Forty-five volcanic events have been identified using the sulphate chemistry of the Law Dome record. The low dating error and comparison with the NGRIP (North Greenland Ice Core Project) volcanic records (on the GICC05 timescale) suggest Law Dome is the most accurately dated Antarctic volcanic dataset, which will improve the dating of individual volcanic events and potentially allow better correlation between ice core records, leading to improvements in global volcanic forcing datasets. One of the most important volcanic events of the last two millennia is the large 1450s CE event, usually assigned to the eruption of Kuwae, Vanuatu. In this study, we review the evidence surrounding the presently accepted date for this event, and make the case that two separate eruptions have caused confusion in the assignment of this event. Volcanic sulphate deposition estimates are important for modelling the climatic response to eruptions. The largest volcanic sulphate events in our record are dated at 1458 CE (Kuwae? Vanuatu), 1257 and 422 CE (unidentified).

5.2 Introduction

Understanding natural causes of climate variability is vital to evaluate the relative impacts of human populations, and, of all the natural causes, volcanic eruptions and solar variation are the two most important (Gao et al., 2007). Volcanic eruptions are an important part of the global climate system because of their radiative forcing (Zielinski, 2000). Sulphur-rich gaseous emissions from eruptions undergo atmospheric oxidation to form stable aerosol compounds that may remain in the atmosphere for several years, during which time they act to cool Earth's surface by reflection of solar radiation (Rampino and Self, 1984; Robock, 2000). Periods of cooling associated with volcanic eruptions must be adequately accounted for in order to determine natural variation in climate, and interpret anthropogenic influences on the climate system (Robock, 2000).

Volcanic aerosols from major eruptions are transported through the stratosphere and deposited across the world, including high latitude polar areas. Ice cores retrieved from these areas offer an archived record that can be analysed (e.g. measuring the electrical properties or sulphate content of the ice) for the unique signature of volcanic events preserved within them. This information can be used to infer the potential climatic impact of an eruption, by calculating estimates of the total sulphate deposition to the ice sheet from a volcanic eruption, provided that events can be dated with sufficient accuracy.

Producing an accurately dated volcanic chronology re- quires a well-dated ice core timescale. The most accurately dated ice cores are dated using annual layer counting methods (Cole-Dai et al., 1997) where seasonal variations in physical or chemical properties marking each year in the ice are counted. However, this requires a high snowfall site to be able to resolve the annual layers; therefore this method cannot be applied at all sites. Where layer counting cannot be applied, ice core timescales are produced based on the identification of reference horizons and assumptions about accumulation rates. This method is capable of producing a reasonably accurate timescale, but it is important to understand the limitations of, and implications of, the use of this "non-independent" method. Incorrect identification of and assignment of dates to

reference horizons will cause errors in the timescale. Often it is difficult to obtain reliable dates for reference horizons beyond recent history, especially in the Southern Hemisphere (SH), as historical documentation of eruptions is poor. The dating accuracy is compromised by variations in snowfall from the average. It is crucial to avoid circular arguments whereby volcanic signatures in ice core records are assigned a date based on some external information (e.g. historical documents, tree ring records, and other ice cores) and then used to verify the dating of that particular event. The assignment of dates does not advance the dating accuracy of the volcanic record – the record will only be as accurate as the record it has been synchronized to, and has the potential to inadvertently reinforce the acceptance of an initially questionable date. Cores dated by non-independent methods remain essential to understanding the spatial distribution patterns of volcanic sulphate aerosols, and dating of deep ice where layer counting cannot be reliably performed. Ice cores dated via accurate layer counting, independent of previously reported volcanic event dates – such as Law Dome – are key to producing high accuracy volcanic chronologies, and improving the dating of events recorded during the first millennium CE, which offers the opportunity to improve correlations between ice cores, as well as better constraining the timing of past volcanic eruptions.

The timing of eruptions is an important factor in producing global volcanic forcing estimates. Presently there are two primary datasets (Crowley et al., 2008; Gao et al., 2008). The Gao dataset places the large, global volcanic horizon of the 1450s at 1453 CE, with a smaller event classified as Northern Hemisphere (NH) only later in that decade (all dates in this work are CE unless stated otherwise). The Crowley dataset has NH event beginning in 1451, and a second event starting in mid-1459, and one SH event starting in 1456. Like Gao, the Crowley study defined the late-1450s volcanic event as NH-only, but suggest the eruption history during this period warrants further investigation (Crowley and Unterman, 2012). Owing to the size of this event, the timing of the event is of importance to climate reconstructions, and we use the accurate, independently dated Law Dome volcanic record to explore the timing of this important event.

DSS (Dome Summit South) is a coastal site, and the chemistry record is influenced by marine aerosols. The site has a high annual accumulation (0.70 ma^{-1} ice equivalent), relatively low mean surface temperatures (−21.8˚C) and wind speeds (8.3 m s^{-1}) (Morgan et al., 1997). Precipitation events at Law Dome occur on average with sufficient frequency to preserve signals at monthly resolution (McMorrow et al., 2001). This allows for high-resolution sampling and this study provides an independently dated, seasonally resolved trace chemistry record spanning the past 2000 years.

5.3 Dating and chemical analysis

The Law Dome record was independently dated using annual layer counting of a suite of chemistry species with seasonally defined behaviours. These include oxygen isotopes ($\delta^{18}O$), deuterium (δD), hydrogen peroxide (H_2O_2) non-sea salt sulphate ($nssSO_4^{2-}$) and sea salt species (Cl^-, Na^+ and Mg^{2+}). Additionally, the ratio of SO_4^{2-}/Cl^- was used as a summer marker. Ice core sampling and analysis methods used were described by Palmer et al. (2001) and Roberts et al., (2009). At 23 BCE, annual layer thickness is reduced to 0.25 ma^{-1} ice equivalent as a result of layer thinning due to ice flow. At this depth, trace ion chemistry was sampled at 25 mm resolution, allowing for 8 to 10 samples per year, which is sufficient for annual dating. Analysis of $\delta^{18}O$ was conducted at 10 mm resolution. Following the methods of Morgan and van Ommen (1997), the summer maxima in $\delta^{18}O$ were fixed as 1 January of each year horizon. Where $\delta^{18}O$ was unavailable, the δD or $nssSO_4^{-2}$ maximum was used. Dating of the discrete samples was performed using linear interpolation between year depth horizons. Six separate ice cores from the Dome Summit South (DSS) site on Law Dome were used in this study. The ice cores were retrieved from DSS site (66˚43’ S, 112˚48’ E), located 4.6 km southeast of the Law Dome summit. Drilling for the main 1196 metre long DSS ice core began in 1987, with drilling completed in 1993. Two additional mid-length cores (DSS97 and DSS99) were drilled in subsequent years at the site to provide better core quality through the top 117m of the original DSS core. In recent years (since 1999) the DSS site has been revisited and series of short overlapping firn cores were drilled in 2001, 2008 and 2009 (cores DSS0102, DSS0809 and DSS0910, respectively) to bring the record

up to 2009. Palmer et al. (2001) produced a single chemistry time series from DSS99, DSS97 and DSS down to 400 m (1300), and we have applied their methods to extend the Law Dome chemistry record from 1995 to 2009. All cores used were dated via annual layer counting. Dating is registered across core boundaries by matching seasonal features in oxygen isotopes and other chemistry species through the periods of overlap between cores. Dating across core boundaries is unambiguous and locked without error. In the event of misalignment of overlapping records, natural variability in accumulation from year to year would result in rapid loss of coherence between annual cycles.

Layer counting identified 11 ambiguous years where the seasonality was not clear. Of these 11 years, 7 years were not counted where evidence for a year was weak, but could not be conclusively discounted. Four years were counted where multiple lines of evidence supported a year. This error estimation technique allows the date at 23 BCE to be a maximum of 7 years older or 4 years younger than dated, with the record dated unambiguously to 1807, and ±1 years to 894. This error estimate is the lowest of all comparable-length Antarctic ice core records, with DML (Dronning Maud Land) ±23 years at 186 (Traufetter et al., 2004) and South Pole ±20 at 176 (Ferris et al., 2011). Eruption dates previously published for Law Dome (Palmer et al., 2001) older than 1818 have been adjusted for a 1-year dating error due to a damaged section of core. This adjustment was made after synchronizing the $\delta^{18}O$ record of a new mid-length core retrieved from the DSS site in 2005 to the existing DSSmain ice core across the period in question.

5.4 Determination of volcanic signals

There are three primary sources of sulphate to the Antarctic continent: sea salt, biogenic and volcanic sulphate, with anthropogenic sources considered minimal (Curran et al., 1998). To identify the signal associated with volcanic eruptions, it is necessary to remove the sea salt and biogenic sulphate components from the total sulphate concentration. We removed the sea salt sulphate component by calculation of the non-sea salt sulphate ($nssSO_4^{2-}$) parameter, using equation 4.

$$nssSO_4^{2-} = [\text{total } SO_4^{2-}] - (0.1201 - r) \cdot [Na^+] \quad \textbf{Equation 4}$$

where 0.1201 is the ratio of SO_4^{2-} to Na^+ in seawater, and r is a fractionation correction of 0.033 (Palmer et al., 2002) to account for sulphate depletion from the formation of frost flowers on sea ice (Rankin, et al., 2000). The $nssSO_4^{2-}$ signal at Law Dome is dominated by strong seasonality associated with the biogenic sulphate cycle. This biogenic signal has a local summer maximum, and winter minimum, and this seasonality can be a barrier to resolving the onset and duration of volcanic signals. To remove the biogenic signal, we calculated the residual $nssSO_4^{2-}$ ($[nssSO_4^{2-}]_{residual}$), shown in Fig. 5.1. The $nssSO_4^{2-}$ record was down-sampled into 8 even bins per year, and the 31-year centred moving average (starting in 1995) of these bins was computed, and then subtracted from the raw $nssSO_4^{2-}$ record. This residual dataset is sensitive to volcanic sulphate inputs. Eight bins per year were chosen as that reflects the average number of samples per year at the end of the record. A 31-year running mean was used to account for natural variations in background sulphate.

Large volcanic events already identified in the record were removed prior to calculation of the residual to avoid incorrectly weighting the ensemble, which would lead to an over- estimation of background sulphate concentrations. Volcanic signals are detected as a rise above background levels (e.g. Cole-Dai et al., 2000; Delmas et al., 1992; Ferris et al., 2011; Langway et al., 1995; Moore et al., 1991; Palmer et al., 2001; Traufetter et al., 2004); therefore, we have identified volcanic signatures from the $[nssSO_4^{2-}]_{residual}$ time series, where values above zero are representative of concentrations above the 31-year average. This method of volcanic determination is based on the method of Palmer et al. (2001), and uses visual classification criteria and knowledge of the sulphate seasonal cycle to discriminate between noise and volcanic signals. To be classified as volcanic, spikes in the residual record must be at least 6 months in duration. Deviations above the average during winter are characteristic of volcanic events at Law Dome as the variable biogenic sulphate source is low, and winter sea salt sulphate contributions can be accurately determined from the seawater ratio of directly measurable sea salt species (e.g. Na^+). Because biogenic sulphate sources

are more variable, residual sulphate peaks in summer only were treated with caution.

Volcanic events have a clearly definable peak, and are characterised by a sharp rise in concentration at the onset of the volcanic event and then taper off. This conservative approach to identification has a bias towards medium and large events, which are most clearly identifiable in our record, and we consider such events to be those most likely to have the greatest impact on climate. Estimates of volcanic sulphate provide information on the climatic effects of volcanic eruptions as the amount of sulphur-rich gas emitted by eruptions can have an effect on global temperatures. The volcanic flux deposition estimates for Law Dome (Table 5.2) are calculated from the residual $nssSO_4^{2-}$ record according to equation 5.

$$Fs = [nssSO_4^{2-}]_{residual} \cdot \rho \cdot l \cdot 10^{-3} \text{ kg km}^{-2} \qquad \textbf{Equation 5}$$

where $[nssSO_4^{2-}]_{residual}$ is the residual $nssSO_4^{2-}$ in μg kg^{-1}, ρ = 917 kg m^{-3} – the density of ice, and *l* is the surface equivalent ice length of each sample (in metres) and corrects for the smaller apparent sample fluxes due to thinning of the ice with increasing depth. We report total volcanic deposition derived by summing the individual sample fluxes to give a total deposition for the duration of the event. Law Dome deposition estimates from this study are ~ 25% lower than those discussed previously for Law Dome by Palmer et al., (2002). The differences result from the residual calculation method used and small improvements in Law Dome flow thinning calculations (used in the calculation of *l*) and fractionation corrections (r in Eq. 1). We note that our lower deposition for the Tambora, Indonesia, eruption (57.2 kg SO_4^{2-} km^{-2}) compares closely to the SH average of 51 kg SO_4^{2-} km^{-2} as determined by Gao et al., (2007). Table 5.2 includes sulphate depositional information from the NGRIP ice core for inter-hemispheric volcanic events. The calculation methods for the NGRIP depositional information can be found in Appendix A3. Because of the variability inherent in site-specific properties (e.g. sulphate depositional regime, accumulation from year to year, aerosol transport pathways), the depositional size of an eruption can vary from site to site. Therefore, it is important to use as many records as possible when

producing volcanic forcing estimates, provided that those records are dated with sufficient accuracy to resolve the same event across cores.

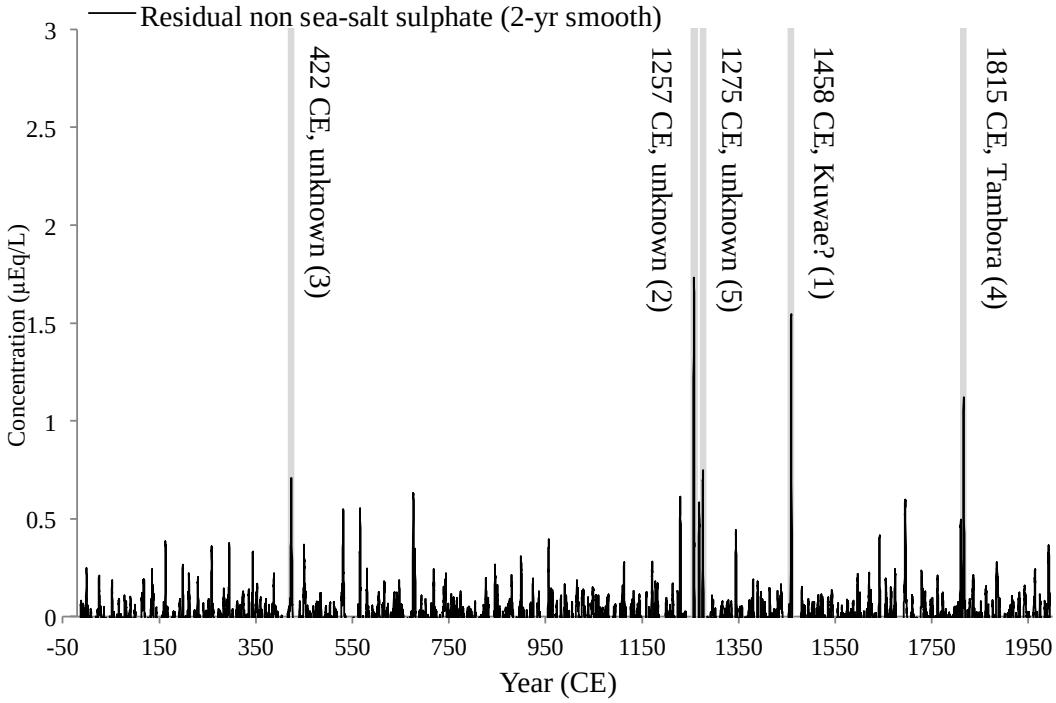

Figure 5.1 – The Law Dome residual non sea salt sulphate record. The peaks shaded in grey represent the five highest event fluxes, with the number in brackets signifying the event size rank in the Law Dome record (1 being highest). A 2-year smooth was used for illustrative purposes.

5.5 Volcanic eruption dating

Atmospheric transport of volcanic aerosols from eruption site to deposition site results in a time delay of typically 6 months to 1 year, and is dependent upon eruption location, atmospheric circulation patterns and site precipitation characteristics. Estimates of this time delay are made by com- paring the onset of the volcanic signal in a dated ice core record to the eruption date of well-documented eruptions (e.g. Tambora, Krakatau). At Law Dome, the average delay is 1 year (1σ = 0.58 years, N =11). The shortest delay of 0.6 years was associated with the 1815 eruption of Tambora, Indonesia, and the longest delay observed was 2.5 years for the 1982 eruption of El Chichón. Palmer et al. (2001) suggested unusual atmospheric patterns associated with the quasi-biennial oscillation could be responsible for this extended delay. 1982–83 period

corresponds with a strong El Niño-Southern Oscillation event that produced anomalous atmospheric circulation patterns over high southern latitudes (Houseago et al., 1998). Those anomalies could have affected the transport of volcanic aerosols following the El Chichón eruption.

5.6 Results and discussion

Forty-five volcanic events have been identified in the Law Dome record between 1995 CE and 23 BCE. Based on total deposition, the largest volcanic events observed in our record are the 1458 (Kuwae?), 1257, 422 (Unidentified) and 1815 (Tambora) events. The sulphate deposition of the 1458 and 1257 eruptions was similar in size, approximately 1.8 times greater than the Tambora eruption. The 422 event signature is observed over a period of 4.3 years, making it the longest event in our 2000-year record, and also appears bimodal in nature and may be a result of two separate eruptions in close temporal proximity. Our record has a period of minimal volcanic activity be- tween 900 and 679. Other records from low accumulation Antarctic sites do see volcanic events during this period (e.g. Ferris et al., 2011) suggesting dilution effects of the higher accumulation at Law Dome make smaller or less sulphate-rich eruptions comparatively difficult to identify when coupled with the variable biogenic sulphate background. The attribution of eruption sources to sulphate spikes in the 695-year period 1995–1300 (Table 5.1) was discussed in detail by Palmer et al. (2001). We have not attributed a source to any other volcanic signatures in this record apart from the 229 event. Although the start date of this event is not clearly identifiable due to a gap in the sulphate record between 229 and 230, there is an increase in $[nssSO_4^{2-}]_{residual}$ values during 230/31. We suggest this event may be the major Holocene eruption of Taupo, New Zealand, on the evidence presented in this study, and dendrochronological work by Hogg et al., (2012) placing the date of this eruption at 232±5.

We have compared the Law Dome volcanic record to three other independent, annually dated ice core records in Table 5.1: NGRIP (Greenland) on the GICC05 timescale, Dronning Maud Land (DML) (Traufetter et al., 2004) and South Pole (SP04C5) (Ferris et al., 2011). We considered the GISP2 (Greenland) volcanic record and will discuss the record where relevant; however,

we found the chronology to be less well resolved compared to NGRIP on the GICC05 timescale. The GICC05 timescale is derived from three, well-dated, independent Greenland records (NGRIP, DYE-3 and GRIP), and are layer counted through our period of interest (Vinther et al., 2006). Of the three Greenland cores in the GICC05 timescale, only NGRIP has sulphate data through our period of interest, and was used by Gao et al., (2008) in 1-year resolution as part of their global volcanic forcing reconstruction. Here the NGRIP SO_4^{2-} data are used in full resolution.

The three cores compared in this work were chosen as they represent the most accurately dated ice core records of comparable length to Law Dome. Volcanic events identified in each record were matched based on their eruption signature characteristics (e.g. signature shape, magnitude). Figure 5.2 illustrates the number of years of difference between the dates of events in Law Dome and the 3 other ice cores. Comparisons with NGRIP show good agreement, averaging a 1-year difference, with a maximum of 3.3 years difference between volcanic deposition dates over the past 1800 years. The agreement between Law Dome and DML for the period 2000–1000 CE is good, with the exception being the 1450s eruption attributed to Kuwae (discussed below). The two records do not agree as closely from 1000–172 CE, with the DML record drifting gradually to be 22 years younger than Law Dome at the 164 (Law Dome) event. Comparisons of the Law Dome and South Pole records show the South Pole record to be more variable, drifting 10 years younger than Law Dome, before coming back into agreement for the 531 event, and drifting to become 17 years older than Law Dome by the 164 event. The 531 event signature is a distinct horizon across the three SH ice core records; therefore we are confident in our matching of this event. The error in the SP045C timescale at this event is ±15 years; therefore synchronicity with Law Dome is permissible and not outside the timescale error bounds. NGRIP has two eruptions in close proximity (529 and 533). The 529 event has the larger sulphate deposition of the two, and has been linked to the eruption of Haruna, Japan (Larsen et al., 2008; Soda, 1996), therefore we have matched our record with the 533 eruption. The accumulation rate of DML (0.073 ma^{-1} ice equivalent ; Schwander, 2003) and SP045C (0.075 ma^{-1} ice equivalent ; Ferris et al., 2011) is considerably lower than the 0.19 ma^{-1} ice equivalent of

NGRIP (Vinther et al., 2006b) and 0.70 ma^{-1} ice equivalent of Law Dome (Morgan et al., 1997). The relatively low accumulation rates at the DML and SP045C sites may increase the chances of a seasonal cycle being absent or ambiguous in nature, thus contributing to the larger error estimates for these cores relative to Law Dome and NGRIP, and may be responsible for the gradual drift in dates relative to Law Dome and NGRIP.

The accuracy of the Law Dome dating allows us to refine some of the present-best dates of volcanic eruptions. This refinement improves existing reconstructions of global volcanic forcing. The Law Dome eruption signature at 566 is in agreement with the NH date for the volcanic index of Gao et al. (2008). We do not observe any eruption in the Law Dome record that is in agreement with the SH date of 578, although we note that it is in agreement with DML. Larsen et al., (2008) suggested that the sequence of volcanic signals detected in the DML ice core at 542, 578 and 685 corresponds to the sequence of volcanic signals detected in Greenland ice cores at 533, 567 and 675. The Law Dome record essentially confirms this interpretation, as the accurate dating places the sequence at late 530, 566 and 676, closely matching the Greenland GICC05 dates. The South Pole (SP04C5) ice core (Ferris et al., 2011) has an event dated 560 with an error of 2%, which also places it within agreement of the NH dating for this eruption, and it is likely the same event in all four ice cores. The distinct volcanic horizon dated late 530 at Law Dome is in close agreement with the 533 NGRIP date for this event. There is also a volcanic event dated 531 in the SP04C5 ice core, which is likely to be the same event. The 533 and 567 CE volcanic events cannot be resolved by the GISP2 core as no measurements are available through this time period, possibly due to damaged core sections. By confirming the Larsen et al. (2008) interpretation that these three events were global, the forcing associated with these events can be more accurately represented.

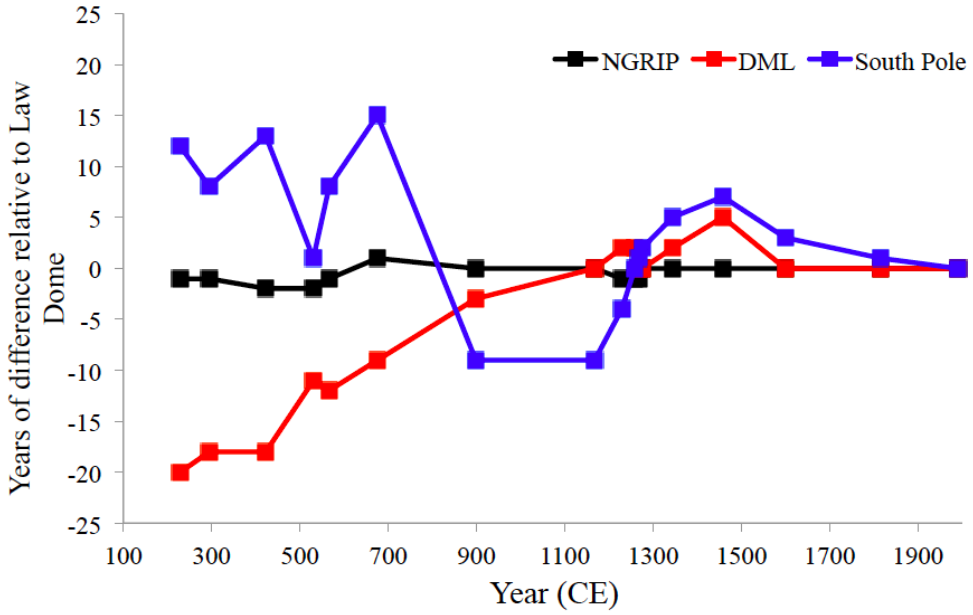

Figure 5.2 – Comparison of Law Dome to other ice core volcanic records. The number of years difference between the dating of volcanic events common to the NGRIP, DML and South Pole (SP045C) ice cores relative to Law Dome. Volcanic event dates have been matched on eruption signature. Squares indicate volcanic event dates. DML and South Pole cores are from relatively low accumulation sites (0.073 and 0.075 m yr^{-1} ice equivalent respectively), which may be a factor in the variability and drifting of those timescales relative to Law Dome (0.70 ma^{-1} ice equivalent). NGRIP at (0.19 ma^{-1} ice equivalent) still agrees well with Law Dome.

5.7 Dating of the major 1450s CE eruption

The largest sulphate spike observed in our 2000-year record is an eruption with a deposition date commencing in mid-1458, and a total deposition of 106.3 kg · SO_4^{2-} km^{-2}, over 2.6 years. Numerous ice core records have recorded a large volcanic signature during the 1450s (e.g. Delmas et al., 1992; Ferris et al., 2011; Hammer et al., 1997; Langway et al., 1995; Moore et al., 1991). Tree ring evidence for cooling, inferred from growth anomalies, has also been observed (e.g. Briffa et al., 1998; LaMarche and Hirschboeck, 1984; Salzer and Hughes, 2007). These signatures have been linked with the eruption of the Kuwae caldera, Vanuatu. Historical records of unusual weather phenomena through this period also provide further evidence for an eruption during the 1450s (Pang, 1993). Because this event is one of the largest in the last two millennia, it is important to

constrain the timing of the event so that its effect on the climate is correctly represented in global climate models.

Despite the magnitude of this event, the dating remains uncertain. Gao et al., (2006) attempted to constrain the dating by averaging the event date from multiple ice core records, concluding that Kuwae likely erupted in either 1452 or 1453. Gao et al. (2006) used 33 ice core records to arrive at a date for the Kuwae eruption signature; however, 14 of the 33 records used (Table 1; Gao et al., 2006) do not extend to 1450. Eleven of the remaining 19 records are not independent layer counted records. Dating is crucial in the case of this event, as it is necessary for the ice core timescale to be sufficiently accurate to resolve – in ice core terms – a very small time frame of 4–5 years. Layer counted records are considered more accurate than those dated using depth-accumulation estimate methods, however, require a sample resolution of 5–8 samples per year to resolve the years with confidence (Cole-Dai et al., 1997). Independence of these records is important – records that assign the date of Kuwae from some external information (e.g. Talos Dome (Stenni et al., 2002) and Plateau Remote (Cole-Dai et al., 2000)) could bias the end result when producing a mean date from all available ice cores. Taking the above into account, 8 cores of the original 33 used remain, including Law Dome (Palmer et al., 2001). The GRIP core has no volcanic signal detected be- tween 1445 and 1465 CE (Gao et al., 2006). Six ice cores – NGRIP (1458±1), GISP2 (1460±2; (Zielinski, 1995), DYE-3 (1457±2) (Clausen et al., 1997) and Crete (1458±2) (Hammer, 1980) (NH) and Siple Station (1454±3) (Cole-Dai et al., 1997) and DML B32 (1453±5) (Traufetter et al., 2004) (SH) – all have a volcanic signal that falls within the error estimate of the Law Dome date of 1458±1. Traufetter et al. (2004) attributed the large sulphate peak present in the DML B32 core at 1453, to Kuwae; however, Ruth et al., (2007), during synchronization of EPICA Dome C (EDC) core to the DML B32 timescale using volcanic markers, used the ice date 1458 for that volcanic signature, a weighted average of the Law Dome (Palmer et al., 2001) and the DML B32 (Traufetter et al., 2004) dating, suggesting some reservation about the DML B32 dating of this event.

Our layer-counted dating places this large event at 1458±1, and when considering the uncertainties with dating errors, the longest transport delay with precedent (2.5 years), the earliest eruption date based on this work is 1455. Comparisons of Law Dome and other layer-counted SH records – DML, Siple Station (Cole-Dai et al., 1997) and SP04C5 (Ferris et al., 2011) – yield deposition dates for the large sulphate peak of 1453±5 in DML, 1454±3 at Siple Station and 1453±7 in SP04C5. This allows for a maximum date range of 1448 to 1458, 1451 to 1457 and 1446 to 1460, respectively. The higher accumulation rate and larger suite of measured chemistry available at Law Dome in comparison to the other SH records allows for better constrained error, giving a deposition date range of between 1457 and 1459. By comparing errors in the records, the common time period for this event deposition is between 1457 and 1459, with the eruption between 1456 and 1458, assuming the average lag time of 1 year.

Examination of NH ice core records shows that several NH ice core records (e.g. NGRIP, Crete, Renland, NGTB20 (Greenland) and A84 (Ellesmere Island, Canada)) have evidence for two volcanic events separated by ~5 years around the 1450s (Bigler et al., 2002; Fisher et al., 1995; Gao et al., 2006). The NGRIP ice core is the best dated of these ice cores, and has two events, dated 1453±1 and 1458±1, the latter in agreement with Law Dome (Fig. 3). Accurately dated tree ring records (e.g. LaMarche and Hirschboek, 1984; Briffa et al., 1998; Salzer and Hughes, 2007) have observed anomalous tree ring growth responses in the period 1452/53. Historical evidence of unusual weather phenomena during 1453 also suggests an eruption took place at this time (Pang, 1993), but this historical evidence is primarily from the NH. The agreement between anomalous tree ring growth and the climatic effects of volcanic eruptions is well established (e.g. LaMarche and Hirschboek, 1984; Scuderi et al., 1990; Salzer and Hughes, 2007), and an example of the exceptional agreement is demonstrated by comparing our record to that of Salzer and Hughes (2007; Table 5.1). Salzer and Hughes used statistical methods to show ring-width minima years can be matched with known volcanoes or ice-core volcanic signals in 44 of 51 cases (86%) for the last millennium in their record. The link between the 1452/53 NH tree ring anomalies and the large 1450s volcanic signal in SH ice cores, now attributed to Kuwae, appears to have come from the South Pole (PS1) ice core (Delmas et al.,

1992), linking the signal in that core to the NH tree ring response dated 1452 by LaMarche and Hirschboeck, (1984). Given that the signal is one of the largest sulphate events in the past millennium in many ice cores, it might seem reasonable to link these two phenomena. However, tree ring signals capture local climate variability, potentially complicating the interpretation of tree ring records, as not all width minima and frost damaged rings are the result of volcanic activity. Additionally, Mann et al., (2012) suggested that tree ring signals may not adequately represent the climatic impact of large eruptions, due to the tree growth not responding to the post-eruption climate system. The 1815 eruption of Tambora, Indonesia, is not detected in the Salzer and Hughes record, and the authors suggested that the local climate system might not have been in a state sensitive to the climatic impact of the Tambora eruption, an interpretation that may be supported by Mann et al., (2012). We believe the early 1450s tree ring signature may have been caused by a NH-dominant eruption. The NGRIP sulphate data clearly indicate two eruptions during the 1450s, as do a number of other NH ice cores. In contrast, the majority of SH ice cores do not observe two volcanic events during the 1450s (e.g. DML, G15, PS1, Plateau Remote, SP2001C1, Talos Dome, DT-401) (Traufetter et al., 2004; Moore et al., 1991; Delmas et al., 1992; Cole-Dai et al., 2000; Stenni et al., 2001; Ren et al., 2010). The SP04C5 core (Ferris et al., 2011) has a volcanic signature preceding the large volcanic event they assigned to Kuwae by 5 years, which is the same temporal spacing as the NGRIP core.

Siple station (Cole-Dai et al., 1997) did report a possible volcanic event in 1443 CE (10 years earlier than the signal they attributed to Kuwae), though the authors point out they cannot be certain the peak did not result from high background SO_4^{2-} in a high accumulation year. At Law Dome, a sampling gap affects our volcanic record through 1452.3–1453.1, which could obscure a short duration (10 months or less) volcanic signature; therefore, we cannot exclude the possibility of a SH signature from the Law Dome record. There are no indications for a volcanic event from the residual record either side of this time period, as there was for the 229 event, which together with the short 10-month length of this gap suggests this was not a major volcanic event. Dating continuity at Law Dome is unaffected, as other data are available through this time period. The weaker

tree-ring evidence for a volcanic event in the later 1450s could be explained by tree growth not responding to the climate system, as suggested by Mann et al. (2012). We note that the record of Salzer and Hughes (2007) does have anomalous tree ring growth coincident with a late 1450s eruption – with frost-damaged rings in 1457/58 and ring width minima through the period of 1459 to 1462.

The large volcanic signal found in many ice cores from both hemispheres has been attributed to the Kuwae caldera, Vanuatu (17° S) (Monzier et al., 1994), and the sulphur-rich characteristics of the eruption (Witter and Self, 2006) support the possibility of Kuwae being responsible for that signal. However, geological evidence from Németh et al., (2007) suggests the large mid-15th century eruption was possibly smaller than first thought, or subaqueous in nature, thus limiting its effect on climate forcing. Until a direct link (e.g. tephra) between the large sulphate spike in ice cores and a volcanic centre is found, it is difficult to safely attribute a source to the 1458 event, and as such we urge caution in assigning Kuwae to any eruption signature during the 1450s. We are confident in our linking of the distinct 1450s sulphate peak in Law Dome and the 1458 NGRIP event, as the dating error constraints of the cores do not permit the 1453±1 NGRIP event being aligned with 1458±1 Law Dome event. The signatures of the 1458 events in the two cores also show similarities in peak shape (Fig. 3). A source for the 1453 eruption could be Aniakchak, Alaska, which Bigler et al., (2002) and Briffa et al., (1998) noted as a possible source of volcanic aerosols in the 1450s, while Salzer and Hughes, (2007) suggest Mount Pelée, Martinique, as another potential volcanic centre, with an eruption date of 1460±20 years (Siebert and Simkin, 2002).

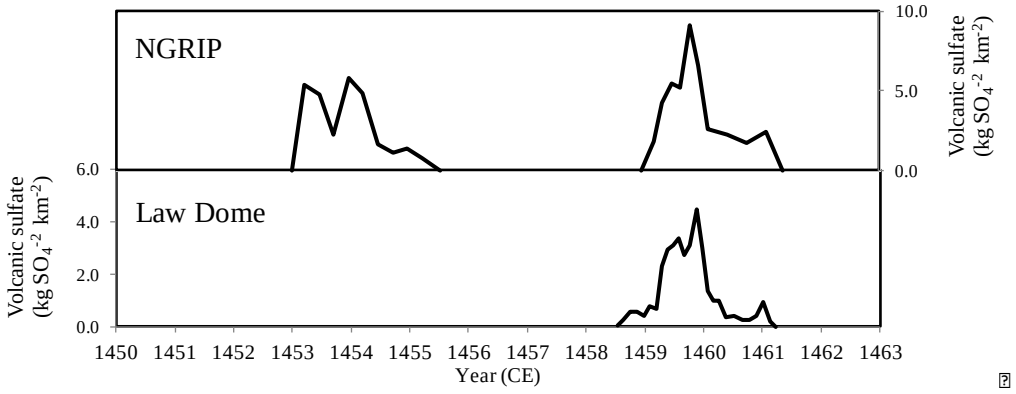

Figure 5.3 – The Law Dome and NGRIP volcanic sulphate records between 1450 –1460. The two distinct volcanic peaks in NGRIP are dated 1453 and 1458 CE; the single clear peak in Law Dome is dated 1458 CE. The two NGRIP peaks are evidence of two separate volcanic eruptions during the 1450s CE.

5.8 Conclusion

The Law Dome represents the currently most accurately dated Antarctic ice core, with error estimates lower than the DML and South Pole ice cores. Using this independently dated, annually resolved ice core record from Law Dome, we have identified and dated 45 volcanic signatures over the past 2000 years. A comparison with volcanic horizons from the NGRIP ice core, on the well-dated GICC05 timescale, shows Law Dome to be in good agreement, with the age difference between global volcanic horizons of ±3 years or better. The improved dating of volcanic events in the first millennium for the SH allows better correlation between SH ice cores, and will allow current volcanic forcing datasets to be updated and extended. This study has confirmed that three 6–7th century eruptions can be synchronized to Greenland records; thus they can be identified as global horizons, which has implications for the forcing calculations related to these three eruptions.

We have also presented a discussion on the dating of the global volcanic event attributed to the Kuwae caldera. This study dates this event at 1458±1, which is in agreement with the GICC05 timescale. The NGRIP sulphate data have two volcanic signatures dated 1453±1 and 1458±1. Two volcanic signatures ~5 years apart are evidenced in many NH ice cores, but only the SP04C5 (Ferris et

al., 2011) has a clear second signal in the SH, which suggests a NH-dominant eruption in the early 1450s. We contend this earlier eruption was likely responsible for the anomalous NH tree ring growth and historical documentation of unusual weather phenomena during 1452/53. By comparing the overlap in error estimates of our Law Dome record and the other best dated SH ice cores (DML and South Pole), we conclude the globally significant volcanic horizon of the 1450s erupted between 1456 and 1458, most likely between mid-1457 and 1458. This information can be used to revise the current volcanic forcing estimate datasets.

5.9 Acknowledgements

The authors wish to acknowledge the contribution of Vin Morgan, the expeditioners involved in drilling the ice cores and the laboratory support staff. C. T. Plummer also acknowledges an Australian Postgraduate Award. Edited by: J. Luterbacher.

Table 5.1 – Comparisons of the Law Dome volcanic event start dates with other independently dated records.

Volcanic Event	Law Dome ice date	NGRIP[1]	DML[2]	South Pole[3]	NH tree ring signature[4]
Pinatubo/Cerro Hudson	1991.7	1992	1992	1991	–
El Chichón	1984.5	–	1982	–	–
Agung	1964.1	–	1964	1963	*1965*
Tarawera	1887.5	–	1886	–	–
Krakatau	1884.5	1884	1884	1887	*1884*
Cosiguina	1836.7	1835	1835	1836	1836
Galunggung	1823.4	–	–	–	–
Tambora	1815.8	1816	1816	1815	–
Unidentified	1809.7	1809	1809	1808	*1809*
Unidentified	1695.3 ± 1	1694	1695	1687	–
Gamkonora	1674.3 ± 1	–	1676	1668	1675
Parker	1641.8 ± 1	1641	1640	1634	1641
Huaynaputina	1600.7 ± 1	1601	1601	1600	*1601*, 1602
Ruiz	1596.7 ± 1	–	1596	1594	*1596*
Raung	1595.5 ± 1	–	–	–	–
Kelut	1587.3 ± 1	1586	–	–	–
Billy Mitchell	1583.6 ± 1	1584	–	–	–
Kuwae?	1458.5 ± 1	1458	–	–	*1457*, 1458–62
Kuwae?	–	1453	1453	1453	*1453*
Unidentified	1344.0 ± 1	1344	1343	1334	1342
Unidentified	1275.6 ± 1	1276	1276	1274	*1275, 1277*
Unidentified	1268.4 ± 1	–	1268	1269	–
Unidentified	1257.4 ± 1	1259	1256	1260	1257
Unidentified	1229.2 ± 1	1230	1227	1235	1230
Unidentified	1170.7 ± 1	1168	1168	1176	*1171*
Unidentified	1014.6 ± 1	–	–	–	*1015*
Unidentified	956.8 ± 1	–	961		*959*
Unidentified	924.5 ± 1	–	–	–	–
Unidentified	900.5 ± 1	897	–	908	900–903
Unidentified	679.2 −4/+1	–	–	–	*681*
Unidentified	676.5 −4/+1	675	685	662	674
Unidentified	566.3 −5/+1	567	578	560	569
Unidentified	530.9 −5/+1	533	542	531	*532*
Unidentified	449.7 −6/+2	–		446	451
Unidentified	422.7 −6/+2	425	441	411	*421*
Unidentified	343.7 −6/+2	–	–	–	344
Unidentified	295.4 −7/+3	297	315	288	–
Unidentified	258.7 −7/+3	258	–	–	–
Taupo?	∼ 229 −7/+3	230	249	217	*230*
Unidentified	198.4 −7/+3	–	–	181	–
Unknown	163.8 −7/+3		186		–
Unknown	136.4 −7/+3				137
Unknown	117.5 −7/+4				*119*
Unknown	52.5 −7/+4				–
Unknown	−2.5 −7/+4				–

All dates CE, and represent the date the volcanic signal is found in each core.
[1] See Appendix A for dating methods.
[2] Traufetter et al. (2004).
[3] Ferris et al. (2011).
[4] Salzer and Hughes (2007), tree ring growth minima (plain text) and and frost damaged rings (italics).
A "–" indicates the volcanic event is not observed in that record; no mark indicates the record does not cover this period. Unknown events are those not previously reported; unidentified are those previously recorded, but the eruption source is not known.

Table 5.2 – Volcanic sulphate deposition at Law Dome. For events identified as inter-hemispheric, NGRIP depositional data are provided also.

Event	Law Dome			NGRIP		
	Start Date	End Date	Deposition ($kg\,SO_4\,km^{-2}$)	Start Date	End Date	Deposition ($kg\,SO_4\,km^{-2}$)
Pinatubo/Cerro Hudson	1991.7	1993.9	19.1 ± 0.8	1992.1	1992.4	5.5 ± 1.9
El Chichón	1984.5	1984.8	< 5.0	–	–	–
Agung	1964.1	1965.2	10.1 ± 0.5	–	–	–
Tarawera	1887.5	1888.2	7.8 ± 0.5	–	–	–
Krakatau	1884.5	1885.9	16.8 ± 0.7	1883.5	1886.2	15.4 ± 2.7
Cosigüina	1836.7	1837.8	8.7 ± 0.5	1835.3	1838.4	33.4 ± 2.1
Galunggung	1823.4	1823.9	6.1 ± 0.9	–	–	–
Tambora	1815.8	1819.3	57.2 ± 1.5	1816.1	1817.9	40.3 ± 1.8
Unidentified	1809.7	1811.1	24.6 ± 1.3	1809.3	1811.8	38.6 ± 2.2
Unidentified	1695.3	1697.2	28.2 ± 1.3	1694.1	1698.0	37.2 ± 2.1
Gamkonora	1674.3	1676.0	14.7 ± 0.5	–	–	–
Parker	1641.8	1643.3	21.3 ± 0.8	1640.9	1643.6	41.6 ± 3.0
Huaynaputina	1600.7	*	*	1601.1	1603.7	48.0 ± 2.4
Ruiz	1596.7	1598.4	18.8 ± 1.6	–	–	–
Raung	1595.5	1596.1	< 5.0	–	–	–
Kelut	1587.3	1588.3	7.9 ± 0.7	1586.0	1586.6	5.4 ± 1.1
Billy Mitchell	1583.6	1584.1	< 5.0	1583.5	1583.7	2.8 ± 0.7
Kuwae?	1458.5	1461.1	106.3 ± 4.0	1459.2	1461.4	41.4 ± 1.8
Kuwae?	–	–	–	1453.2	1455.2	27.99 ± 1.8
Unidentified	1344.0	1346.2	24.6 ± 1.0	1344.9	1347.7	33.3 ± 2.4
Unidentified	1275.6	1278.0	55.5 ± 1.4	1277.3	1278.5	8.6 ± 1.4
Unidentified	1268.4	1269.4	32.3 ± 2.6	–	–	–
Unidentified	1257.4	1259.2	101.1 ± 4.3	1258.1	1261.8	98.6 ± 2.2
Unidentified	1229.2	1231.1	26.9 ± 1.0	1229.5	1232.7	61.3 ± 3.0
Unidentified	1170.7	1171.9	14.5 ± 0.5	1167.4	1170.4	36.5 ± 1.8
Unidentified	1014.6	1015.9	11.0 ± 0.9	–	–	–
Unidentified	956.8	958.0	15.5 ± 1.1	–	–	–
Unidentified	924.5	925.4	11.8 ± 0.8	–	–	–
Unidentified	900.5	901.1	15.2 ± 0.9	–	–	–
Unidentified	679.2	681.1	19.4 ± 0.9	–	–	–
Unidentified	676.5	677.7	29.8 ± 2.0	674.2	676.7	31.1 ± 2.5
Unidentified	566.3	567.7	25.2 ± 1.5	566.9	569.4	42.9 ± 2.5
Unidentified	530.9	533.2	37.0 ± 1.9	532.1	536.5	56.2 ± 3.7
Unidentified	449.7	452.3	27.9 ± 1.7	–	–	–
Unidentified**	422.7	427.0	63.1 ± 1.6	425.1	426.9	17.5 ± 1.5
Unidentified	343.7	345.2	16.0 ± 1.3	–	–	–
Unidentified	295.4	297.0	27.6 ± 1.6	297.1	297.7	8.9 ± 1.3
Unidentified	258.7	260.0	24.5 ± 1.6	258.1	262.1	55.4 ± 2.9
Taupo?	~ 229	232.3	*	230.1	231.6	10.8 ± 2.0
Unidentified	198.4	200.0	17.1 ± 0.7	–	–	–
Unidentified	163.8	164.9	29.9 ± 2.5			
Unknown	136.4	137.0	13.2 ± 1.4			
Unknown	117.5	119.3	12.7 ± 0.8			
Unknown	52.5	54.1	14.4 ± 0.6			
Unknown	-2.5	1.3	19.5 ± 1.5			

All dates CE.
* Eruption signature incomplete.
** Possibly two close eruptions.
A "–" indicates the volcanic event is not observed in that record. The NGRIP record does extend beyond 186 CE. Unknown events are those not previously reported; unidentified are those previously recorded, but the eruption source is not known.

Chapter 6 – Conclusion

The ice core records from Law Dome, East Antarctica have been analysed for an array of chemistry species. This study has filled a gap in the DSS Holocene record by new analysis of 187 metres of existing DSS ice, covering the time period 2,140 – 4,453 b2k. The high latitude Southern Hemisphere in particular lacks adequate spatial and temporal coverage of high resolution data for determining long term climate patterns, therefore the addition of this new ice core data is a very important step. An extensive effort to annually layer count the Law Dome record has extended the high-resolution record to from 1300 CE to 333 BCE with an error of +13/-7; comparable or better than the few long Antarctic ice core records currently available. The high-resolution layer counted Law Dome record has been used to construct new millennial-length reconstructions of ENSO and South Eastern Australia rainfall patterns beyond the instrumental period (Tozer et al., 2015; Vance et al., 2015, 2013), contributed to a 2000 year Antarctic temperature reconstruction (PAGES 2k Consortium, 2013) and establish an accurate accumulation history for Law Dome (Roberts et al., 2015). By using the accurate annual dating of Law Dome, it was demonstrated that the major 1450s eruption of Kuwae, Vanuatu, erupted between 1456 and 1458 CE rather than the earlier estimate of 1453 CE and that a smaller event occurred at 1453 CE, which may have had greater influence on the NH-dominated tree ring reconstructions of temperature available at the time. This new information has been reflected in updated volcanic forcing estimates which are used by the model community (Sigl et al., 2015). Beyond the annually layer counted period, the identification of volcanic events has improved the Law Dome timescale through additional dating constraints by synchronisation to other records.

The Holocene records of sea salt, sulphate and MSA have been investigated for long term environmental changes. Sea salt concentrations were lowest at 12,000 b2k, increasing 117% to modern day levels which were reached by 5,000 b2k. Sea salt concentrations declined with increasing accumulation through the LGM-Holocene transition, indicative of a dry-depositional regime. From 12,000 b2k sea salt concentrations increased in line with accumulation, suggesting that the site was increasingly dominated by wet aerosol deposition.

Sulphate concentrations remained steady throughout the Holocene, increasing 40% since 3,250 b2k. The MSA record has an early Holocene maximum at 9,000 b2k, 660 years after the isotope maximum associated with early Holocene optimum as recorded at DSS. The MSA record also has a strong decline between 5,100 and 5,650 b2k, with the lowest Holocene MSA levels at 5,250 b2k. The timing of this decline is broadly consistent with abrupt changes in the Siple Dome MSA and EDML sea salt records (Saltzman et al., 2006; Fischer et al., 2007a) and a period of cooler sea surface temperatures in the Atlantic sector of the Southern Ocean (Divine et al., 2010).

Aerosols at DSS today are essentially fully wet deposited (van Ommen et al., 2004). DSS at the Last Glacial Maximum was dominated by dry deposition of aerosols. The sodium flux record indicates the transition to the wet depositional regime was underway by 12,000 b2k and became fully wet deposited between 8-7,000 b2k. The timing of this is consistent with modelling and paleorecords showing a southward shift in zonal westerlies and storm track closer to the coast and increased cyclogenesis (e.g. Kim et al., 2012; Renssen et al., 2005; Varma et al., 2012), increasing accumulation and enhancing sea salt aerosol transport to DSS.

The ratio of SO_4^{2-}/Na^+ ratio today varies as a function of distance to the coast and altitude, with greater values moving inland as larger sea salt particles drop out. The SO_4^{2-}/Na^+ ratio has changed from 0.38 at 12,000 b2k to 0.23 today. The ratio change was driven by increasing sea salt concentrations while sulphate concentrations remained stable. The ratio change may be interpreted as DSS becoming relatively more coastal with a contracting ice sheet and increasing cyclonic activity over the site increasing the sea salt load. The physical reorganisation of Law Dome was completed by ~8,000 b2k, but sea salt concentrations continued to rise after this time, pointing to other factors such as continuing changes in cyclonic activity impacting on sea salt deposition to DSS.

Comparisons of DSS sea salts and Holocene SST reconstructions around the Southern Ocean show an inverse trend, but the strength of correlations between locations is variable. Correlation is strongest with the TN057-13PC4 off the Dronning Maud Land coast, but a moderate correlation is found in locations

as far north as New Zealand. The regional relationship between SST reconstructions and DSS sea salts requires further exploration as to the exact mechanisms driving these processes. An inverse correlation is consistent with increased zonal wind over the Southern Ocean and/or movement of the wind belt into the source region for Law Dome aerosols simultaneously depressing SST and entraining more sea salt aerosols. Wind driven upwelling and feedbacks associated with this have been proposed as drivers of SST changes (e.g. Anderson et al., 2009; Divine et al., 2010; Etourneau et al., 2013; Shevenell et al., 2011) with currents acting to distribute heat flux regionally across the Southern Ocean. The ultimate driver of these processes is likely to be solar insolation changes and its global effects on oceanic and atmospheric circulation patterns.

The sea salt-sea ice presence relationship is not well defined and few sea ice reconstruction records are available through the Holocene. The reconfiguration of Law Dome to present conditions was reached between 7-8,000 b2k. The correlation between SST and DSS sea salt concentrations persists beyond this time. A correlation with the TN057 marine sediment core derived proxy records off the Dronning Maud Land coast suggests that sea ice extent either varied on regional scales around the EAIS or is responding to other factors. The stronger relationship between SST and sea salt concentration suggests DSS may be more responsive to SST than sea ice presence as is seen at inland ice core sites.

MSA concentrations around Law Dome are positively correlated with sea ice extent (and by extension melting of that sea ice extent) in the area 80-140 degrees in the present era (Curran et al., 2003). However, there is no consistent relationship between MSA, SST and sea ice presence on a Holocene-length timescale evident in this study from the few Holocene-length records available. Formation of MSA is a complicated process dependent on DMS production, flux to the atmosphere, oxidation in the atmosphere and post depositional movement and readmission to the atmosphere. It is not possible to make a definitive conclusion on the MSA record from DSS without further understanding these processes and without better understanding what MSA is responding to on 100-year periodicity.

Chapter 7 – Recommendations for further research

7.1 Improving data resolution

As the Holocene becomes a key focus area for understanding a warming climate, obtaining more detailed climate information from this period is of increasing importance. Records of seasonal snowfall and trace chemistry offer potential to develop proxies that go beyond the limited instrumental period thus putting current changes into long term context. The seasonal dating in this work (Chapter 3) directly contributed to this endeavour through records of volcanism, snowfall and El Niño–Southern Oscillation (ENSO) and Interdecadal Pacific Oscillation (IPO) reconstructions. Annual layer counting (ALC) beyond 2332 b2k would greatly assist in expanding paleovolcanic records by improving dating and better accounting for their impacts on global climates as a natural forcing. Annual layer counting at DSS using the isotope record has been shown feasible to at least 6,900 b2k (van Ommen et al., 2004). The viability of a high-resolution sampling regime for the Holocene should be investigated for trace ion chemistry also. Seasonal chemistry data through the Holocene offers an improved and more detailed volcanic history for the Southern Hemisphere. Details on SAM and ENSO climate modes and possible clues as to their genesis. Although MSA will have been lost from the DSS ice core in storage, qualitative interpretations of sea ice extent may be possible. Timing of local site changes and fractionation processes might be better constrained.

The ability to annually layer count the chemical stratigraphy in ice is hampered by progressively thinning layers and decreasing sample volumes with depth. Continuous flow analysis is a common approach used for ice core analysis that could be applied to DSS cores. Continuous flow analysis works by producing a constant stream of water by melting successive ice core samples and dividing the stream between multiple instruments for measurement. This achieves a finer resolution than conventional discrete sampling as used in this study.

Recent advances using capillary ion chromatograph systems have enabled measurement of major trace ion species in ice cores from aliquots of 300μL (e.g. Rodriguez et al., 2015). Due to the progressive thinning of ice layers it is

necessary to reduce sample sizes to maintain data resolution, thus reducing sample volumes. With capillary IC requiring less sample volume than conventional IC methods, it will enable analysis at resolutions not currently possible. The small volume analysis would allow for triplicate measurements on <1 mL of sample. Replicate measurements are not routine with conventional IC methods due to low sample volumes. The ability to provide replicates could improve reliability of ice core data. Capillary IC should be evaluated for routine use in future ice core analysis.

With progressively finer sampling it will be necessary to establish a minimum level at which an ice core can reliably record an annual signal. Different ionic species will have different physical limits restricting how finely the ice can be sampled and still give reliable seasonality without interference from diffusion or movement along grain boundaries. New sampling techniques appropriate to the required sampling regime should also be developed, maintaining the clean techniques necessary for ultra-low level trace ion measurements required for ice core analysis.

The uncertainty surrounding the dating accuracy of the DSS ice core could be improved by analysis for beryllium-10 (^{10}Be) events dated between 774-775 CE and 993-994 CE. These dating horizons have been used to assess the layer counted timescale at ice cores sites NGRIP, NEEM-2011-S1 and WAIS divide (Sigl et al., 2015). ^{10}Be analysis would serve as an independent check of the layer count at DSS.

7.2 Ocean-atmosphere linkages

Links between marine sediment core reconstructions of sea ice presence and sea surface temperature (SST) and ice core chemistry demonstrate regional connections between atmospheric composition and oceans. Sediment cores closer to Law Dome with sea ice presence information would provide insight into timing of advance and retreat of the Wilkes Land ice margin, and establish better constraints on extent and seasonality, two parameters which have significant impact on albedo and radiation budgets for determination of heat fluxes. The

regional extent of the SST and DSS sea salt concentration relationship should be further investigated by incorporating more SST reconstructions. This information would assist in identifying the underlying mechanism, its drivers and on what scale they operate on.

7.3 A new ice core

DSSmain has significant patches of poor ice quality from brittle ice. At depth, increasing ice overburden pressurizes trapped air bubbles causing fracture of cores upon exposure to atmospheric pressure (Neff, 2014). Thermal and physical shocks also play a role. Fractured ice cores degrade analyses, reducing resolution and causing contamination. This made the task of synchronising the DSS volcanic record to the AICC2012 timescale difficult. The period from 4,055 to 8,178 b2k is one of the more poorly constrained whilst conversely one which experiences many significant changes. The drilling process provides important opportunities to reduce brittle fractures in ice cores, and any new deep core from Law Dome would benefit from advances in technology and experiences from other deep drilling campaigns since DSSmain was drilled. At WAIS divide, during the brittle ice zone, the drill would break the core in to 3 pieces at depth before returning the ice to the surface, reducing the need to handle long cores at the surface (Souney et al., 2014). To reduce thermal shocks cores were stored at temperatures close to that at the depth which they are drilled. Other steps that can be taken in the transport phase include delaying the transport time to allow for the ice to relax and the use of tight-fitting nylon netting to preserve stratigraphy and prevent further damage of fragmented sections during transport (Neff, 2014).

MSA is easily lost to the atmosphere during ice core storage (Abram et al., 2008; Roberts et al., 2009). Parts of the DSSmain core have been stored over 25 years before analysis, limiting our ability to interpret the MSA record. Comparisons with modern day MSA concentrations can only be considered relatively rather than absolutely for much of the Holocene. It has been reported that ice core samples that had been cut, melted and refrozen show no MSA loss after 15 years of frozen storage (Abram et al., 2013). Therefore it is recommended

for discrete analysis that ice core samples are melted and refrozen to preserve MSA. For CFA analysis of MSA it is recommended that any new core from DSS be analysed as quickly as possible to minimise losses.

References

Abelmann, A., Gersonde, R., Cortese, G., Kuhn, G., Smetacek, V., 2006. Extensive phytoplankton blooms in the Atlantic sector of the glacial Southern Ocean. Paleoceanography 21, 1–9. DOI:10.1029/2005PA001199

Abram, N.J., Curran, M.A.J., Mulvaney, R., Vance, T., 2008. The preservation of methanesulphonic acid in frozen ice-core samples. J. Glaciol. 54, 680–684. DOI:10.3189/002214308786570890

Abram, N.J., Wolff, E.W., Curran, M.A.J., 2013. A review of sea ice proxy information from polar ice cores. Quat. Sci. Rev. 79, 168–183. DOI:10.1016/j.quascirev.2013.01.011

Aciego, S., Bourdon, B., Schwander, J., Baur, H., Forieri, A., 2011. Toward a radiometric ice clock: uranium ages of the Dome C ice core. Quat. Sci. Rev. 30, 2389–2397. DOI:10.1016/j.quascirev.2011.06.008

Adams, N., 1996. The detection and analysis of gravity wave observed over Casey in East Antarctica using radiosonde data. Aust. Meteorol. Mag. 45, 219–232.

Ahrens, C.D., 2012. Essentials of Meteorology: An Invitation To The Atmosphere, 6th ed. Brooks/Cole, Belmont.

Aizen, V.B., Aizen, E.M., Melack, J.M., Kreutz, K.J., Cecil, L.D., 2004. Association between atmospheric circulation patterns and firn-ice core records from the Inilchek glacierized area, central Tien Shan, Asia. J. Geophys. Res. D Atmos. 109, D08304. DOI:10.1029/2003JD003894

Albert, M.R., 2002. Effects of snow and firn ventilation on sublimation rates. Ann. Glaciol. 35, 52–56.

Alley, R.B., Ágústsdóttir, A.M., 2005. The 8k event: Cause and consequences of a major Holocene abrupt climate change. Quat. Sci. Rev. 24, 1123–1149. DOI:10.1016/j.quascirev.2004.12.004

Alley, R.B., Mayewski, P.A., Sowers, T., Stuiver, M., Taylor, K.C., Clark, P.U., 1997a. Holocene climatic instability: A prominent, widespread event 8200 yr ago. Geology 25, 483–486. DOI:10.1130/0091-7613

Alley, R.B., Shuman, C.A., Meese, D.A., Gow, A.J., Taylor, K.C., Cuffey, K.M., Fitzpatrick, J.J., Grootes, P.M., Zielinski, G.A., Ram, M., Spinelli, G., Elder, B., 1997b. Visual-stratigraphic dating of the GISP2 ice core: Basis, reproducibility, and application. J. Geophys. Res. 102, 26367. DOI:10.1029/96JC03837

Allison, I., Wendler, G., Radok, U., 1993. Climatology of the East Antarctic ice sheet (100°E to 140°E) derived from automatic weather stations. J. Geophys. Res. 98, 8815. DOI:10.1029/93JD00104

Allison, L.C., Johnson, H.L., Marshall, D.P., Munday, D.R., 2010. Where do winds drive the antarctic circumpolar current? Geophys. Res. Lett. 37, 1–5. DOI:10.1029/2010GL043355

Alvarez-Aviles, L., Simpson, W.R., Douglas, T.A., Sturm, M., Perovich, D.,

Domine, F., 2008. Frost flower chemical composition during growth and its implications for aerosol production and bromine activation. J. Geophys. Res. 113, D21304. DOI:10.1029/2008JD010277

Anderson, R.F., Ali, S., Bradtmiller, L.I., Nielsen, S.H.H., Fleisher, M.Q., Anderson, B.E., Burckle, L.H., 2009. Wind-driven upwelling in the Southern Ocean and the deglacial rise in atmospheric CO2. Science 323, 1443–1448. DOI:10.1126/science.1167441

Armbruster, D.A., Pry, T., 2008. Limit of blank, limit of detection and limit of quantitation. Clin. Biochem. Rev. 29 Suppl 1, S49-52.

Arsene, C., Barnes, I., Becker, K.H., 1999. FT-IR product study of the photo-oxidation of dimethyl sulfide: Temperature and O2 partial pressure dependence. Phys. Chem. Chem. Phys. 1, 5463–5470.

Baillie, M.G.L., McAneney, J., 2015. Tree ring effects and ice core acidities clarify the volcanic record of the first millennium. Clim. Past 11, 105–114. DOI:10.5194/cp-11-105-2015

Bard, E., Raisbeck, G., Yiou, F., Jouzel, J., 2000. Solar irradiance during the last 1200 years based on cosmogenic nuclides. Tellus B 52, 985–992. DOI:10.1034/j.1600-0889.2000.d01-7.x

Bates, T.S., Calhoun, J. a., Quinn, P.K., 1992. Variations in the methanesulfonate to sulfate molar ratio in submicrometer marine aerosol particles over the south Pacific Ocean. J. Geophys. Res. Atmos. 97, 9859–9865. DOI:10.1029/92JD00411

Becagli, S., Castellano, E., Cerri, O., Curran, M., Frezzotti, M., Marino, F., Morganti, A., Proposito, M., Severi, M., Traversi, R., Udisti, R., 2009. Methanesulphonic acid (MSA) stratigraphy from a Talos Dome ice core as a tool in depicting sea ice changes and southern atmospheric circulation over the previous 140 years. Atmos. Environ. 43, 1051–1058. DOI:10.1016/j.atmosenv.2008.11.015

Benassai, S., Becagli, S., Gragnani, R., Magand, O., Proposito, M., Fattori, I., Traversi, R., Udisti, R., 2005. Sea-spray deposition in Antarctic coastal and plateau areas from ITASE traverses. Ann. Glaciol. 41, 32–40. DOI:10.3189/172756405781813285

Berger, A., Loutre, M.F., 1991. Insolation values for the climate of the last 10 million years. Quat. Sci. Rev. 10, 297–317. DOI:10.1016/0277-3791(91)90033-Q

Bergin, M.H., Jaffrezo, J., Davidson, C.I., Dibb, J.E., Hillamo, R., Maenhaut, W., Kuhns, H.D., Makela, T., 1995. The contributions of snow, fog, and dry deposition to the summer flux of anions and cations at Summit, Greenland. J. Geophys. Res. 100, 275–288.

Bertler, N., Mayewski, P.A., Aristarain, A., Barrett, P., Becagli, S., Bernardo, R., Bo, S., Xiao, C., Curran, M., Qin, D., Dixon, D., Ferron, F., Fischer, H., Frey, M., Frezzotti, M., Fundel, F., Genthon, C., Gragnani, R., Hamilton, G., Handley, M., Hong, S., Isaksson, E., Kang, J., Ren, J., Kamiyama, K., Kanamori, S., Ka, E., Kaspari, S., Kreutz, K., Kurbatov, A., Meyerson, E., Ming, Y., Zhang, M., Motoyama, H., Mulvaney, R.,

Oerter, H., Osterberg, E., Smith, B., Sneed, S., Proposito, M., Pyne, A., Ruth, U., Simo, J., Williamson, B., Winther, J.-G., Li, Y., Wolff, E., Li, Z., Zielinski, A., 2005. Snow chemistry across Antarctica. Ann. Glaciol. 41, 167–179.

Bigler, M., Wagenbach, D., Fischer, H., Kipfstuhl, J., Miller, H., Sommer, S., Stauffer, B., 2002. Sulphate record from a northeast Greenland ice core over the last 1200 years based on continuous flow analysis. Ann. Glaciol. 35, 250–256.

Bradley, R.S., 1999. Paleoclimatology: reconstructing climates of the Quaternary, 2nd ed. Academic Press, San Diego.

Briffa, K.R., Jones, P.D., Osborn, T.J., 1998. Influence of volcanic eruptions on Northern Hemisphere summer temperature over the past 600 years. Nature 393, 450–455. DOI:10.1038/30943

Broecker, W.S., Peng, T.-H., 1982. Tracers In The Sea. Lamont-Doherty Geological Observatory, Palisades.

Bromwich, D.H., 1988. Snowfall in high southern latitudes. Rev. Geophys. 26, 149. DOI:10.1029/RG026i001p00149

Buck, C.F., Mayewski, P.A., Spencer, M.J., Whitlow, S., Twickler, M.S., Barrett, D., 1992. Determination of major ions in snow and ice cores by ion chromatography. J. Chromatogr. A 594, 225–228. DOI:10.1016/0021-9673(92)80334-Q

Carleton, A.M., 1989. Antarctic Sea-Ice relationships with indices of the atmosphere cirulation of the Southern Hemisphere. Clim. Dyn. 3, 207–220.

Casey, K.A., Fudge, T.J., Neumann, T.A., Steig, E.J., Cavitte, M.G.P., Blankenship, D.D., 2014. The 1500m South Pole ice core: recovering a 40 ka environmental record. Ann. Glaciol. 55, 137–146. DOI:10.3189/2014AoG68A016

Cayan, D.R., 1992. Latent and Sensible Heat Flux Anomalies over the Northern Oceans: Driving the Sea Surface Temperature. J. Phys. Oceanogr.

Charlson, R.J., Lovelock, J.E., Andreae, M.O., Warren, S.G., 1987. Oceanic phytoplankton, atmospheric sulphur, cloud albedo and climate. Nature 326, 655–661. DOI:10.1038/326655a0

Chiang, J.C.H., Bitz, C.M., 2005. Influence of high latitude ice cover on the marine Intertropical Convergence Zone. Clim. Dyn. 25, 477–496. DOI:10.1007/s00382-005-0040-5

Clark, P.U., Dyke, A.S., Shakun, J.D., Carlson, A.E., Clark, J., Wohlfarth, B., Mitrovica, J.X., Hostetler, S.W., McCabe, A.M., 2009. The Last Glacial Maximum. Science 325, 710–4. DOI:10.1126/science.1172873

Clausen, H.B., Hammer, C.U., Hvidberg, C.S., Dahl-Jensen, D., Steffensen, J.P., Kipfstuhl, J., Legrand, M., 1997. A comparison of the volcanic records over the past 4000 years from the Greenland Ice Core Project and Dye 3. J. Geophys. Res. 102, 26707–26723.

Clement, A.C., Seager, R., Cane, M.A., 1999. Orbital controls on the El

Niño/Southern Oscillation and the tropical climate. Paleoceanography 14, 441. DOI:10.1029/1999PA900013

CLIMAP, P.M., 1981. Seasonal reconstructions of the Earth's surface at the last glacial maximum. Geol. Soc. Am. Map Chart Ser. 36, 1–18.

Colbeck, S.C., 1989. Air movement in snow due to windpumping. J. Glaciol. 35, 209–213.

Cole-Dai, J., Mosley-Thompson, E., Thompson, L.G., 1997. Annually resolved southern hemisphere volcanic history from two Antarctic ice cores. J. Geophys. Res. 102, 16761. DOI:10.1029/97JD01394

Cole-Dai, J., Mosley-Thompson, E., Wight, S.P., Thompson, L.G., 2000. A 4100-year record of explosive volcanism from an East Antarctica ice core. J. Geophys. Res. 105, D14, 24431-24441.

Consortium, P. 2k, 2013. Continental-scale temperature variability during the past two millennia. Nat. Geosci. 6, 339–346. DOI:10.1038/ngeo1797

Crosta, X., Pichon, J.-J., Burckle, L.H., 1998. Reappraisal of Antarctic seasonal sea-ice at the Last Glacial Maximum. Geophys. Res. Lett. 25, 2703–2706. DOI:10.1029/98GL02012

Crowley, T.J., Quinn, T.M., Taylor, F.W., Henin, C., Joannot, P., 1997. Evidence for a volcanic cooling signal in a 335-year coral record from New Caledonia. Paleoceanography 12, 633–639. DOI:10.1029/97PA01348

Crowley, T.J., Unterman, M.B., 2012. Technical details concerning development of a 1200-yr proxy index for global volcanism. Earth Syst. Sci. Data Discuss. 5, 1–28. DOI:10.5194/essdd-5-1-2012

Crowley, T.J., Zielinski, G.A., Vinther, B., Udisti, R., Kreutz, K., Cole-Dai, J., Castellano, E., 2008. Volcanism and the Little Ice Age. PAGES News 16, 22–23.

Cunningham, J., Waddington, E.D., 1993. Air flow and dry deposition of non-sea salt sulfate in polar firn: Paleoclimatic implications. Atmos. Environ. Part A. Gen. Top. 27, 2943–2956. DOI:10.1016/0960-1686(93)90327-U

Curran, M.A.J., Jones, G.B., 2000. Dimethyl sulfide in the Southern Ocean: Seasonality and flux. J. Geophys. Res. 105, D16, 20451. DOI:10.1029/2000JD900176

Curran, M.A.J., Palmer, A.S., 2001. Suppressed ion chromatography methods for the routine determination of ultra low level anions and cations in ice cores. J. Chromatogr. A 919, 107–113. DOI:10.1016/S0021-9673(01)00790-7

Curran, M.A.J., Palmer, A.S., van Ommen, T.D., Morgan, V.I., Phillips, K.L., McMorrow, A.J., Mayewski, P.A., 2002. Post-depositional movement of methanesulphonic acid at Law Dome , Antarctica , and the influence of accumulation rate. Ann. Glaciol. 35, 333–339.

Curran, M.A.J., van Ommen, T.D., Morgan, V., 1998. Seasonal characteristics of the major ions in the high accumulation Dome Summit South ice core, Law Dome, Antarctica. Ann. Glaciol. 27, 385–390.

Curran, M.A.J., van Ommen, T.D., Morgan, V.I., Phillips, K.L., Palmer, A.S., 2003. Ice core evidence for Antarctic sea ice decline since the 1950s. Science 302, 1203–1206. DOI:10.1126/science.1087888

Dansgaard, W., 1964. Stable isotopes in precipitation. Tellus 16, 436–468. DOI:10.1111/j.2153-3490.1964.tb00181.x

Dansgaard, W., Johnsen, S.J., 1969. A Flow Model and a Time Scale for the Ice Core from Camp Century, Greenland. J. Glaciol. 8, 215–223.

Davidson, C.I., Bergin, M.H., Kuhns, H.D., 1996. The Deposition of Particles and Gases to Ice Sheets. In: Wolff, E.W., Bales, R.C. (Eds.), Chemical Exchange Between the Atmosphere and Polar Snow. Springer, New York, pp. 275–306.

Davies, T.D., Vincent, C.E., Brimblecombe, P., 1982. Preferential elution of strong acids from a Norwegian ice cap. Nature 300, 161–163. DOI:10.1038/300161a0

de Menocal, P.B., 2015. Palaeoclimate: End of the African Humid Period. Nat. Geosci. 8, 86–87. DOI:10.1038/ngeo2355

Delmas, R.J., Kirchner, S., Palais, J.M., Petit, J.-R., 1992. 1000 years of explosive volcanism recorded at the South Pole. Tellus B 44, 335–350. DOI:10.1034/j.1600-0889.1992.00011.x

deMenocal, P., Bond, G., 1997. Holocene Climate Less Stable That Previously Thought. EOS, Trans. Am. Geophys. Union 78, 447,454.

Denis, D., Crosta, X., Barbara, L., Massé, G., Renssen, H., Ther, O., Giraudeau, J., 2010. Sea ice and wind variability during the Holocene in East Antarctica: insight on middle–high latitude coupling. Quat. Sci. Rev. 29, 3709–3719. DOI:10.1016/j.quascirev.2010.08.007

Divine, D.V., Koç, N., Isaksson, E., Nielsen, S., Crosta, X., Godtliebsen, F., 2010. Holocene Antarctic climate variability from ice and marine sediment cores: Insights on ocean–atmosphere interaction. Quat. Sci. Rev. 29, 303–312. DOI:10.1016/j.quascirev.2009.11.012

Dixon, D., Mayewski, P.A., Kaspari, S., Sneed, S., Handley, M., 2004. A 200 year sub-annual record of sulfate in West Antarctica, from 16 ice cores. Ann. Glaciol. 39, 545–556. DOI:10.3189/172756404781814113

Dunbar, N.W., Zielinski, G.A., Voisins, D.T., 2003. Tephra layers in the Siple Dome and Taylor Dome ice cores, Antarctica: Sources and correlations. J. Geophys. Res. 108, 2374. DOI:10.1029/2002JB002056

Ellison, C.R.W., Chapman, M.R., Hall, I.R., 2006. Surface and Deep Ocean Interactions During the Cold Climate Event 8200 Years Ago. Science (80-.). 312, 1929–1932. DOI:10.1126/science.1127213

Emslie, S.D., Woehler, E.J., 2005. A 9000-year record of Adélie penguin occupation and diet in the Windmill Islands, East Antarctica. Antarct. Sci. 17, 57–66. DOI:10.1017/S0954102005002427

Enomoto, H., Ohmura, A., 1990. The Influences of Atmospheric Half-Yearly Cycle on The Sea Ice Extent in The Antarctic. J. Geophys. Res. 95, 9497–

9511. DOI:10.1029/JC095iC06p09497

Etheridge, D.M., Steele, L.P., Langenfelds, R.L., Francey, R.J., Barnola, J.M., Morgan, V.I., 1996. Natural and anthropogenic changes in atmospheric CO2 over the last 1000 years from air in Antarctic ice and firn. J. Geophys. Res. 101, 4115–4128. DOI:10.1029/95JD03410

Etourneau, J., Collins, L.G., Willmott, V., Kim, J.H., Barbara, L., Leventer, A., Schouten, S., Sinninghe Damst´, J.S., Bianchini, A., Klein, V., Crosta, X., Massé, G., 2013. Holocene climate variations in the western Antarctic Peninsula: Evidence for sea ice extent predominantly controlled by changes in insolation and ENSO variability. Clim. Past 9, 1431–1446. DOI:10.5194/cp-9-1431-2013

Ferris, D.G., Cole-Dai, J., Reyes, A.R., Budner, D.M., 2011. South Pole ice core record of explosive volcanic eruptions in the first and second millennia A.D. and evidence of a large eruption in the tropics around 535 A.D. J. Geophys. Res. 116, D17308. DOI:10.1029/2011JD015916

Ferry, A.J., Crosta, X., Quilty, P.G., Fink, D., Howard, W., Armand, L.K., 2015. First records of winter sea ice concentration in the southwest Pacific sector of the Southern Ocean. Paleoceanography 30, 1525–1539. DOI:10.1002/2014PA002764

Fischer, H., 2004. Prevalence of the Antarctic Circumpolar Wave over the last two millenia recorded in Dronning Maud Land ice. Geophys. Res. Lett. 31, L08202. DOI:10.1029/2003GL019186

Fischer, H., Fundel, F., Ruth, U., Twarloh, B., Wegner, A., Udisti, R., Becagli, S., Castellano, E., Morganti, A., Severi, M., Wolff, E., Littot, G., Röthlisberger, R., Mulvaney, R., Hutterli, M. a., Kaufmann, P., Federer, U., Lambert, F., Bigler, M., Hansson, M., Jonsell, U., de Angelis, M., Boutron, C., Siggaard-Andersen, M.-L., Steffensen, J.P., Barbante, C., Gaspari, V., Gabrielli, P., Wagenbach, D., 2007a. Reconstruction of millennial changes in dust emission, transport and regional sea ice coverage using the deep EPICA ice cores from the Atlantic and Indian Ocean sector of Antarctica. Earth Planet. Sci. Lett. 260, 340–354. DOI:10.1016/j.epsl.2007.06.014

Fischer, H., Mieding, B., 2005. A 1,000-year ice core record of interannual to multidecadal variations in atmospheric circulation over the North Atlantic. Clim. Dyn. 25, 65–74. DOI:10.1007/s00382-005-0011-x

Fischer, H., Siggaard-Andersen, M.-L., Ruth, U., Röthlisberger, R., Wolff, E., 2007b. Glacial/interglacial changes in mineral dust and sea-salt records in polar ice cores: Sources, transport, and deposition. Rev. Geophys. 45, RG1002. DOI:10.1029/2005RG000192

Fisher, D.A., Koerner, R.M., Reeh, N., 1995. Holocene climatic records from Agassiz Ice Cap, Ellesmere Island, NWT. The Holocene 5, 19–24.

Fletcher, M.-S., Moreno, P.I., 2011. Zonally symmetric changes in the strength and position of the Southern Westerlies drove atmospheric CO2 variations over the past 14 k.y. Geology 39, 419–422. DOI:10.1130/G31807.1

Fletcher, M.S., Moreno, P.I., 2012. Have the Southern Westerlies changed in a

zonally symmetric manner over the last 14,000 years? A hemisphere-wide take on a controversial problem. Quat. Int. 253, 32–46. DOI:10.1016/j.quaint.2011.04.042

Foster, A.F.M., Curran, M.A.J., Smith, B.T., van Ommen, T.D., Morgan, V.I., 2006. Covariation of sea ice and methanesulphonic acid in Wilhelm II Land, East Antarctica. Ann. Glaciol. 44, 429–432. DOI:10.3189/172756406781811394

Frankignoul, C., 1985. Sea Surface Temperature Anomalies, Planetary Waves,. Rev. Geophys. 23, 357–390.

Fuhrer, K., Neftel, A., Anklin, M., Staffelbach, T., Legrand, M., 1996. High-resolution ammonium ice core record covering a complete glacial-interglacial cycle. J. Geophys. Res. 101, 4147. DOI:10.1029/95JD02903

Gao, C., Oman, L., Robock, A., Stenchikov, G.L., 2007. Atmospheric volcanic loading derived from bipolar ice cores: Accounting for the spatial distribution of volcanic deposition. J. Geophys. Res. 112, D09109. DOI:10.1029/2006JD007461

Gao, C., Robock, A., Ammann, C., 2008. Volcanic forcing of climate over the past 1500 years: An improved ice core-based index for climate models. J. Geophys. Res. 113, D23111. DOI:10.1029/2008JD010239

Gao, C., Robock, A., Self, S., Witter, J.B., Steffenson, J.P., Clausen, H.B., Siggaard-Andersen, M.L., Johnsen, S., Mayewski, P.A., Ammann, C., 2006. The 1452 or 1453 A.D. Kuwae eruption signal derived from multiple ice core records: Greatest volcanic sulfate event of the past 700 years. J. Geophys. Res. Atmos. 111, 1–11. DOI:10.1029/2005JD006710

Gersonde, R., 2003. Last glacial sea surface temperatures and sea-ice extent in the Southern Ocean (Atlantic-Indian sector): A multiproxy approach. Paleoceanography 18, 1061. DOI:10.1029/2002PA000809

Gersonde, R., Crosta, X., Abelmann, A., Armand, L., 2005. Sea-surface temperature and sea ice distribution of the Southern Ocean at the EPILOG Last Glacial Maximum - A circum-Antarctic view based on siliceous microfossil records. Quat. Sci. Rev. 24, 869–896. DOI:10.1016/j.quascirev.2004.07.015

Gibson, J.A.E., Garrick, R.C., Burton, H.R., McTaggart, A.R., 1990. Dimethylsulfide and the alga Phaeocystis pouchetii in Antarctic coastal waters. Mar. Biol. 104, 339–346.

Glen, J.W., 1955. The creep of polycrystalline ice. Proc. R. Soc. A 228, 519–538.

Gong, S.L., Barrie, L.A., Prospero, J.M., Savoie, D.L., Ayers, G.P., Blanchet, J.-P., Spacek, L., 1997. Modeling sea-salt aerosols in the atmosphere: 2. Atmospheric concentrations and fluxes. J. Geophys. Res. 102, D3, 3819. DOI:10.1029/96JD03401

Goodwin, I.D., van Ommen, T.D., Curran, M.A.J., Mayewski, P.A., 2004. Mid latitude winter climate variability in the South Indian and southwest Pacific regions since 1300 AD. Clim. Dyn. 22, 783–794. DOI:10.1007/s00382-

004-0403-3

Goodwin, I.D., Zweck, C., 2000. Glacio-isostasy and Glacial Ice Load at Law Dome, Wilkes Land, East Antarctica. Quat. Res. 53, 285–293. DOI:10.1006/qres.1999.2125

Gow, A.J., Meese, D.A., Alley, R.B., Fitzpatrick, J.J., Anandakrishnan, S., Woods, G.A., Elder, B.C., 1997. Physical and structural properties of the Greenland Ice Sheet Project 2 ice core : A review. J. Geophys. Res. 102, C12, 26559–26575.

Graf, H.-F., Shirsat, S.V., Oppenheimer, C., Jarvis, M.J., Podzun, R., Jacob, D., 2010. Continental scale Antarctic deposition of sulphur and black carbon from anthropogenic and volcanic sources. Atmos. Chem. Phys. 10, 2457–2465. DOI:10.5194/acp-10-2457-2010

Guglielmin, M., Convey, P., Malfasi, F., Cannone, N., 2015. Glacial fluctuations since the "Medieval Warm Period" at Rothera Point (western Antarctic Peninsula). The Holocene, 26 (1), 154-158. DOI:10.1177/0959683615596827

Hall, A., Visbeck, M., 2004. Synchronous Variability in the Southern Hemisphere Atmosphere, Sea Ice, and Ocean Resulting from the Annular Mode. J. Clim. 15, 3043–3057. DOI:10.1175/1520-0442(2002)015<3043:SVITSH>2.0.CO;2

Hammer, C.U., 1977. Past volcanism revealed by Greenland Ice Sheet impurities. Nature 270, 482–486. DOI:10.1038/270482a0

Hammer, C.U., 1980. Acidity of polar ice cores in relation to absolute dating, past volcanism, and radio echoes. J. Glaciol. 25, 359–372.

Hammer, C.U., Clausen, H.B., Langway, C.C., 1997. 50,000 years of recorded global volcanism. Clim. Change 35, 1–15.

Harder, S., Warren, S.G., Charlson, R.J., 2000. Sulfate in air and snow at the South Pole: Implications for transport and deposition at sites with low snow accumulation. J. Geophys. Res. 105, 22,825-22,832.

Heikoop, J.M., Tsujita, C.J., Risk, M.J., Tomascik, T., 1996. Corals as Proxy Recorders of Volcanic Activity: Evidence from Banda Api, Indonesia. Palaios 11, 286. DOI:10.2307/3515236

Hodell, D.A., Kanfoush, S.L., Shemesh, A., Crosta, X., Charles, C.D., Guilderson, T.P., 2001. Abrupt Cooling of Antarctic Surface Waters and Sea Ice Expansion in the South Atlantic Sector of the Southern Ocean at 5000 cal yr B.P. Quat. Res. 56, 191–198. DOI:10.1006/qres.2001.2252

Hodgson, D.A., McMinn, A., Kirkup, H., Cremer, H., Gore, D., Melles, M., Roberts, D., Montiel, P., 2003. Colonization, succession, and extinction of marine floras during a glacial cycle: A case study from the Windmill Islands (east Antarctica) using biomarkers. Paleoceanography 18. DOI:10.1029/2002PA000775

Hodgson, D.A., Sime, L.C., 2010. Palaeoclimate: Southern westerlies and CO2. Nat. Geosci. 3, 666–667. DOI:10.1038/ngeo970

Hogg, A., Lowe, D.J., Palmer, J., Boswijk, G., Ramsey, C.B., 2012. Revised calendar date for the Taupo eruption derived by 14C wiggle-matching using a New Zealand kauri 14C calibration data set. The Holocene 22, 439–449. DOI:10.1177/0959683611425551

Holland, P.R., Kwok, R., 2012. Wind-driven trends in Antarctic sea-ice drift. Nat. Geosci. 5, 872–875. DOI:10.1038/ngeo1627

Houseago, R.E., McGregor, G.R., King, J.C., Harangozo, S.A., 1998. Climate anomaly wave-train patterns linking southern low and high latitudes during South Pacific warm and cold events. Int. J. Climatol. 18, 1181–1193. DOI:10.1002/(SICI)1097-0088(199809)18:11<1181::AID-JOC332>3.0.CO;2-X

Huang, J., Jaeglé, L., 2016. Wintertime enhancements of sea salt aerosol in polar regions consistent with a sea-ice source from blowing snow. Atmos. Chem. Phys. Discuss. 1–23. DOI:10.5194/acp-2016-972

Huber, T.M., Schwikowski, M., Gäggeler, H.W., 2001. Continuous melting and ion chromatographic analyses of ice cores. J. Chromatogr. A 920, 193–200. DOI:10.1016/S0021-9673(01)00613-6

IPCC, 2014. IPCC, 2014: Climate Change 2014: Synthesis Report. Contribution of Working Groups I, II and III to the Fifth Assessment Report of the Intergovernmental Panel on Climate Change, AR5. ed. IPCC, Geneva.

Johnsen, S.J., Dahl-Jensen, D., Dansgaard, W., Gundestrup, N., 1995. Greenland palaeotemperatures derived from GRIP bore hole temperature and ice core isotope profiles. Tellus B 47, 624–629. DOI:10.1034/j.1600-0889.47.issue5.9.x

Jourdain, B., Preunkert, S., Cerri, O., Castebrunet, H., Udisti, R., Legrand, M., 2008. Year-round record of size-segregated aerosol composition in central Antarctica (Concordia station): Implications for the degree of fractionation of sea-salt particles. J. Geophys. Res. 113, D14308. DOI:10.1029/2007JD009584

Kaleschke, L., Richter, A., Burrows, J., Afe, O., Heygster, G., Notholt, J., Rankin, A.M., Roscoe, H.K., Hollwedel, J., Wagner, T., Jacobi, H.W., 2004. Frost flowers on sea ice as a source of sea salt and their influence on tropospheric halogen chemistry. Geophys. Res. Lett. 31, 4–7. DOI:10.1029/2004GL020655

Kärkäs, E., Teinilä, K., Virkkula, A., Aurela, M., 2005. Spatial variations of surface snow chemistry during two austral summers in western Dronning Maud Land, Antarctica. Atmos. Environ. 39, 1405–1416. DOI:10.1016/j.atmosenv.2004.11.027

Kaufmann, P., Fundel, F., Fischer, H., Bigler, M., Ruth, U., Udisti, R., Hansson, M., de Angelis, M., Barbante, C., Wolff, E.W., Hutterli, M., Wagenbach, D., 2010. Ammonium and non-sea salt sulfate in the EPICA ice cores as indicator of biological activity in the Southern Ocean. Quat. Sci. Rev. 29, 313–323. DOI:10.1016/j.quascirev.2009.11.009

Khosrawi, F., Urban, J., Pitts, M.C., Voelger, P., Achtert, P., Kaphlanov, M., Santee, M.L., Manney, G.L., Murtagh, D., Fricke, K.H., 2011.

Denitrification and polar stratospheric cloud formation during the Arctic winter 2009/2010. Atmos. Chem. Phys. 11, 8471–8487. DOI:10.5194/acp-11-8471-2011

Kim, J.-H., Crosta, X., Willmott, V., Renssen, H., Bonnin, J., Helmke, P., Schouten, S., Sinninghe Damsté, J.S., 2012. Holocene subsurface temperature variability in the eastern Antarctic continental margin. Geophys. Res. Lett. 39, n/a-n/a. DOI:10.1029/2012GL051157

Kim, S.-J., Lü, J., Kim, B.-M., 2014. The Southern Annular Mode (SAM) in PMIP2 simulations of the last glacial maximum. Adv. Atmos. Sci. 31, 863–878. DOI:10.1007/s00376-013-3179-8

Knudson, K.P., Hendy, I.L., Neil, H.L., 2011. Re-examining Southern Hemisphere westerly wind behavior: Insights from a late Holocene precipitation reconstruction using New Zealand fjord sediments. Quat. Sci. Rev. 30, 3124–3138. DOI:10.1016/j.quascirev.2011.07.017

Kobashi, T., Severinghaus, J.P., Brook, E.J., Barnola, J.-M., Grachev, A.M., 2007. Precise timing and characterization of abrupt climate change 8200 years ago from air trapped in polar ice. Quat. Sci. Rev. 26, 1212–1222. DOI:10.1016/j.quascirev.2007.01.009

Kohfeld, K.E., Graham, R.M., de Boer, A.M., Sime, L.C., Wolff, E.W., Le Quéré, C., Bopp, L., 2013. Southern Hemisphere westerly wind changes during the Last Glacial Maximum: Paleo-data synthesis. Quat. Sci. Rev. 68, 76–95. DOI:10.1016/j.quascirev.2013.01.017

Kohfeld, K.E., Harrison, S.P., 2001. DIRTMAP: the geological record of dust. Earth-Science Rev. 54, 81–114. DOI:10.1016/S0012-8252(01)00042-3

Kreutz, K.J., Mayewski, P.A., Meeker, L.D., Twickler, M.S., Whitlow, S.I., Pittalwala, I.I., 1997. Bipolar Changes in Atmospheric Circulation During the Little Ice Age. Science (80-.). 277, 1294–1296. DOI:10.1126/science.277.5330.1294

Kreutz, K.J., Mayewski, P.A., Pittalwala, I.I., Meeker, L.D., Twickler, M.S., Whitlow, S.I., 2000. Sea level pressure variability in the Amundsen Sea region inferred from a West Antarctic glaciochemical record. J. Geophys. Res. 105, 4047. DOI:10.1029/1999JD901069

Krinner, G., Genthon, C., 1998. GCM similations of the last glacial maximum surface climate of Greenland and Antarctica. Clim. Dyn. 14, 741–758.

Kwok, R., Comiso, J.C., 2002. Spatial patterns of variability in Antarctic surface temperature : Connections to the Southern Hemisphere Annular Mode and the Southern Oscillation. Geophys. Res. Lett. 29, 50-1-50–4. DOI:10.1029/2002GL015415

LaMarche, V.C., Hirschboeck, K.K., 1984. Frost rings in trees as records of major volcanic eruptions. Nature 307, 121–126. DOI:10.1038/307121a0

Lambeck, K., Chappell, J., 2001. Sea level change through the last glacial cycle. Science (80-.). 292, 679–686. DOI:10.1126/science.1059549

Lambeck, K., Yokoyama, Y., Purcell, T., 2002. Into and out of the last glacial

maximum: Sea-level change during oxygen isotope stages 3 and 2. Quat. Sci. Rev. 21, 343–360. DOI:10.1016/S0277-3791(01)00071-3

Lambert, F., Bigler, M., Steffensen, J.P., Hutterli, M., Fischer, H., 2012. Centennial mineral dust variability in high-resolution ice core data from Dome C, Antarctica. Clim. Past 8, 609–623. DOI:10.5194/cp-8-609-2012

Lambert, F., Delmonte, B., Petit, J.R., Bigler, M., Kaufmann, P.R., Hutterli, M. a, Stocker, T.F., Ruth, U., Steffensen, J.P., Maggi, V., 2008. Dust-climate couplings over the past 800,000 years from the EPICA Dome C ice core. Nature 452, 616–619. DOI:10.1038/nature06763

Lamy, F., Kilian, R., Arz, H.W., Francois, J.-P., Kaiser, J., Prange, M., Steinke, T., 2010. Holocene changes in the position and intensity of the southern westerly wind belt. Nat. Geosci. 3, 695–699. DOI:10.1038/ngeo959

Langway, C.C., Osada, K., Clausen, H.B., Hammer, C.U., Shoji, H., 1995. A 10-century comparison of prominent bipolar volcanic events in ice cores. J. Geophys. Res. 100, D8, 16241–16247. DOI:10.1029/95JD01175

Larsen, L.B., Vinther, B.M., Briffa, K.R., Melvin, T.M., Clausen, H.B., Jones, P.D., Siggaard-Andersen, M.-L., Hammer, C.U., Eronen, M., Grudd, H., Gunnarson, B.E., Hantemirov, R.M., Naurzbaev, M.M., Nicolussi, K., 2008. New ice core evidence for a volcanic cause of the A.D. 536 dust veil. Geophys. Res. Lett. 35, L04708. DOI:10.1029/2007GL032450

Lavigne, F., Degeai, J.-P., Komorowski, J.-C., Guillet, S., Robert, V., Lahitte, P., Oppenheimer, C., Stoffel, M., Vidal, C.M., Surono, Pratomo, I., Wassmer, P., Hajdas, I., Hadmoko, D.S., de Belizal, E., 2013. Source of the great A.D. 1257 mystery eruption unveiled, Samalas volcano, Rinjani Volcanic Complex, Indonesia. Proc. Natl. Acad. Sci. U. S. A. 110, 16742–16747. DOI:10.1073/pnas.1307520110

Legrand, M., 1987. Chemistry of Antarctic snow and ice. J. Phys. 48, 3, 77-86.

Legrand, M., Delmas, R.J., 1987. A 220-year continuous record of volcanic H2SO4 in the Antarctic ice sheet. Nature 327, 671–676. DOI:10.1038/327671a0

Legrand, M., Dominé, F., Léopold, A., 1996. Acidic gases (HCl, HF, HNO3, HCOOH, and CH3COOH): a review of ice core data and some preliminary discussions on their air-snow relationships. In: Wolff, E.W., Bales, R.C. (Eds.), Chemical Exchange Between the Atmosphere and Polar Snow. Springer, New York, pp. 19–44.

Legrand, M., Mayewski, P., 1997. Glaciochemistry of polar ice cores: A review. Rev. Geophys. 35, 219–243. DOI:10.1029/96RG03527

Legrand, M.R., Delmas, R.J., 1988. Formation of HCl in the Antarctic atmosphere. J. Geophys. Res. Atmos. 93, 7153–7168. DOI:10.1029/JD093iD06p07153

Levine, J.G., Yang, X., Jones, A.E., Wolff, E.W., 2014. Sea salt as an ice core proxy for past sea ice extent: A process-based model study. J. Geophys. Res. Atmos. 119, 1–20. DOI:10.1002/2013JD020925

Li, J., Wang, J.X.L., 2003. A modified zonal index and its physical sense. Geophys. Res. Lett. 30, 34(1-4). DOI:10.1029/2003GL017441

Liss, P.S., Malin, G., Turner, S.M., Holligan, P.M., 1994. Dimethyl sulphide and Phaeocystis: A review. J. Mar. Syst. 5, 41-52.

Mackintosh, A.N., Verleyen, E., O'Brien, P.E., White, D.A., Jones, R.S., McKay, R., Dunbar, R., Gore, D.B., Fink, D., Post, A.L., Miura, H., Leventer, A., Goodwin, I., Hodgson, D.A., Lilly, K., Crosta, X., Golledge, N.R., Wagner, B., Berg, S., van Ommen, T., Zwartz, D., Roberts, S.J., Vyverman, W., Masse, G., 2014. Retreat history of the East Antarctic Ice Sheet since the Last Glacial Maximum. Quat. Sci. Rev. 100, 10–30. DOI:10.1016/j.quascirev.2013.07.024

Mann, M.E., Fuentes, J.D., Rutherford, S., 2012. Underestimation of volcanic cooling in tree-ring-based reconstructions of hemispheric temperatures. Nat. Geosci. 5, 202–205. DOI:10.1038/ngeo1394

Mann, M.E., Zhang, Z., Rutherford, S., Bradley, R.S., Hughes, M.K., Shindell, D., Ammann, C., Faluvegi, G., Ni, F., 2009. Global Signatures and Dynamical Origins of the Little Ice Age and Medieval Climate Anomaly. Science (80-.). 326, 1256–1260. DOI:10.1126/science.1177303

Masson-Delmotte, V., Buiron, D., Ekaykin, A., Frezzotti, M., Gallée, H., Jouzel, J., Krinner, G., Landais, A., Motoyama, H., Oerter, H., Pol, K., Pollard, D., Ritz, C., Schlosser, E., Sime, L.C., Sodemann, H., Stenni, B., Uemura, R., Vimeux, F., 2011. A comparison of the present and last interglacial periods in six Antarctic ice cores. Clim. Past 7, 397–423. DOI:10.5194/cp-7-397-2011

Masson, V., Vimeux, F., Jouzel, J., Morgan, V., Delmotte, M., Ciais, P., Hammer, C., Johnsen, S., Lipenkov, V.Y., Mosley-Thompson, E., Petit, J.-R., Steig, E.J., Stievenard, M., Vaikmae, R., 2000. Holocene Climate Variability in Antarctica Based on 11 Ice-Core Isotopic Records. Quat. Res. 54, 348–358. DOI:10.1006/qres.2000.2172

Mayewski, P.A., Legrand, M.R., 1990. Recent increase in nitrate concentration of Antarctic snow. Nature 346, 258–260. DOI:10.1038/346258a0

Mayewski, P.A., Maasch, K.A., White, J.W.C., Steig, E.J., Meyerson, E., Goodwin, I., Morgan, V.I., van Ommen, T., Curran, M.A.J., Souney, J., Kreutz, K., 2004a. A 700 year record of Southern Hemisphere extratropical climate variability. Ann. Glaciol. 39, 127–132. DOI:10.3189/172756404781814249

Mayewski, P.A., Rohling, E.E., Curt Stager, J., Karlén, W., Maasch, K.A., David Meeker, L., Meyerson, E.A., Gasse, F., van Kreveld, S., Holmgren, K., Lee-Thorp, J., Rosqvist, G., Rack, F., Staubwasser, M., Schneider, R.R., Steig, E.J., 2004b. Holocene climate variability. Quat. Res. 62, 243–255. DOI:10.1016/j.yqres.2004.07.001

McCormick, M.P., Thomason, L.W., Trepte, C.R., 1995. Atmospheric effects of the Mt Pinatubo eruption. Nature 373, 399–404. DOI:10.1038/373399a0

McCracken, K.G., McDonald, F.B., Beer, J., Raisbeck, G., Yiou, F., 2004. A phenomenological study of the long-term cosmic ray modulation, 850–

1958 AD. J. Geophys. Res. 109, A12103. DOI:10.1029/2004JA010685

McGee, D., Donohoe, A., Marshall, J., Ferreira, D., 2014. Changes in ITCZ location and cross-equatorial heat transport at the Last Glacial Maximum, Heinrich Stadial 1, and the mid-Holocene. Earth Planet. Sci. Lett. 390, 69–79. DOI:10.1016/j.epsl.2013.12.043

McGlone, M.S., Turney, C.S.M., Wilmshurst, J.M., Renwick, J., Pahnke, K., 2010. Divergent trends in land and ocean temperature in the Southern Ocean over the past 18,000 years. Nat. Geosci. 3, 622–626. DOI:10.1038/ngeo931

McMorrow, A.J., Curran, M.A.J., van Ommen, T.D., Morgan, V., Pook, M.J., Allison, I., 2001. Intercomparison of firn core and meteorological data. Antarct. Sci. 13, 329–337.

Meese, D.A., Gow, A.J., Alley, R.B., Zielinski, G.A., Grootes, P.M., Ram, M., Taylor, K.C., Mayewski, P.A., Bolzan, J.F., 1997. The Greenland Ice Sheet Project 2 depth-age scale: Methods and results. J. Geophys. Res. 102, 26411–26423.

Mellor, G., 1997. Introduction to Physical Oceanography. Am. J. Phys. 65, 1028. DOI:10.1119/1.18716

Minikin, A., Legrand, M., Hall, J., Wagenbach, D., Kleefeld, C., Wolff, E., Pasteur, E.C., Ducroz, F., 1998. Sulfur-containing species (sulfate and methanesulfonate) in coastal Antarctic aerosol and precipitation. J. Geophys. Res. 103, 10975. DOI:10.1029/98JD00249

Minikin, A., Wagenbach, D., Graf, W., Kipfstuhl, J., 1994. Spatial and seasonal variations of the snow chemistry at the central Filchner–Ronne Ice Shelf, Antarctica. Ann. Glaciol. 20, 283–290.

Monzier, M., Robin, C., Eisenb, J., 1994. Kuwae (1452 A.D.): the forgotten caldera. J. Volcanol. Geotherm. Res. 59, 207–218.

Moore, J., Paren, J., Oerter, H., 1992. Sea Salt Dependent Electrical Conduction in Polar Ice. J. Geophys. Res. 97, 19,803-18,812.

Moore, J.C., 1993. High-resolution dielectric profiling of ice cores. J. Glaciol. 39, 132, 245-248.

Moore, J.C., Maeno, N., 1991. Application of the dielectric profiling technique to ice core studies. Proc. NIPR Symp. Polar Meteorol. Glaciol. 4, 81-92.

Moore, J.C., Mulvaney, R., Paren, J.G., 1989. Dielectric stratigraphy of ice: A new technique for determining total ionic concentrations in polar ice cores. Geophys. Res. Lett. 16, 10, 1,177-1,180.

Moore, J.C., Narita, H., Maeno, N., 1991. A continuous 770-year record of volcanic activity from East Antarctica. J. Geophys. Res. 96, 17,353-17,359.

Moore, J.C., Paren, J.G., 1987. A New Technique for Dielectric Logging of Antarctic Ice Cores. Le J. Phys. Colloq. 48, C1-155-C1-160. DOI:10.1051/jphyscol:1987123

Morgan, V., van Ommen, T.D., Elcheikh, A., Jun, L., 1998. Variations in shear deformation rate with depth at Dome Summit South, Law Dome, East Antarctica. Ann. Glaciol. 27, 135–139.

Morgan, V.I., Wookey, C.W., Li, J., van Ommen, T.D., Skinner, W., Fitzpatrick, M.F., 1997. Site information and initial results from deep ice drilling on Law Dome, Antarctica. J. Glaciol. 43, 3–10.

Moy, C.M., Seltzer, G.O., Rodbell, D.T., Anderson, D.M., 2002. Variability of El Niño/Southern Oscillation activity at millennial timescales during the Holocene epoch. Nature 420, 162–165. DOI:10.1038/nature01194

Mulvaney, R., Pasteur, E.C., Peel, D.A., Saltzman, S., Whung, P.-Y., 1992. The ratio of MSA to non-sea-salt sulphate in Antarctic Peninsula ice cores. Tellus A 44B, 295–303.

Mulvaney, R., Wolff, E.W., 1993. Evidence for Winter / Spring Denitrification of the Stratosphere in the Nitrate Record of Antarctic Fim Cores, 98, D3, 5213–5220.

Mulvaney, R., Wolff, E.W., 1994. Spatial variability of the major chemistry of the Antarctic ice sheet. Ann. Glaciol. 20, 440–447. DOI:doi:10.3189/172756494794587159

Narcisi, B., Petit, J.R., Delmonte, B., Scarchilli, C., Stenni, B., 2012. A 16,000-yr tephra framework for the Antarctic ice sheet: a contribution from the new Talos Dome core. Quat. Sci. Rev. 49, 52–63. DOI:10.1016/j.quascirev.2012.06.011

Neff, P.D., 2014. A review of the brittle ice zone in polar ice cores. Ann. Glaciol. 55, 72–82. DOI:10.3189/2014AoG68A023

Neftel, A., Jacob, P., Klockow, D., 1986. Long-term record of H202 in polar ice cores. Tellus 38B, 262–270.

Németh, K., Cronin, S.J., White, J.D.L., 2007. Kuwae Caldera and Climate Confusion. Open Geol. J. 1, 7–11.

Neumann, T.A., Waddington, E.D., 2004. Effects of firn ventilation on isotopic exchange. J. Glaciol. 50, 183–194.

Nielsen, S.H.H., Koç, N., Crosta, X., 2004. Holocene climate in the Atlantic sector of the Southern Ocean: Controlled by insolation or oceanic circulation? Geology 32, 317. DOI:10.1130/G20334.1

Norris, S.J., Brooks, I.M., Moat, B.I., Yelland, M.J., de Leeuw, G., Pascal, R.W., Brooks, B., 2012. Field measurements of aerosol production from whitecaps in the open ocean. Ocean Sci. Discuss. 9, 3359–3392. DOI:10.5194/osd-9-3359-2012

Oerter, H., Wilhelms, F., Jung-Rothenhäusler, F., Göktas, F., Miller, H., Graf, W., Sommer, S., 2000. Accumulation rates in Dronning Maud Land, Antarctica, as revealed by dielectric-profiling measurements of shallow firn cores. Ann. Glaciol. 30, 27–34. DOI:10.3189/172756400781820705

Orsi, A.J., Cornuelle, B.D., Severinghaus, J.P., 2012. Little Ice Age cold interval in West Antarctica: Evidence from borehole temperature at the

West Antarctic Ice Sheet (WAIS) Divide. Geophys. Res. Lett. 39, 1–7. DOI:10.1029/2012GL051260

Pahnke, K., Zahn, R., Elderfield, H., Schulz, M., 2003. 340,000-Year Centennial-Scale Marine Record of Southern Hemisphere Climatic Oscillation. Science (80-.). 301, 948–952. DOI:10.1126/science.1084451

Palais, J.M., Kirchner, S., Delmas, R.J., 1990. Identification of some global volcanic horizons by major element analysis of fine ash in Antarctic ice. Ann. Glaciol. 14, 216–220.

Palmer, A.S., 2002. Environmental Signals from Chemical Measurements on Law Dome Ice Cores, Unpub. PhD thesis, University of Tasmania.

Palmer, A.S., Morgan, V.I., Curran, M.A.J., Van Ommen, T.D., Mayewski, P.A., 2002. Antarctic volcanic flux ratios from Law Dome ice cores. Ann. Glaciol. 35, 329–332. DOI:10.3189/172756402781816771

Palmer, A.S., van Ommen, T.D., Curran, M.A.J., Morgan, V., Souney, J.M., Mayewski, P.A., 2001. High-precision dating of volcanic events (A.D. 1301-1995) using ice cores from Law Dome, Antarctica. J. Geophys. Res. Atmos. 106, 28089–28095. DOI:10.1029/2001JD000330

Pang, K.D., 1993. Climatic impact of the mid-fifteenth century Kuwae caldera formation, as reconstructed from historical and proxy data. EOS Trans. 74, 106.

Parrenin, F., Dreyfus, G., Durand, G., Fujita, S., Gagliardini, O., Gillet, F., Jouzel, J., Kawamura, K., Lhomme, N., Masson-Delmotte, V., Ritz, C., Schwander, J., Shoji, H., Uemura, R., Watanabe, O., Yoshida, N., 2007. Ice flow modelling at EPICA Dome C and Dome Fuji, East Antarctica. Clim. Past Discuss. 3, 19–61. DOI:10.5194/cpd-3-19-2007

Parrenin, F., Petit, J.-R., Masson-Delmotte, V., Wolff, E., Basile-Doelsch, I., Jouzel, J., Lipenkov, V., Rasmussen, S.O., Schwander, J., Severi, M., Udisti, R., Veres, D., Vinther, B.M., 2012. Volcanic synchronisation between the EPICA Dome C and Vostok ice cores (Antarctica) 0–145 kyr BP. Clim. Past 8, 1031–1045. DOI:10.5194/cp-8-1031-2012

Pasteur, E.C., Mulvaney, R., 2000. Migration of methane sulphonate in Antarctic firn and ice. J. Geophys. Res. 105, 11525. DOI:10.1029/2000JD900006

Paterson, W.S.B., 1994. The Physics of Glaciers, Third. ed. Pergamon, Oxford.

Pedro, J.B., van Ommen, T.D., Rasmussen, S.O., Morgan, V.I., Chappellaz, J., Moy, A.D., Masson-Delmotte, V., Delmotte, M., 2011. The last deglaciation: timing the bipolar seesaw. Clim. Past 7, 671–683. DOI:10.5194/cp-7-671-2011

Petit, J.R., Jouzel, J., Pourchet, M., Merlivat, L., 1982. A detailed study of snow accumulation and stable isotope content in Dome C (Antarctica). J. Geophys. Res. 87, 4301–4308. DOI:10.1029/JC087iC06p04301

Petit, J.R., Raynaud, D., Basile, I., Chappellaz, J., Ritz, C., Delmotte, M., Legrand, M., Lorius, C., Pe, L., Jouzel, J., Raynaud, D., Barkov, N.I.,

Barnola, J.-M., Basile, I., Bender, M., Chappellaz, J., Davis, M., Delaygue, G., Delmotte, M., Kotlyakov, V.M., Legrand, M., Lipenkov, V.Y., Lorius, C., PÉpin, L., Ritz, C., Saltzman, E., Stievenard, M., 1999. Climate and atmospheric history of the past 420,000 years from the Vostock ice core, Antarctica. Nature 399, 429–436. DOI:10.1038/20859

Plummer, C.T., 2009. Effect of Accumulation Rate on the Preservation of Trace Ion Chemistry at Law Dome, East Antarctica. Unpub. Honours thesis, University of Tasmania.

Plummer, C.T., Curran, M.A.J., van Ommen, T.D., Rasmussen, S.O., Moy, A.D., Vance, T.R., Clausen, H.B., Vinther, B.M., Mayewski, P.A., 2012. An independently dated 2000-yr volcanic record from Law Dome, East Antarctica, including a new perspective on the dating of the 1450s CE eruption of Kuwae, Vanuatu. Clim. Past 8, 1929–1940. DOI:10.5194/cp-8-1929-2012

Pomeroy, J.W., Jones, H.G., 1996. Wind-blown Snow: Sublimation, Transport and Changes to Polar Snow. In: Wolff, E.W., Bales, R.C. (Eds.), Chemical Exchange Between the Atmosphere and Polar Snow. Springer, New York, pp. 453–489.

Power, S., Casey, T., Folland, C., Colman, A., Mehta, V., 1999. Inter-decadal modulation of the impact of ENSO on Australia. Clim. Dyn. 15, 319–324. DOI:10.1007/s003820050284

Quinn, P.K., Kapustin, V.N., Bates, T.S., 1996. Chemical and optical properties of marine boundary layer aerosol particles of the mid-Pacific in relation to sources and meteorological transport. J. Geophys. Res. 101, 6931–6951.

Rampino, M.R., Self, S., 1982. Historic eruptions of Tambora (1815), Krakatau (1883), and Agung (1963), their stratospheric aerosols, and climatic impact. Quat. Res. 18, 127–143. DOI:10.1016/0033-5894(82)90065-5

Rampino, M.R., Self, S., 1984. Sulphur-rich volcanic eruptions and stratospheric aerosols. Nature 310, 677–679. DOI:10.1038/310677a0

Rankin, A.M., Auld, V., Wolff, E.W., 2000. Frost flowers as a source of fractionated sea salt aerosol in the polar regions. Geophys. Res. Lett. 27, 3469–3472. DOI:10.1029/2000GL011771

Rankin, A.M., Wolff, E.W., Martin, S., 2002. Frost flowers: Implications for tropospheric chemistry and ice core interpretation. J. Geophys. Res. Atmos. 107, AAC 4-1-AAC 4-15. DOI:10.1029/2002JD002492

Rankin, A.M., Wolff, E.W., Mulvaney, R., 2004. A reinterpretation of sea-salt records in Greenland and Antarctic ice cores? Ann. Glaciol. 39, 276–282. DOI:10.3189/172756404781814681

Rasmussen, S.O., Andersen, K.K., Svensson, A.M., Steffensen, J.P., Vinther, B.M., Clausen, H.B., Siggaard-Andersen, M.-L., Johnsen, S.J., Larsen, L.B., Dahl-Jensen, D., Bigler, M., Röthlisberger, R., Fischer, H., Goto-Azuma, K., Hansson, M.E., Ruth, U., 2006. A new Greenland ice core chronology for the last glacial termination. J. Geophys. Res. 111, D06102. DOI:10.1029/2005JD006079

Ren, J., Li, C., Hou, S., Xiao, C., Qin, D., Li, Y., Ding, M., 2010. A 2680 year volcanic record from the DT-401 East Antarctic ice core. J. Geophys. Res. 115, D11301. DOI:10.1029/2009JD012892

Renssen, H., Goosse, H., Fichefet, T., Masson-Delmotte, V., Koç, N., 2005. Holocene climate evolution in the high-latitude Southern Hemisphere simulated by a coupled atmosphere–sea ice–ocean–vegetation model. The Holocene 15, 951–964. DOI:10.1191/0959683605hl869ra

Rintoul, S.R., Hughes, C.W., Olbers, D., 2001. The Antarctic Circumpolar Current System, International Geophysics, 77, 271-302. DOI:10.1016/S0074-6142(01)80124-8

Risbey, J.S., Pook, M.J., McIntosh, P.C., Wheeler, M.C., Hendon, H.H., 2009. On the Remote Drivers of Rainfall Variability in Australia. Mon. Weather Rev. 137, 3233–3253. DOI:10.1175/2009MWR2861.1

Roberts, D., McMinn, A., Cremer, H., Gore, D.B., Melles, M., 2004. The Holocene evolution and palaeosalinity history of Beall Lake, Windmill Islands (East Antarctica) using an expanded diatom-based weighted averaging model. Palaeogeogr. Palaeoclimatol. Palaeoecol. 208, 121–140. DOI:10.1016/j.palaeo.2004.02.032

Roberts, J., Curran, M., Poynter, S., Moy, A., Ommen, T. van, Vance, T., Tozer, C., Graham, F.S., Young, D.A., Plummer, C., Pedro, J., Blankenship, D., Siegert, M., 2016. Correlation confidence limits for unevenly sampled data. Comput. Geosci. DOI:10.1016/j.cageo.2016.09.011

Roberts, J., Plummer, C., Vance, T., van Ommen, T., Moy, A., Poynter, S., Treverrow, A., Curran, M., George, S., 2015. A 2000-year annual record of snow accumulation rates for Law Dome, East Antarctica. Clim. Past 11, 697–707. DOI:10.5194/cp-11-697-2015

Roberts, J.L., Van Ommen, T.D., Curran, M.A.J., Vance, T.R., 2009. Methanesulphonic acid loss during ice-core storage: Recommendations based on a new diffusion coefficient. J. Glaciol. 55, 784–788. DOI:10.3189/002214309790152474

Robock, A., 2000. Volcanic eruptions and climate. Rev. Geophys. 38, 191–219.

Rodriguez, E.S., Poynter, S., Curran, M., Haddad, P.R., Shellie, R.A., Nesterenko, P.N., Paull, B., 2015. Capillary ion chromatography with on-column focusing for ultra-trace analysis of methanesulfonate and inorganic anions in limited volume Antarctic ice core samples. J. Chromatogr. A 1409, 182–188. DOI:10.1016/j.chroma.2015.07.034

Roscoe, H.K., Brooks, B., Jackson, A. V., Smith, M.H., Walker, S.J., Obbard, R.W., Wolff, E.W., 2011. Frost flowers in the laboratory: Growth, characteristics, aerosol, and the underlying sea ice. J. Geophys. Res. Atmos. 116, 1–12. DOI:10.1029/2010JD015144

Röthlisberger, R., Crosta, X., Abram, N.J., Armand, L., Wolff, E.W., 2010. Potential and limitations of marine and ice core sea ice proxies: an example from the Indian Ocean sector. Quat. Sci. Rev. 29, 296–302. DOI:10.1016/j.quascirev.2009.10.005

Röthlisberger, R., Hutterli, M. a., Wolff, E.W., Mulvaney, R., Fischer, H., Bigler, M., Goto-Azuma, K., Hansson, M.E., Ruth, U., Siggaard, M.L., Steffensen, J.P., 2002a. Nitrate in Greenland and Antarctic ice cores: A detailed description of post-depositional processes. Ann. Glaciol. 35, 209–216. DOI:10.3189/172756402781817220

Röthlisberger, R., Mudelsee, M., Bigler, M., de Angelis, M., Fischer, H., Hansson, M., Lambert, F., Masson-Delmotte, V., Sime, L., Udisti, R., Wolff, E.W., 2008. The southern hemisphere at glacial terminations: insights from the Dome C ice core. Clim. Past Discuss. 4, 761–789. DOI:10.5194/cpd-4-761-2008

Röthlisberger, R., Mulvaney, R., Wolff, E.W., Hutterli, M.A., Bigler, M., de Angelis, M., Hansson, M.E., Steffensen, J.P., Udisti, R., 2003. Limited dechlorination of sea-salt aerosols during the last glacial period: Evidence from the European Project for Ice Coring in Antarctica (EPICA) Dome C ice core. J. Geophys. Res. 108, 4526. DOI:10.1029/2003JD003604

Röthlisberger, R., Mulvaney, R., Wolff, E.W., Hutterli, M.A., Bigler, M., Sommer, S., Jouzel, J., 2002b. Dust and sea salt variability in central East Antarctica (Dome C) over the last 45 kyrs and its implications for southern high-latitude climate. Geophys. Res. Lett. 29, 1963. DOI:10.1029/2002GL015186

Ruth, U., Barnola, J.-M., Beer, J., Bigler, M., Blunier, T., Castellano, E., Fischer, H., Fundel, F., Huybrechts, P., Kaufmann, P., Kipfstuhl, S., Lambrecht, A., Morganti, A., Oerter, H., Parrenin, F., Rybak, O., Severi, M., Udisti, R., Wilhelms, F., Wolff, E., 2007. "EDML1": a chronology for the EPICA deep ice core from Dronning Maud Land, Antarctica, over the last 150 000 years. Clim. Past 3, 475–484. DOI:10.5194/cp-3-475-2007

Salby, M.L., 2012. Physics of the Atmosphere and Climate, 2nd ed. Cambridge University Press, New York.

Salinger, M.J., Renwick, J.A., Mullan, A.B., 2001. Interdecadal Pacific Oscillation and South Pacific climate. Int. J. Climatol. 21, 1705–1721. DOI:10.1002/joc.691

Saltzman, E.S., Dioumaeva, I., Finley, B.D., 2006. Glacial/interglacial variations in methanesulfonate (MSA) in the Siple Dome ice core, West Antarctica. Geophys. Res. Lett. 33, L11811. DOI:10.1029/2005GL025629

Salzer, M.W., Hughes, M.K., 2007. Bristlecone pine tree rings and volcanic eruptions over the last 5000 yr. Quat. Res. 67, 57–68. DOI:10.1016/j.yqres.2006.07.004

Savoie, D.L., Arimoto, R., Keene, W.C., Prospero, J.M., Duce, R.A., Galloway, J.N., 2002. Marine biogenic and anthropogenic contributions to non-sea-salt sulfate in the marine boundary layer over the North Atlantic Ocean. J. Geophys. Res. 107, D18, 4356. DOI:10.1029/2001JD000970

Schlosser, E., Oerter, H., Masson-Delmotte, V., Reijmer, C., 2008. Atmospheric influence on the deuterium excess signal in polar firn: implications for ice-core interpretation. J. Glaciol. 54, 117–124. DOI:10.3189/002214308784408991

Schlosser, E., Powers, J.G., Duda, M.G., Manning, K.W., 2011. Interaction between Antarctic sea ice and synoptic activity in the circumpolar trough: Implications for ice-core interpretation. Ann. Glaciol. 52, 9–17. DOI:10.3189/172756411795931859

Schoemann, V., Becquevort, S., Stefels, J., Rousseau, V., Lancelot, C., 2005. Phaeocystis blooms in the global ocean and their controlling mechanisms: A review. J. Sea Res. 53, 43–66. DOI:10.1016/j.seares.2004.01.008

Schwander, J., 2003. Timescales for the EPICA ice cores. In: EGS-AGU Joint Assembly, Nice, France, abstract #9965.

Severi, M., Becagli, S., Castellano, E., Morganti, A., Traversi, R., Udisti, R., Ruth, U., Fischer, H., Huybrechts, P., Wolff, E., Parrenin, F., Kaufmann, P., Lambert, F., Steffensen, J.P., 2007. Synchronisation of the EDML and EDC ice cores for the last 52 kyr by volcanic signature matching. Clim. Past Discuss. 3, 409–433. DOI:10.5194/cpd-3-409-2007

Shevenell, A.E.E., Ingalls, A.E.E., Domack, E.W.W., Kelly, C., 2011. Holocene Southern Ocean surface temperature variability west of the Antarctic Peninsula. Nature 470, 250–254. DOI:10.1038/nature09751

Siebert, L., Simkin, T., 2002. Volcanoes of the World: an Illustrated Catalog of Holocene Volcanoes and their Eruptions. Smithsonian Institution, Global Volcanism Program Digital Information Series, GVP-3 [volcano.si.edu/volcano.cfm?vn=360120].

Sigg, A., Neftel, A., 1988. Seasonal variations in hydrogen peroxide in polar ice cores. Ann. Glaciol. 10, 157–162.

Sigl, M., McConnell, J.R., Layman, L., Maselli, O., McGwire, K., Pasteris, D., Dahl-Jensen, D., Steffensen, J.P., Vinther, B., Edwards, R., Mulvaney, R., Kipfstuhl, S., 2013. A new bipolar ice core record of volcanism from WAIS Divide and NEEM and implications for climate forcing of the last 2000 years. J. Geophys. Res. Atmos. 118, 1151–1169. DOI:10.1029/2012JD018603

Sigl, M., Winstrup, M., McConnell, J.R., Welten, K.C., Plunkett, G., Ludlow, F., Büntgen, U., Caffee, M., Chellman, N., Dahl-Jensen, D., Fischer, H., Kipfstuhl, S., Kostick, C., Maselli, O.J., Mekhaldi, F., Mulvaney, R., Muscheler, R., Pasteris, D.R., Pilcher, J.R., Salzer, M., Schüpbach, S., Steffensen, J.P., Vinther, B.M., Woodruff, T.E., 2015. Timing and climate forcing of volcanic eruptions for the past 2,500 years. Nature 523, 543–549. DOI:10.1038/nature14565

Simmonds, I., 1996. Climatic Role of Southern Hemisphere Extratropical Cyclones and Their Relationship with Sea Ice. Pap. Proc. R. Soc. Tasmania, 130, 2, 95-100.

Simonsen, S.B., Johnsen, S.J., Popp, T.J., Vinther, B.M., Gkinis, V., Steen-Larsen, H.C., 2011. Past surface temperatures at the NorthGRIP drill site from the difference in firn diffusion of water isotopes. Clim. Past 7, 1327–1335. DOI:10.5194/cp-7-1327-2011

Smith, B.T., van Ommen, T.D., Curran, M.A.J., 2004. Methanesulphonic acid movement in solid ice cores. Ann. Glaciol. 39, 540–544.

DOI:10.3189/172756404781814645

Smith, D.E., Harrison, S., Firth, C.R., Jordan, J.T., 2011. The early Holocene sea level rise. Quat. Sci. Rev. 30, 1846–1860. DOI:10.1016/j.quascirev.2011.04.019

Soda, T., 1996. Explosive activities of Haruna volcano and their impacts on human life in the sixth century A.D. Geogr. Reports Tokyo Metrop. Univ. 31, 37–52.

Souney, J.M., Mayewski, P.A., Goodwin, I.D., Meeker, L.D., Morgan, V., Curran, M.A.J., van Ommen, T.D., Palmer, A.S., 2002. A 700-year record of atmospheric circulation developed from the Law Dome ice core, East Antarctica. J. Geophys. Res. 107, D22, 4608. DOI:10.1029/2002JD002104

Souney, J.M., Twickler, M.S., Hargreaves, G.M., Bencivengo, B.M., Kippenhan, M.J., Johnson, J.A., Cravens, E.D., Neff, P.D., Nunn, R.M., Orsi, A.J., Popp, T.J., Rhoades, J.F., Vaughn, B.H., Voigt, D.E., Wong, G.J., Taylor, K.C., 2014. Core handling and processing for the WAIS Divide ice-core project. Ann. Glaciol. 55, 15–26. DOI:10.3189/2014AoG68A008

Spahni, R., Schwander, J., Flückiger, J., Stauffer, B., Chappellaz, J., Raynaud, D., 2003. The attenuation of fast atmospheric CH 4 variations recorded in polar ice cores. Geophys. Res. Lett. 30, 11, 1571. DOI:10.1029/2003GL017093

Steig, E., Morse, D.L., Waddington, E.D., Stuiver, M., Grootes, P.M., Mayewski, P.A., Twickler, M.S., Whitlow, S.I., 2000. Wisconsian and Holocene climate history from an ice core at Taylor Dome, western Ross embayment, Antarctica. Geogr. Ann. 82, 213–235.

Steig, E.J., Mayewski, P.A., Dixon, D.A., Kaspari, S.D., Frey, M.M., Schneider, D.P., Arcone, S.A., Hamilton, G.S., Spikes, V.B., Albert, M., Meese, D., Gow, A.J., Shuman, C.A., White, J.W.C., Sneed, S., Flaherty, J., Wumkes, M., 2005. High-resolution ice cores from US ITASE (West Antarctica): development and validation of chronologies and determination of precision and accuracy. Ann. Glaciol. 41, 77–84.

Stenni, B., Proposito, M., Gragnani, R., Flora, O., Jouzel, J., Falourd, S., Frezzotti, M., 2002. Eight centuries of volcanic signal and climate change at Talos Dome (East Antarctica). J. Geophys. Res. 107, D9, 4076. DOI:10.1029/2000JD000317

Stothers, R.B., 1984. The great tambora eruption in 1815 and its aftermath. Science 224, 1191–8. DOI:10.1126/science.224.4654.1191

Stothers, R.B., 1999. Volcanic dry fogs, climate cooling, and plague pandemics in europe and the Middle East. Clim. Change 42, 713–723.

Svensson, A., Andersen, K.K., Bigler, M., Clausen, H.B., Dahl-Jensen, D., Davies, S.M., Johnsen, S.J., Muscheler, R., Parrenin, F., Rasmussen, S.O., Röthlisberger, R., Seierstad, I., Steffensen, J.P., Vinther, B.M., 2008. A 60 000 year Greenland stratigraphic ice core chronology. Clim. Past 4, 47–57. DOI:10.5194/cp-4-47-2008

Svensson, A., Andersen, K.K., Bigler, M., Clausen, H.B., Dahl-Jensen, D., Davies, S.M., Johnsen, S.J., Muscheler, R., Rasmussen, S.O., Röthlisberger, R., Steffensen, J.P., Vinther, B.M., 2006. The Greenland Ice Core Chronology 2005, 15-42 ka. Part 2: comparison to other records. Quat. Sci. Rev. 25, 3258–3267. DOI:10.1016/j.quascirev.2006.08.003

Tabazadeh, A., Toon, O.B., 1996. The presence of metastable HNO3/H2O solid phases in the stratosphere inferred from ER 2 data. J. Geophys. Res. 101, 9071–9078. DOI:10.1029/96JD00062

Takata, M., Iizuka, Y., Hondoh, T., Fujita, S., Fujii, Y., Shoji, H., 2004. Stratigraphic analysis of Dome Fuji Antarctic ice core using an optical scanner. Ann. Glaciol. 39, 467–472. DOI:10.3189/172756404781813899

Taylor, K.C., Alley, R.B., Meese, D.A., Spencer, M.K., Brook, E.J., Dunbar, N.W., Finkel, R.C., Gow, A.J., Kurbatov, A. V., Lamorey, G.W., Mayewski, P.A., Meyerson, E.A., Nishiizumi, K., Zielisnki, G.A., 2004. Dating the Siple Dome (Antarctica) ice core by manual and computer interpretation of annual layering. J. Glaciol. 50, 453–461. DOI:10.3189/172756504781829864

Tegen, I., 2003. Modeling the mineral dust aerosol cycle in the climate system. Quat. Sci. Rev. 22, 1821–1834. DOI:10.1016/S0277-3791(03)00163-X

Thomas, E.R., Wolff, E.W., Mulvaney, R., Steffensen, J.P., Johnsen, S.J., Arrowsmith, C., White, J.W.C., Vaughn, B., Popp, T., 2007. The 8.2ka event from Greenland ice cores. Quat. Sci. Rev. 26, 70–81. DOI:10.1016/j.quascirev.2006.07.017

Thompson, A.M., 1992. The Oxidizing Capacity of the Earth's Atmosphere: Probable Past and Future Changes. Science. 256, 1157–1165. DOI:10.1126/science.256.5060.1157

Thompson, L.G., Mosley-Thompson, E., Davis, M.E., Henderson, K.A., Brecher, H.H., Zagorodnov, V.S., Mashiotta, T.A., Lin, P.-N., Mikhalenko, V.N., Hardy, D.R., Beer, J., 2002. Kilimanjaro ice core records: evidence of holocene climate change in tropical Africa. Science 298, 589–593. DOI:10.1126/science.1073198

Toggweiler, J.R., Russell, J.L., Carson, S.R., 2006. Midlatitude westerlies, atmospheric CO2, and climate change during the ice ages. Paleoceanography 21, 1–15. DOI:10.1029/2005PA001154

Tozer, C.R., Vance, T.R., Roberts, J., Kiem, A.S., Curran, M.A.J., Moy, A.D., 2015. An ice core derived 1013-year catchment scale annual rainfall reconstruction in subtropical eastern Australia. Hydrol. Earth Syst. Sci. Discuss. 12, 12483–12514. DOI:10.5194/hessd-12-12483-2015

Traufetter, F., Oerter, H., Fischer, H., Weller, R., Miller, H., 2004. Spatio-temporal variability in volcanic sulphate deposition over the past 2 kyr in snow pits and firn cores from Amundsenisen, Antarctica. J. Glaciol. 50, 137–146. DOI:10.3189/172756504781830222

Trenberth, K.E., Large, W.G., Olson, J.G., 1990. The Mean Annual Cycle in Global Ocean Wind Stress. J. Phys. Oceanogr. 20, 11, 1742-1760.

Udisti, R., Becagli, S., Benassai, S., De Angelis, M., Hansson, M.E., Jouzel, J., Schwander, J., Steffensen, J.P., Traversi, R., Wolff, E., 2004. Sensitivity of chemical species to climatic changes in the last 45 kyr as revealed by high-resolution Dome C (East Antarctica) ice-core analysis. Ann. Glaciol. 39, 457–466. DOI:10.3189/172756404781814096

Udisti, R., Dayan, U., Becagli, S., Busetto, M., Frosini, D., Legrand, M., Lucarelli, F., Preunkert, S., Severi, M., Traversi, R., Vitale, V., 2012. Sea spray aerosol in central Antarctica. Present atmospheric behaviour and implications for paleoclimatic reconstructions. Atmos. Environ. 52, 109–120. DOI:10.1016/j.atmosenv.2011.10.018

van Ommen, T., 2015. Northern push for the bipolar see-saw. Nature 520, 630–631. DOI:10.1038/520630a

van Ommen, T.D., Morgan, V., 1996. Peroxide concentrations in the Dome Summit South ice core, Law Dome, Antarctica. J. Geophys. Res. 101, 15147. DOI:10.1029/96JD00838

van Ommen, T.D., Morgan, V., 1997. Calibrating the ice core paleothermometer using seasonality. J. Geophys. Res. 102, 9351–9357. DOI:10.1029/96JD04014

van Ommen, T.D., Morgan, V., Curran, M.A.J., 2004. Deglacial and Holocene changes in accumulation at Law Dome, East Antarctica. Ann. Glaciol. 39, 359–365. DOI:10.3189/172756404781814221

van Ommen, T.D.T., Loulergue, L., Chappellaz, J., Morgan, V.V.I., Spahni, R., Schilt, A., Curran, M., MacFarling-Muere, C., Etheridge, D.M., Stocker, T., 2007. The 8200 B.P. climate event in the Southern Hemisphere. In: EGU General Assembly. European Geosciences Union, Vienna.

Vance, T.R., Roberts, J.L., Plummer, C.T., Kiem, A.S., van Ommen, T.D., 2015. Interdecadal Pacific variability and eastern Australian megadroughts over the last millennium. Geophys. Res. Lett. 42, 129–137. DOI:10.1002/2014GL062447

Vance, T.R., van Ommen, T.D., Curran, M.A.J., Plummer, C.T., Moy, A.D., 2013. A Millennial Proxy Record of ENSO and Eastern Australian Rainfall from the Law Dome Ice Core, East Antarctica. J. Clim. 26, 710–725. DOI:10.1175/JCLI-D-12-00003.1

Varma, V., Prange, M., Merkel, U., Kleinen, T., Lohmann, G., Pfeiffer, M., Renssen, H., Wagner, A., Wagner, S., Schulz, M., 2012. Holocene evolution of the Southern Hemisphere westerly winds in transient simulations with global climate models. Clim. Past 8, 391–402. DOI:10.5194/cp-8-391-2012

Veres, D., Bazin, L., Landais, A., Toyé Mahamadou Kele, H., Lemieux-Dudon, B., Parrenin, F., Martinerie, P., Blayo, E., Blunier, T., Capron, E., Chappellaz, J., Rasmussen, S.O., Severi, M., Svensson, A., Vinther, B., Wolff, E.W., 2013. The Antarctic ice core chronology (AICC2012): an optimized multi-parameter and multi-site dating approach for the last 120 thousand years. Clim. Past 9, 1733–1748. DOI:10.5194/cp-9-1733-2013

Vinther, B.M., Andersen, K.K., Jones, P.D., Briffa, K.R., Cappelen, J., 2006a.

Extending Greenland temperature records into the late eighteenth century. J. Geophys. Res. Atmos. 111, 1–13. DOI:10.1029/2005JD006810

Vinther, B.M., Buchardt, S.L., Clausen, H.B., Dahl-Jensen, D., Johnsen, S.J., Fisher, D.A., Koerner, R.M., Raynaud, D., Lipenkov, V., Andersen, K.K., Blunier, T., Rasmussen, S.O., Steffensen, J.P., Svensson, A.M., 2009. Holocene thinning of the Greenland ice sheet. Nature 461, 385–388. DOI:10.1038/nature08355

Vinther, B.M., Clausen, H.B., Johnsen, S.J., Rasmussen, S.O., Andersen, K.K., Buchardt, S.L., Dahl-Jensen, D., Seierstad, I.K., Siggaard-Andersen, M.-L., Steffensen, J.P., Svensson, A., Olsen, J., Heinemeier, J., 2006b. A synchronized dating of three Greenland ice cores throughout the Holocene. J. Geophys. Res. 111, D13102. DOI:10.1029/2005JD006921

Virkkula, A., Asmi, E., Teinilä, K., Frey, A., Aurela, M., 2009. Review of Aerosol Research at the Finnish Antarctic Research Station Aboa and its Surroundings in Queen Maud Land , Antarctica. Geophysica 45, 163–181.

von Grafenstein, U., Erlenkeuser, H., Müller, J., Jouzel, J., Johnsen, S., 1998. The cold event 8200 years ago documented in oxygen isotope records of precipitation in Europe and Greenland. Clim. Dyn. 14, 73–81. DOI:10.1007/s003820050210

Waddington, E.D., Cunningham, J., Harder, S.L., 1996. The Effects of Snow Ventilation on Chemical Concentrations. In: Wolff, E.W., Bales, R.C. (Eds.), Chemical Exchange Between the Atmosphere and Polar Snow. Springer, New York, pp. 403–452.

Wagenbach, D., 1996. Coastal Antarctica: Atmospheric Chemical Composition and Atmospheric Transport. In: Wolff, E.W., Bales, R.C. (Eds.), Chemical Exchange Between the Atmosphere and Polar Snow. Springer, New York, pp. 173–199.

Wagenbach, D., Ducroz, F., Mulvaney, R., Keck, L., Minikin, A., Legrand, M., Hall, J.S., Wolff, E.W., 1998. Sea-salt aerosol in coastal Antarctic regions. J. Geophys. Res. 103, 10961. DOI:10.1029/97JD01804

Wagner, A.J., Morrill, C., Otto-Bliesner, B.L., Rosenbloom, N., Watkins, K.R., 2013. Model support for forcing of the 8.2 ka event by meltwater from the Hudson Bay ice dome. Clim. Dyn. 41, 2855–2873. DOI:10.1007/s00382-013-1706-z

Walker, M., Johnsen, S., Rasmussen, S.O., Popp, T., Steffensen, J.-P., Gibbard, P., Hoek, W., Lowe, J., Andrews, J., Björck, S., Cwynar, L.C., Hughen, K., Kershaw, P., Kromer, B., Litt, T., Lowe, D.J., Nakagawa, T., Newnham, R., Schwander, J., 2009. Formal definition and dating of the GSSP (Global Stratotype Section and Point) for the base of the Holocene using the Greenland NGRIP ice core, and selected auxiliary records. J. Quat. Sci. 24, 3–17. DOI:10.1002/jqs.1227

Wallace, J., Smith, C., Jiang, Q., 1990. Spatial Patterns of Atmosphere-Ocean Interaction in the Northern Winter. J. Clim. 3, 990-998.

Wallace, J.M., Hobbs, P. V., 2006. Atmospheric Science: An Introductory Survey, 2nd ed. Academic Press, Burlington.

Wang, Q., Danilov, S., Fahrbach, E., Schröter, J., Jung, T., 2012. On the impact of wind forcing on the seasonal variability of Weddell Sea Bottom Water transport. Geophys. Res. Lett. 39, L06603. DOI:10.1029/2012GL051198

Weller, R., Traufetter, F., Fischer, H., Oerter, H., Piel, C., Miller, H., 2004. Postdepositional losses of methane sulfonate, nitrate, and chloride at the European Project for Ice Coring in Antarctica deep-drilling site in Dronning Maud Land, Antarctica. J. Geophys. Res. 109, D07301. DOI:10.1029/2003JD004189

Winstrup, M., Svensson, A.M., Rasmussen, S.O., Winther, O., Steig, E.J., Axelrod, A.E., 2012. An automated approach for annual layer counting in ice cores. Clim. Past 8, 1881–1895. DOI:10.5194/cp-8-1881-2012

Witter, J.B., Self, S., 2006. The Kuwae (Vanuatu) eruption of AD 1452: potential magnitude and volatile release. Bull. Volcanol. 69, 301–318. DOI:10.1007/s00445-006-0075-4

Wolff, E., 1996. Location, Movement and Reactions of Impurities in Solid Ice. In: Wolff, E.W., Bales, R.C. (Eds.), Chemical Exchange Between the Atmosphere and Polar Snow. Springer, New York, pp. 541–560.

Wolff, E.W., Fischer, H., Fundel, F., Ruth, U., Twarloh, B., Littot, G.C., Mulvaney, R., Röthlisberger, R., de Angelis, M., Boutron, C.F., Hansson, M., Jonsell, U., Hutterli, M.A., Lambert, F., Kaufmann, P., Stauffer, B., Stocker, T.F., Steffensen, J.P., Bigler, M., Siggaard-Andersen, M.L., Udisti, R., Becagli, S., Castellano, E., Severi, M., Wagenbach, D., Barbante, C., Gabrielli, P., Gaspari, V., 2006. Southern Ocean sea-ice extent, productivity and iron flux over the past eight glacial cycles. Nature 440, 491–496. DOI:10.1038/nature04614

Wolff, E.W., Hall, J.S., Mulvaney, R., Pasteur, E.C., Wagenbach, D., Legrand, M., 1998. Relationship between chemistry of air, fresh snow and firn cores for aerosol species in coastal Antarctica. J. Geophys. Res. 103, 11057. DOI:10.1029/97JD02613

Wolff, E.W., Miners, W.D., Moore, J.C., Paren, J.G., 1997. Factors Controlling the Electrical Conductivity of Ice from the Polar RegionsA Summary. J. Phys. Chem. B 101, 6090–6094. DOI:10.1021/jp9631543

Wolff, E.W., Rankin, A.M., Röthlisberger, R., 2003. An ice core indicator of Antarctic sea ice production? Geophys. Res. Lett. 30, 22, 2158. DOI:10.1029/2003GL018454

Wong, G., 2007. Investigating the Dominant Source of Sea Salt to Antarctica: Sea Salt Signal in Ice Core GD17, Unpub. Honours thesis, University of Tasmania.

Yalcin, K., Wake, C.P., Germani, M.S., 2003. A 100-year record of North Pacific volcanism in an ice core from Eclipse Icefield, Yukon Territory, Canada. J. Geophys. Res. 108, D1, 4012. DOI:10.1029/2002JD002449

Yang, Q., Mayewski, P.A., Linder, E., Whitlow, S.I., Twickler, M.S., 1996. Chemical species spatial distribution and relationship to elevation and snow accumulation rate over the Greenland Ice Sheet. J. Geophys. Res. 101, 18629–18637. DOI:10.1029/96JD01061

Yang, X., Pyle, J.A., Cox, R.A., 2008. Sea salt aerosol production and bromine release: Role of snow on sea ice. Geophys. Res. Lett. 35, L16815. DOI:10.1029/2008GL034536

Yuan, X., Martinson, D.G., Liu, W.T., 1999. Effect of air-sea-ice interaction on winter 1996 Southern Ocean subpolar storm distribution. J. Geophys. Res. Atmos. 104, 1991–2007. DOI:10.1029/98JD02719

Yung, Y.L., Lee, T., Wang, C.-H., Shieh, Y.-T., 1996. Dust: A Diagnostic of the Hydrologic Cycle During the Last Glacial Maximum. Science (80-.). 271, 962–963. DOI:10.1126/science.271.5251.962

Zielinski, G.A., 1995. Stratospheric loading and optical depth estimates of explosive volcanism over the last 2100 years. J. Geophys. Res. 100, 20937–20955.

Zielinski, G.A., 2000. Use of paleo-records in determining variability within the volcanism-climate system. Quat. Sci. Rev. 19, 417–438. DOI:10.1016/S0277-3791(99)00073-6

Zielinski, G.A., Mayewski, P.A., Meeker, L.D., Grönvold, K., Germani, M.S., Whitlow, S., Twickler, M.S., Taylor, K., 1997. Volcanic aerosol records and tephrochronology of the Summit, Greenland, ice cores. J. Geophys. Res. 102, 26625. DOI:10.1029/96JC03547

Appendices

Appendix A1 – Example chromatograms

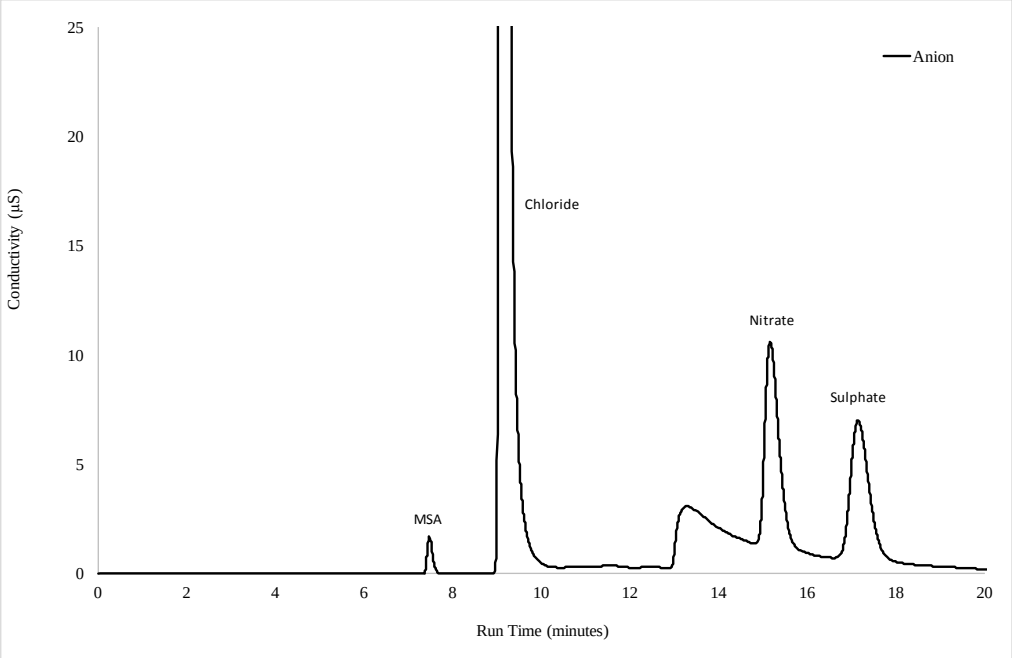

Figure A1-1 – Anion chromatogram. Chloride peaks at 180 µS.

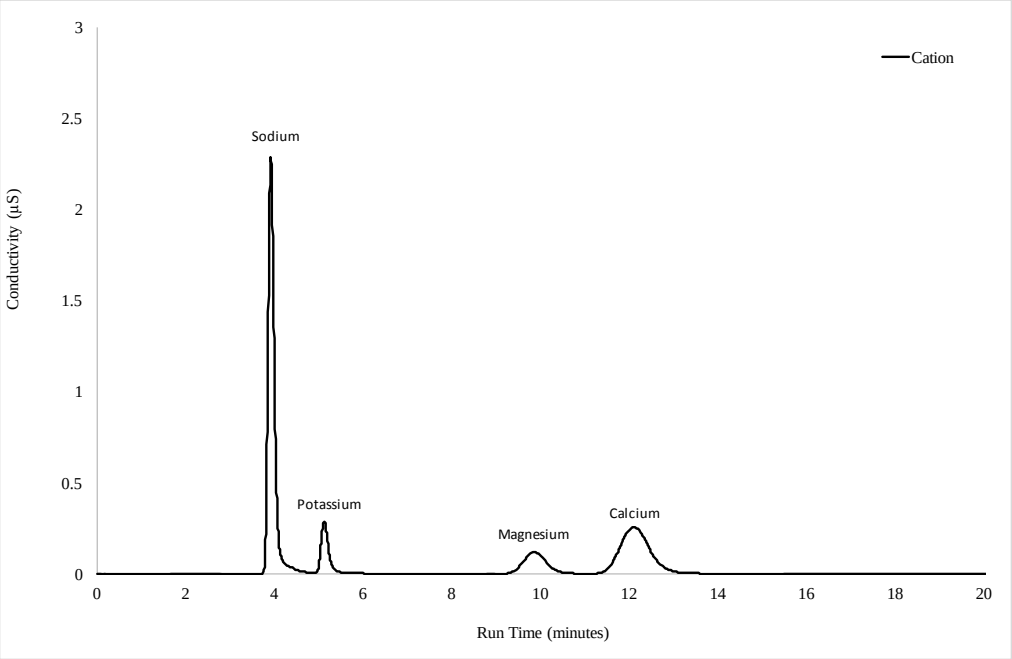

Figure A1-2 – Cation chromatogram.

Appendix A2 – Holocene volcanic record

Following on from the 2000 years of volcanic eruption data discussed in Chapter 5, the remainder of the Holocene volcanic record is presented in Table A1. Events between 23 BCE and 333 BCE have layer counted dates and uncertainties. The Law Dome age model was constructed by including some volcanic events that were synchronised with the EDC volcanic record on the AICC2012 timescale through the Holocene [Table 3.2, chapter 3]. Volcanic events not identified as part of the AICC2012 timescale from the EDC volcanic record have been dated using the age model described in Chapter 3.5.

A2.1 Identification of volcanic events

Volcanic events have been identified as deviations from the background in the sulphate record. Identification of events in the deeper (older) DSS record is more difficult due to decreasing sample resolution and layer thinning which smooths out signals associated with short-term variations like volcanic eruptions. Only large volcanic events can be detected resulting in fewer events being identified compared with the high resolution ALC record. Additionally, there are several gaps in the Law Dome deep chemistry record due to areas of poor core quality that make a continuous volcanic record difficult to obtain. This is a particularly important factor for synchronisation of volcanic records as being able to match the records in a continuous manner increases confidence in tie points.

Table A1 – Volcanic events at Law Dome beyond 23 BCE (2022 b2k). Depths and ages represent the peak in volcanic sulphate. AICC2012 refers to events dated by synchronisation to EDC on the AICC2012 timescale used in the age model (detailed in Chapter 3).

Depth (m)	Date (b2k)	Uncertainty (years)	Dating Method
796.78	2,024	+4/-7	Layer counting
802.10	2,051	+6/-7	Layer counting
809.12	2,088	+9/-7	Layer counting
812.22	2,102	+10/-7	Layer counting
821.28	2,152	+13/-7	Layer counting
825.22	2,175	+13/-7	Layer counting
832.10	2,215	+13/-7	Layer counting
838.33	2,251	+13/-7	Layer counting
868.16	2,440	20	Matched to AICC2012
881.00	2,540	20	Age model
888.02	2,603	20	Age model
898.16	2,702	20	Age model
905.36	2,784	20	Age model
935.84	3,182	20	Age model
949.32	3,375	20	Matched to AICC2012
951.98	3,423	20	Matched to AICC2012
952.60	3,435	20	Matched to AICC2012
964.75	3,637	20	Age model
965.05	3,648	20	Age model
966.49	3,674	20	Matched to AICC2012
970.31	3,735	20	Matched to AICC2012
972.46	3,769	20	Age model
983.81	3,988	20	Age model
985.52	4,012	20	Age model
987.43	4,055	20	Matched to AICC2012
1002.46	4,412	50	Age model
1003.45	4,433	50	Age model
1022.81	4,922	50	Age model

Depth (m)	Date (b2k)	Uncertainty (years)	Dating Method
1060.02	6,059	50	Age model
1082.77	7,084	80	Age model
1083.87	7,141	80	Age model
1096.84	7,881	80	Age model
1102.33	8,463	100	Age model
1106.83	9,158	100	Age model
1119.02	11,349	200	Age model

Appendix A3 Calculation of NGRIP volcanic sulphate deposition

The NGRIP SO_4^{2-} dataset is based on measurements performed on two NGRIP ice cores. Data covering 1973–1999 stem from the NGRIP 2000 S6 shallow core, while the 186–1973 interval is derived from the NGRIP1 1996 main core. The entire dataset was measured in 50 mm resolution, corresponding to an average time resolution of 4 samples per year in the deepest (oldest) ice and 10 samples per year in the uppermost (youngest) sections of the NGRIP ice. The measurement data were converted into SO_4^{2-} deposition using equation A1 without the sea salt correction. Detection of volcanic signals in the NGRIP 50 mm resolution SO_4^{2-} deposition dataset was carried out using the methodology outlined in Traufetter et al. (2004). In this approach running medians (RM_i) and median absolute deviations (MAD_i) of a moving window of n data are calculated. Peaks were then found when deposition exceeded the running threshold value.

$$\text{year} = RM_i + k \cdot MAD_i \qquad \textbf{Equation A1}$$

The parameters k = 5 and n = 100 were determined empirically. Furthermore, peak width was defined as the number of samples surrounding a detected sample, all exceeding a running threshold calculated with k = 0.5. The total volcanic deposition for each event was then calculated as the sum of the deposition stemming from each 50 mm sample forming a given peak, subtracting the background SO_4^{2-} deposition (the background being calculated as the running mean of the SO_4^{2-} deposition data where no volcanic signals were detected, again with n = 100 as the window length.). Peak deposition uncertainties were finally

calculated from the standard deviation of the background SO_4^{2-} deposition. The NGRIP sulphate data are available from www.iceandclimate.dk/data/.

Appendix A4 Cores used in chapter 5 2000-yr volcanics publication

Table A2 – These six ice cores are within 1 km of the DSS site (66°43'S 112°48'E), Law Dome, East Antarctica, and were used to produce the continuous Law Dome chemistry time series. Ice cores were selected to cover different time periods to give the highest quality dataset through that time period. DSS99 covers an older time period than DSS97, as DSS97 has continuous trace ion data to 1882 CE (96 m) only. DSS97, DSS99 and DSSmain down to 400 m were used previously by Palmer et al., (2001).

Core	Drill Location	Length (m)	Drill start date	Bottom Date	Time period spanned in Law Dome record (CE)
DSS0910	DSS	7	Dec. 2009	2003 CE	2009.0 – 2005.5
DSS0809	DSS	10	Dec. 2008	2001 CE	2005.5 – 2001.5
DSS0102	DSS	9	Dec. 2001	1994 CE	2001.5 – 1995.5
DSS97	DSS	240	Dec. 1997	1792 CE	1995.5 – 1888.0
DSS99	DSS	125	Feb. 2000	1840 CE	1888.0 – 1840.5
DSSmain	DSS	1196	Dec. 1987	≈90 ka	1840.5 – 23 BCE

Appendix A5 Core locations used in Figure 4.11

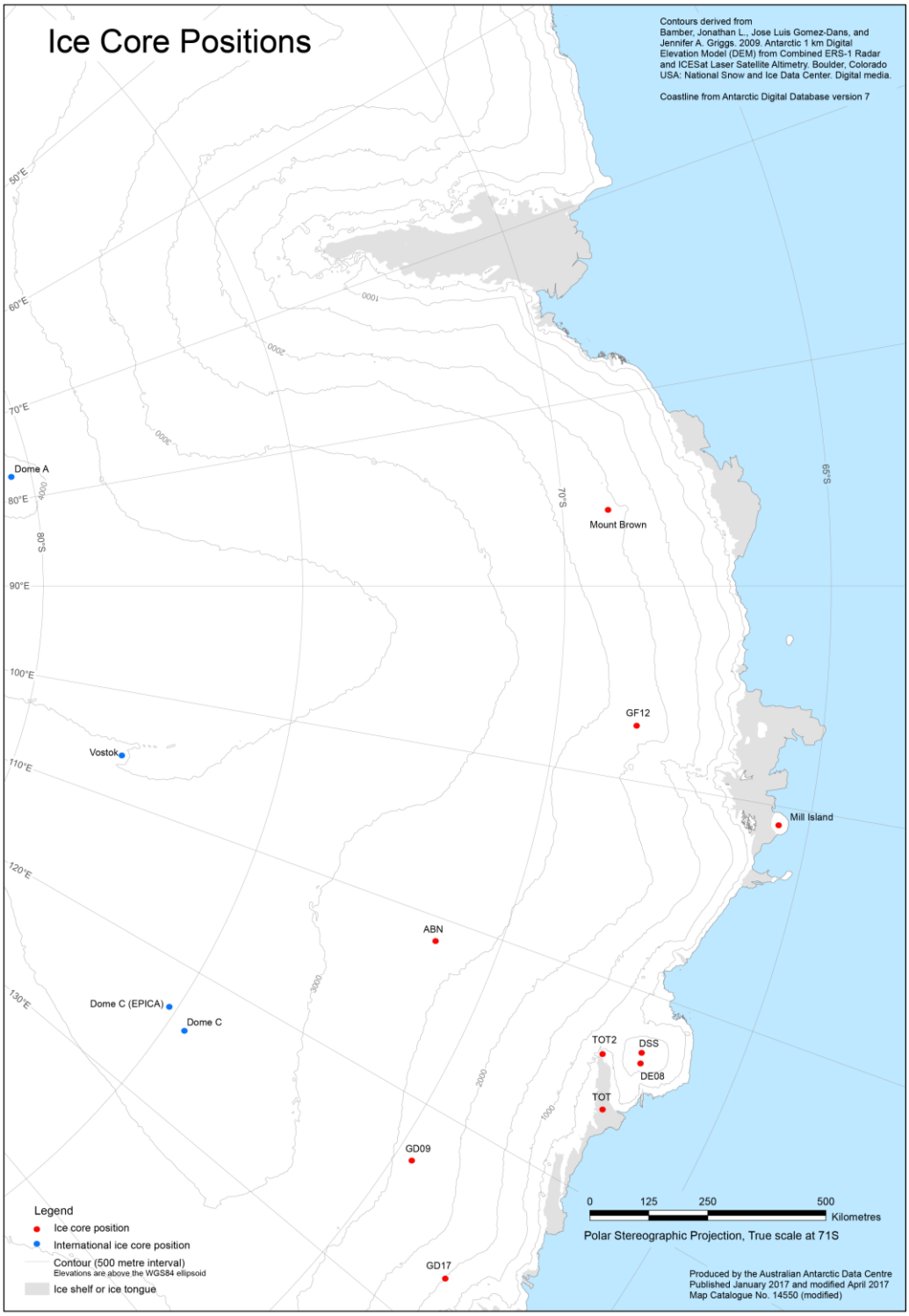

Figure A2 – East Antarctic ice core locations referred to in Figure 4.11 (section 4.7). Red dots show cores locations used.